



UNIVERSITÀ DEGLI STUDI DI TRENTO

DEPARTMENT OF INDUSTRIAL ENGINEERING

Master degree in Mechatronics Engineering

**KINEMATIC
OPTIMIZATION OF A RACING CAR
SUSPENSION USING THE “g-g” DIAGRAM**

Supervisor:

Ing. Francesco Biral

Graduant:

Alessandro Luchetti

Academic year 2017-2018

Copyright

Alessandro Luchetti, 2018

All rights reserved

"We're all on the limit, the car is on the limit, the human being is on the limit,...

That's what it's all about motor racing."

- Ayrton Senna

ABSTRACT

This thesis describes a way to find the best double wishbone suspension configuration thanks to which is possible to guarantee the desired dynamic behaviour of a racing car.

Starting from a dynamic vehicle model, which includes the Pacejka's Magic Formula tire model, the curves of camber and toe angle that optimized the "g-g" diagrams at each velocity are found.

The following step consists in founding the suspension configuration that best approximates these curves.

Then, once fixed the Motion ratio behaviour between the wheel displacement and the shock absorber, the missing kinematic points, directly linked to this parameter, are added to the suspension model.

At the end of the work is defined the list of all the optimized kinematic points that best replicate the main curves: camber, toe and motion ratio.

Key words. *Vehicle dynamics – Double wishbone – Kinematic suspension design – Hardpoints – Tire model – Multi-body vehicle models – Numerical optimization – Formula SAE – Camber – Toe angle – Motion ratio*

TABLE OF CONTENTS

INTRODUCTION.....	1
1. FSAE.....	3
1.1 E-Agle Trento racing team.....	3
1.2 Chimera.....	4
2. Suspension configuration for a racing car	6
3. Characteristic wheel angles.....	8
4. Characteristic parameters and their influence on vehicle dynamics.....	12
4.1 Kingpin axis.....	12
4.2 Centers of velocities	14
4.2.1 Front view.....	16
4.2.2 Side view.....	18
5. I OPTIMIZATION: Camber and toe optimized curves using the “g-g” diagram	20
5.1 Dynamic vehicle model	20
5.1.1 Dynamic model equations.....	21
5.1.2 Dynamics of vertical forces	22
5.1.3 Dynamics of tire drift angles	22
5.1.4 Steering dynamics	23
5.1.5 Wheel dynamics (spin)	23
5.1.6 Final dynamic equations set.....	24
5.1.7 Matlab environment	24
5.2 The “g-g” diagram optimization	27
5.2.1 Longitudinal acceleration and braking.....	31
5.2.2 Lateral maximum acceleration.....	33
5.2.3 Considerations.....	35
5.3 Camber and toe curves optimization	36
5.3.1 Genetic algorithm.....	38
5.3.2 Results	42
6. II OPTIMIZATION: Kinematic suspension optimization.....	46
6.1 Objective function	46
6.2 Constraints	47
6.3 Variables.....	51
6.4 Results	52
7. III Optimization: Suspension Motion ratio	57

7.1	Motion ratio theory.....	57
7.2	Motion ratio optimization.....	61
7.2.1	Objective function	61
7.2.2	Constraints and variables	62
7.2.3	Results	67
7.3	Validation Model with Motion ratio	71
7.3.1	Sensors	72
7.3.2	Assumptions.....	74
7.3.3	Lengths check	75
7.3.4	Results	76
CONCLUSIONS AND FUTURE WORK.....		79
REFERENCES		81
APPENDIX A: Magic Formula.....		82
APPENDIX B: IPOPT algorithm.....		89
APPENDIX C: FSAE suspension rules		93

LIST OF FIGURES

FIGURE 1 - FORMULA SAE ITALY & FORMULA ELECTRIC ITALY - VARANO JULY 11-15, 2018	3
FIGURE 2 - E-AGLE TRENTO RACING TEAM EMBLEM	4
FIGURE 3 - FIRST FSAE VEHICLE OF THE UNIVERSITY OF TRENTO - VARANO 2017	4
FIGURE 4 - DEGREES OF FREEDOM AND SUSPENSION MOTION: DEFINITIONS	6
FIGURE 5 - CHIMERA REAR PUSH-ROD CONFIGURATION / FIGURE 6 - CHIMERA FRONT PULL-ROD CONFIGURATION....	7
FIGURE 7 - SAE TIRE AXIS SYSTEM.....	8
FIGURE 8 - NEGATIVE CAMBER.....	9
FIGURE 9 - TOP VIEW: TOE-IN	10
FIGURE 10 - OVERSTEER BEHAVIOUR / FIGURE 11 - UNDERSTEER BEHAVIOUR	11
FIGURE 12 - FRONT SUSPENSION PACKAGING	12
FIGURE 13 - CENTER OF INSTANTANEOUS ROTATION GEOMETRY CONSTRUCTION	14
FIGURE 14 - CHASLES'S THEOREM	15
FIGURE 15 - INSTANT AXIS	15
FIGURE 16 - ROLL CENTER CONSTRUCTION	16
FIGURE 17 - JACKING EFFECT WITH A HIGH ROLL CENTER	17
FIGURE 18 - GEOMETRICAL REPRESENTATION OF THE CAMBER CHANGE RATE	17
FIGURE 19 - SCRUB RESPECT TO IC HEIGHT	18
FIGURE 20 - CALCULATION OF THE ANTI-SQUAT PERCENTAGE.....	19
FIGURE 21 - ROLL AXIS MODEL.....	20
FIGURE 22 - SIGN CONVENTION	21
FIGURE 23 - ACKERMAN STEERING (CHASSIS - TOP VIEW)	23
FIGURE 24 - THE TIRE COORDINATE SYSTEM	25
FIGURE 25 - DRAG AND DOWNFORCES IN DYNAMIC MODEL	26
FIGURE 26 - THE "G-G" DIAGRAM CORRESPONDS TO THE VELOCITY OF 15 [M/s]	30
FIGURE 27 - HALF "G-G" DIAGRAM OPTIMIZATION	30
FIGURE 28 - TORQUE CURVE OF EMRAX 208 HIGH VOLTAGE CC.....	32
FIGURE 29 - MAXIMUM LONGITUDINAL ACCELERATION POINTS.....	33
FIGURE 30 - MINIMUM LONGITUDINAL ACCELERATION POINTS.....	33
FIGURE 31 - MAXIMUM LATERAL ACCELERATION POINTS	34
FIGURE 32 - ELLIPSE OF ADHERENCE	35
FIGURE 33 - MATLAB USER INTERFACE WITH DEFAULT VALUES	36
FIGURE 34 - THREE-DIMENSIONAL "G-G" DIAGRAMS AT 15 [M/s] AND 20 [M/s] VELOCITY	36
FIGURE 35 - TOP VIEW: "G-G" DIAGRAMS AT 15 [M/s] AND 20 [M/s] VELOCITY	37
FIGURE 36 - CAMBER DUE TO ROLL ANGLE.....	38
FIGURE 37 - TOE DUE TO ROLL ANGLE	39
FIGURE 38 - ELITE CHILD	40
FIGURE 39 - CROSSOVER CHILD	40
FIGURE 40 - MUTATION CHILD	40
FIGURE 41 - GENETIC ALGORITHM OPTIMIZATION INTERFACE	41
FIGURE 42 - CAMBER AND ROLL ANGLE (CHIMERA VS OPTIMIZED)	42
FIGURE 43 - TOE AND ROLL ANGLE (CHIMERA VS OPTIMIZED).....	42
FIGURE 44 - INITIAL CAMBER ANGLE WITH ZERO ROLL ANGLE	43
FIGURE 45 - INITIAL TOE ANGLE WITH ZERO ROLL ANGLE.....	43
FIGURE 46 - MATLAB USER INTERFACE WITH INITIAL DEFAULT VALUES	45
FIGURE 47 - ROLL ANGLE VALUES DURING THE VARANO THE MELEGARI TRACK	46
FIGURE 48 - REAR LEFT SUSPENSION MODEL WITH CHIMERA VEHICLE INITIAL VALUES.....	47

FIGURE 49 – REAR-VIEW	48
FIGURE 50 - TOP-VIEW / FIGURE 51 - LATERAL-VIEW	48
FIGURE 52 – SUSPENSION MODEL WITH POINTS NAME	49
FIGURE 53 - WHEEL RF DEGREES OF FREEDOM	49
FIGURE 54 - ARMS LENGTHS WITH THEIR VARIABLES	50
FIGURE 55 - REAR LEFT SUSPENSION CONFIGURATION WITH OPTIMIZED RESULTS.....	53
FIGURE 56 - DEPENDENT VARIABLES RESULTS DURING THE EIGHT ROLL ANGLE STEPS	53
FIGURE 57 – OPTIMIZED AND MAPLE MODEL CAMBER Vs ROLL ANGLE	54
FIGURE 58 - OPTIMIZED AND MAPLE MODEL TOE Vs ROLL ANGLE	54
FIGURE 59 - WHEEL GROUP	55
FIGURE 60 - KINGPIN AXIS.....	55
FIGURE 61 - ROLL CENTER GEOMETRIC CONSTRUCTION	56
FIGURE 62 – ROCKERS OF CHIMERA VEHICLE	57
FIGURE 63 - TOTAL MOTION RATIO	58
FIGURE 64 - PUSH ROD MOTION RATIO DIMENSIONS	58
FIGURE 65 - REAR ROCKER MOTION RATIO DIMENSIONS.....	59
FIGURE 66 - E-MOTION RENNTTEAM AALEN VEHICLE	59
FIGURE 67 - DESIRED MOTION RATIO 1:1.....	61
FIGURE 68 - SUSPENSION MODEL WITH THE NEW COMPONENTS THAT AFFECT THE MOTION RATIO	62
FIGURE 69 - TOTAL FINAL MODEL	63
FIGURE 70 - 3D CHIMERA METAL JOINT WITH NON-ALIGNED POINTS.....	63
FIGURE 71 - STRESSES OF THE CHIMERA VEHICLE'S LOWER ARM	63
FIGURE 72 - ALIGNMENT PLANE OF POINTS	64
FIGURE 73 – REAR VIEW OF REAR LEFT SUSPENSION	64
FIGURE 75 – ROCKER'S DIMENSIONS.....	65
FIGURE 76 – ROCKER'S DIMENSIONS IN THEIR REFERENCE FRAME	65
FIGURE 77 – CHIMERA'S SHOCK ABSORBER	66
FIGURE 78 – ASSEMBLY OF THE 3D PRINTED JOINT WITH THE PUSH ROD	67
FIGURE 79 - MOTION RATIO CURVE WITH OPTIMIZED POINTS.....	68
FIGURE 80 - OPTIMIZED AND MAPLE MODEL MOTION RATIO	68
FIGURE 81 - ROCKER ROTATION ANGLE	69
FIGURE 82 - INITIAL ROCKER CONFIGURATION (WHEEL DISPLACEMENT SET AT ZERO)	69
FIGURE 83 - FINAL OPTIMIZED SUSPENSION HARDPOINTS	70
FIGURE 84 - OPTIMIZED REAR SUSPENSIONS CONFIGURATION	70
FIGURE 85 - INSTRUMENTS LAYOUT FOR THE MOTION RATIO VALIDATION	71
FIGURE 86 - KEYENCE LK-G157	72
FIGURE 87 - LASER STATION	72
FIGURE 88 - DISPLACEMENT SENSOR CALIBRATION	73
FIGURE 89 - LINEAR REGRESSION.....	73
FIGURE 90 - WAYSEAR KTC 150 / SHOCK ABSORBER CONNECTION	74
FIGURE 91 - CAD MODEL REAR LEFT SUSPENSION / FIGURE 92 - BUILT MODEL REAR LEFT SUSPENSION.....	75
FIGURE 93 - SHOCK ABSORBER TRAVEL.....	76
FIGURE 94 - WHEEL TRAVEL	76
FIGURE 95 - WHEEL AND SHOCK ABSORBER DISPLACEMENT	76
FIGURE 96 - MOTION RATIO MEASURED	77
FIGURE 97 - MOTION RATIO FROM IDEAL MAPLE MODEL	77
FIGURE 98 - MOTION RATIO MEASURED AND THE ONE FROM MAPLE MODEL	78

FIGURE A. 1 -TIRE FORCES AND MOMENTS.....	82
FIGURE A. 2 - SIDE ANGLE (TOP VIEW) / FIGURE A. 3 - INCLINATION/CAMBER ANGLE (REAR VIEW)	82
FIGURE A. 4 - LATERAL TIRE DEFORMATION.....	83
FIGURE A. 5 – TIRE TRACTION.....	83
FIGURE A. 7 - CURVE PRODUCED BY THE ORIGINAL SINE VERSION OF THE MAGIC FORMULA, EQN (A.1).....	84
FIGURE A. 8 - MAGIC FORMULA MODEL: LONGITUDINAL SLIP RATIO VS LONGITUDINAL FORCE/NOMINAL LOAD	85
FIGURE A. 9 - MAGIC FORMULA MODEL: LATERAL SLIP ANGLE VS LATERAL FORCE/NOMINAL LOAD	85
FIGURE A. 10 -VERTICAL LOAD EFFECT ON LONGITUDINAL SLIP RATIO VS LONGITUDINAL FORCE/NOMINAL LOAD CURVE	86
FIGURE A. 11 - VERTICAL LOAD EFFECT ON LATERAL SLIP ANGLE VS LATERAL FORCE/NOMINAL LOAD CURVE	86
FIGURE A. 12 - CAMBER EFFECT ON LATERAL SLIP ANGLE VS LATERAL FORCE/NOMINAL LOAD CURVE	86
FIGURE A. 13 - CAMBER EFFECT ON LONGITUDINAL SLIP RATIO VS LONGITUDINAL FORCE/NOMINAL LOAD CURVE	87
FIGURE A. 14 - THREE-DIMENSIONAL GRAPH OF COMBINED SLIP FORCE CHARACTERISTICS	87
FIGURE A. 15 - ELLIPSE OF ADHERENCE	88
 FIGURE B. 1 - EXAMPLE A BARRIER FUNCTION / FIGURE B. 2 - EXAMPLE B BARRIER FUNCTION	90
 FIGURE C. 1 - KEEP-OUT-ZONES FOR THE DEFINITION OF AN OPEN-WHEELED VEHICLE	93
FIGURE C. 2 - SKIDPAD TRACK LAYOUT.....	96

LIST OF TABLES

TABLE 1 - LOWER AND UPPER BOUNDARIES FOR EACH TOE COEFFICIENT.....	39
TABLE 2 - LOWER AND UPPER BOUNDARIES FOR EACH TOE COEFFICIENT.....	39
TABLE 3 - COEFFICIENTS FINAL RESULTS	42
TABLE 4 - ROLL ANGLE DEFAULT DISCRETIZED VALUES	52
TABLE 5 - OPTIMIZATION RESULTS	53
TABLE 6 - TYPICAL FSAE PARAMETERS RANGES.....	56
TABLE 7 - MOTION RATIO COMPARISON	60
TABLE 8 - WHEEL DISPLACEMENT OPTIMIZATION STEPS.....	62
TABLE 9 - OPTIMIZATION MOTION RATIO RESULTS.....	68
TABLE 10 - ARMS LENGTHS	75

INTRODUCTION

After my experience with the Formula student (FSAE) team of the University of Trento, in which I started as structural design of the suspensions group, I decided to optimize a racing car suspension as far as the kinematic aspect is concerned.

The thesis describes the optimization activity performed on one double wishbone suspension of the first car designed and built by the University of Trento.

Even if the analyzed suspension is the rear left one, all the optimizations are suitable for all the four suspensions of the FSAE car and, in general, for any type of suspension, not necessary from the racing world. In fact, the implemented code is modular and some variables initially fixed and set at zero can be unlocked.

In this thesis different optimization tools are used in order to find the optimum suspension's kinematic points, which are called *hardpoints*. These points affect the suspension motion and by doing that they are closely related to the dynamic behaviour of the racing car: handling stability, comfortability and handling of the steering.

In the first section of the thesis are described the possible suspensions' configurations, together with their characteristic parameters, explaining how their values affect the dynamic behaviour of the vehicle. Most of these parameters conflict to each other so it is necessary to reach a compromise based on the most important need to achieve: to guarantee the best contact between the tire and the ground during the suspension travel. With the aim to design a better suspension, all of these trade-offs have to be taken into account after each optimization cycle. Moreover, in case of any modifications, it is necessary to check and verify the compliance with the FSAE 2018 technical regulation (Appendix C).

The second section of the thesis is dedicated to the optimization work, performed on the existing FSAE racing car.

The first step starts from the study of the “g-g” diagram of the current FSAE car; this diagram is important in the design of a racing car since it represents the acceleration capability. An 8DOF nonlinear dynamic model, which includes the Magic Formula tire model, is used to find the best camber and toe equations that generate the optimized “g-g” diagram.

In the following chapter is found the best kinematic suspension configuration able to approximate the optimal *camber* and *toe* curves, previously extracted from the “g-g” diagram.

The last optimization activity consists in founding the optimized hardpoints that lead to the desired *Motion ratio* value between the displacement of the shock absorber and the wheel during the suspension travel.

At the end, it is done a comparison between the Motion ratio found with the kinematic suspension model, implemented in Maple software, and the real one measured on the vehicle through different tests; this comparison is done in order to measure the goodness of the ideal model, validating it if close to the real one.

All the three optimizations described, related to the “g-g” diagram, to the suspension configuration with regards to the camber and toe angle, and to the suspension Motion ratio are performed in three different times but they influence each other with the same order in which they are implemented.

All the work is done in Matlab environment. It is used the Ipopt software package and a genetic algorithm in Matlab to find the optimized solutions. On the other hand, the equations that describe the models and act as constraints in the optimizations, are found and implemented thanks to Maple software.

1. FSAE

Formula SAE, or Formula Student, is a competition among worldwide universities which is organized by the Society of Automotive Engineers (SAE). Established in 1981, with the aim of giving to university students the opportunity to put into practice the knowledge acquired during their studies. It encourages them to design, built and compete with a Formula-style race car.

This competition includes the design and the manufacturing of a racing car, evaluated during series of tests based on its design quality and engineering efficiency. These tests are both dynamic and static at the end of which are given some points whose sum gives the final score. Static events include business presentation, cost and design report, and dynamic events include acceleration, skid pad, autocross and endurance (APPENDIX C).

Figure 1 shows all the university teams during the FSAE competition of July 2017 in the municipality of Varano De' Melegari (PR) which is the first time that the University of Trento has participated.



Figure 1 - Formula SAE Italy & Formula Electric Italy - Varano July 11-15, 2018

Retrieved January 5, 2018, from <http://www.ata.it/content/event-formula-ata/formula-sae-italy-formula-electric-italy-2018-1>

1.1 E-Agle Trento racing team

The first sae team of the University of Trento was born in June of 2016 by the initiative of Paolo Bosetti, professor at the degree course of Mechatronics Engineering at the same University. Today the team is composed of seventy-eight students coming mainly from the Engineering and Economics departments.

The team is organized in six areas concerning: the Design, Dynamics&Modelling, Electrical&Electronics, Economics&Management, Materials&Fabrication and Racing. These

groups work according to a transversal and integrated logic that allows to work in a cohesive way.

The team's name is "*E-AGLE Trento racing team*". The letter "E" wants to emphasize that the designed car is totally electric. The choice to develop directly an electric vehicle and not a combustion one comes from the strong desire of promoting and enhancing the technology behind sustainable mobility. Moreover, it was possible thanks the high preparation in mechanic and electronic field that the mechatronics center of University of Trento gives to its student. Instead, the word "EAGLE", in the team name, refers to the emblem of the city of Trento where there is the eagle of San Venceslao.

An eagle it is also present in the emblem of the Trento racing team which is shown in *Figure 2*.



Figure 2 - E-AGLE Trento racing team emblem
Retrieved January 5, 2018, from <http://www.e-agletrentoracingteam.it/>

1.2 Chimera

The name of the first car is *Chimera* because initially it was a utopia to design and build it. Instead thanks to the mutual collaboration among members of the FSAE team of University of Trento it has been possible. The vehicle structure can be seen in *Figure 3*.



Figure 3 - First FSAE vehicle of the University of Trento - Varano 2017

During the thesis work with the name *Chimera* we refer to this specific racing car.

The main characteristics of this car can be summarized in the following points:

FRAME CONSTRUCTION: Tubular space frame with 3D metal printed joints

MATERIAL: Steel

OVERALL L / W / H: 2700 [mm] x 1500 [mm] x 1200 [mm]

WHEELBASE: 1540 [mm]

TRACK (Fr / Rr): 1200 [mm] / 1180 [mm]

WEIGHT WITH 68 Kg DRIVER (Fr / Rr): 320 [Kg] (40% / 50%)

SUSPENSION: 4 custom independent shock-dampers

TIRES (Fr / Rr): 6x16"

RIM (Fr / Rr): 10"

MOTOR TYPE: Emrax 208

NUMBER OF MOTORS: 2 independent motors

MOTOR LOCATION: Rear mounted

MOTOR MAX POWER: 80 KW peak each

MOTOR CONTROLLER: Digital three-phase Servo Amplifier BAMOCAR D3

MAX SYSTEM VOLTAGE: 504 V

ELECTRODE MATERIALS: Lithium Ion Cell Batteries 18650 Form Factor

COMBINED ACCUMULATOR CAPACITY: 6.7 KWh

TRANSMISSION RATIO (PRIMARY/SECONDARY): 1 to 3.57

DRIVE TYPE: Rear 2WD

DIFFERENTIAL: Electronic

COOLING: 2 side mounted radiators – water cooled

BRAKE SYSTEM: 2 separate circuits – custom brake discs – 4 pistons caliper

ELECTRONICS: Custom designed distributed electronic system for sensor acquisition and car dynamic control

2. Suspension configuration for a racing car

The suspension of a vehicle is the set of components thanks to which the frame is connected to the wheels, or more generally indicates the connection between the sprung masses of the vehicle with the unsprung masses. These connections dictate the path of relative motion and they also control the forces that are transmitted between them. For this, the study of the suspension system of the car and the optimization design is to ensure the basic performance of the car. The car performances are important because have a decisive effect on the results of the competition.

Different types of suspensions exist. The *independent suspensions* are the most used in automotive in which the wheels of the same axle are connected individually to the vehicle chassis, so there is no influence between the travel of one suspension and the other. It permits to control the wheel's motion relative to the car body in a single prescribed path by the designer.

A single wheel body has six degrees of freedom of motion in a three-dimensional world: three components of linear motion and three components of rotational motion as can be seen in *Figure 4*.

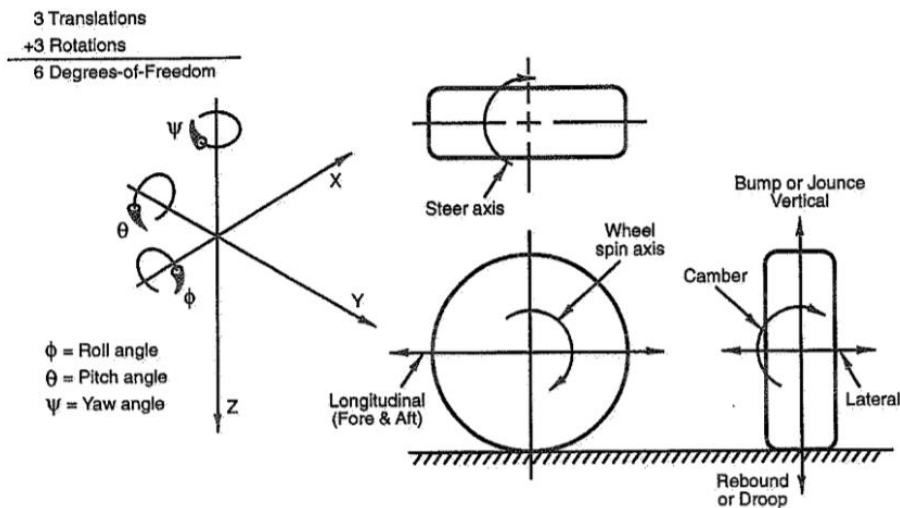


Figure 4 - Degrees of freedom and suspension motion: definitions
taken from: Milliken-Race Car Vehicle Dynamics (1997)

Considering that only one path of motion of the knuckle relative to the body is allowed the suspension must provide five degrees of restrain (D.O.R). The study of independent suspension geometries is to determine how to restrain the knuckle limited motion in five directions.

The independent suspension geometry widely used in the racing car is the *double wishbone suspension* which used two wishbone-shaped arms to locate the wheel. Each wishbone has two mounting points to the chassis and one joint at the knuckle. The shock absorber and coil spring mount to the wishbone to control vertical movement. Double wishbone designs allow to carefully control the motion of the wheel throughout suspension travel, controlling such

parameters as camber angle, caster angle, toe pattern, roll center height, scrub radius and more which will be explained in the next sections. Furthermore, this geometry offers excellent characteristic of stiffness and resistance with a low weight.

Two wishbones could have equal length or not. Usually are used two A-shaped control arms with different lengths. This type of suspensions is called SLA “*short long arms*” in fact the upper arm is shorter than the lower one to allow a camber gain in the curve phase.

The double wishbone suspensions can be divided into two equivalent suspensions types from the kinematic point of view: *Push-rod* configuration (*Figure 5*) and *Pull-rod* configuration (*Figure 6*). In the first case the rod, that thanks the rocker compress the shock absorber, is stressed to compression, instead in the pull-rod case is subject to traction. From a mechanical design point of view the choice of pull-rod configuration is better because allows to use a smaller thickness of the rod reducing the total weight. This is possible because the elastic instability problem is only present in compression.

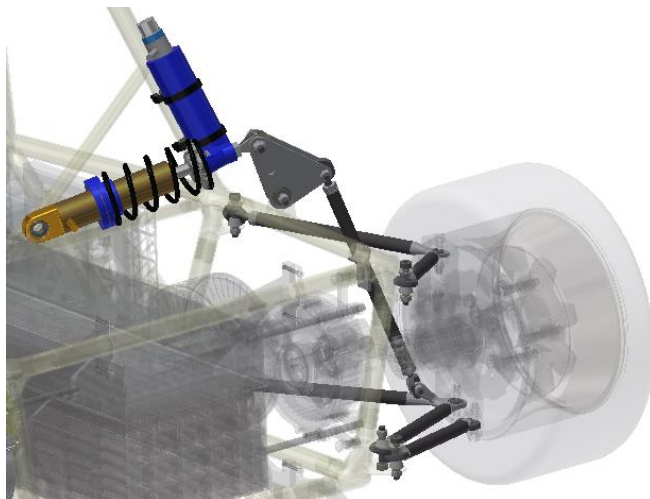


Figure 5 - Chimera rear push-rod configuration

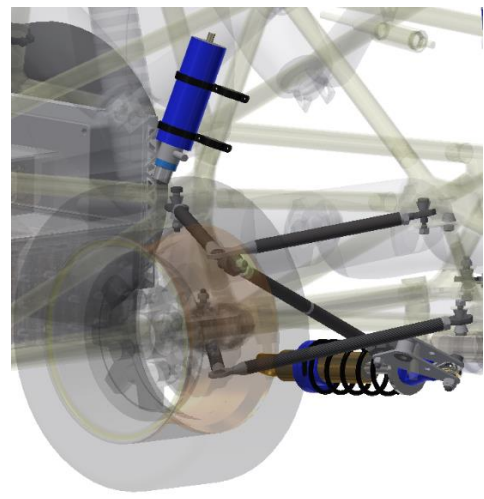


Figure 6 - Chimera front pull-rod configuration

3. Characteristic wheel angles

One of the goal of the vehicle design is to allow the maximum grip of the tires in all the possible cases. It permits to the wheels to exchange high loads with the ground allowing possible higher lateral and longitudinal accelerations. By optimizing the maximum grip a better vehicle results during the race in terms of lap times can be obtained.

This result is reached thanks the control of the wheel position during the suspensions travel. During the vehicle race in fact some characteristic angles as the *camber* or the *toe angle* have a greater influence on the tire grip and their optimal instant value is obtained with a controlled motion of the suspension.

The tire axis system adopted for vehicle dynamics and tire work is shown in *Figure 7*.

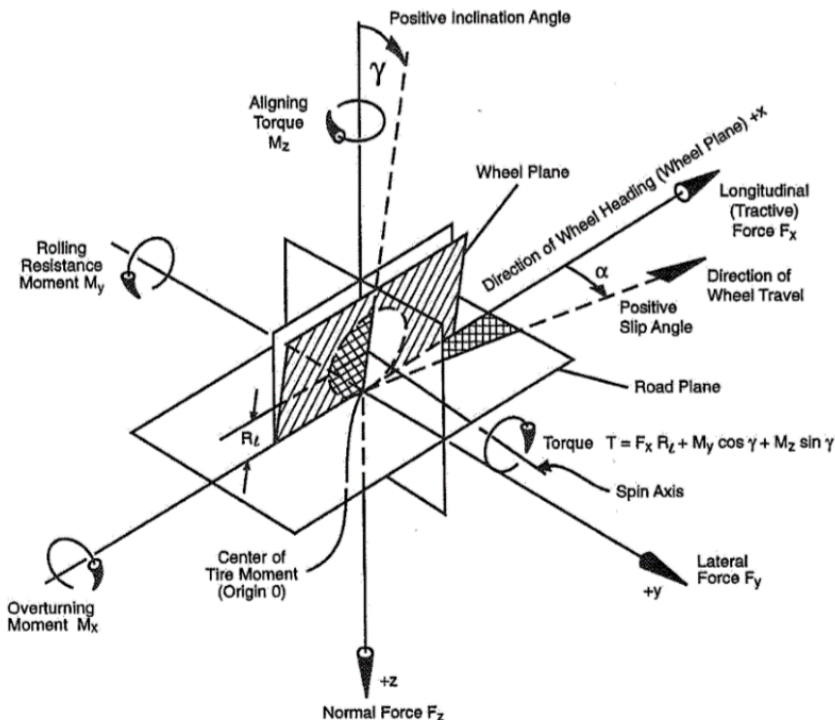


Figure 7 - SAE tire axis system
taken from: Milliken-Race Car Vehicle Dynamics (1997)

The axis system in *Figure 7*, from SAE J670, has its origin in the center of the tire footprint. The origin, O, is the intersection of the z axis with the road plane assumed to be a flat level. The x axis is at the intersection of the wheel plane with the road plane. The z axis is vertical and passes through O. The y axis is perpendicular to x and z and lies in the road plane.

In *Figure 7* is shown the wheel at a positive inclination angle γ and a positive slip angle α . The inclination angle is positive if the wheel is tilted to the right when viewed from behind the rolling tire.

The *camber angle* Φ , according to SAE terminology of *Figure 7*, is defined as the angle between a tilted wheel plane and the vertical one. It is defined positive if the wheel leans outward at the top relative to the vehicle, or negative if it leans inward. It should be also noted that for the front and rear left tire, the camber angle is opposite to the inclination angle γ . For the front and rear right tire, it has the same sign. A negative camber can be seen in *Figure 8*.

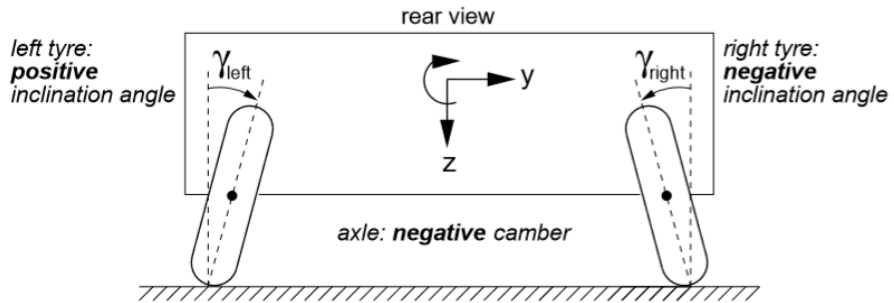


Figure 8 - Negative camber
taken from: Eindhoven University of Technology Mechanical Engineering - Dynamics & Control
Dr. Ir. I.J.M. Besselink lecture notes 2015

A negative angle of camber can provide a higher handling quality when compared to positive camber one. In fact it improves the grip for the outer wheel while cornering maximizing its contact patch area. During cornering the load transfer occurs from the inner wheel to the outer wheel that is much more important for handling when compared to inner one. The maximum lateral force on the outer wheel is increased since the outer tire is placed at a more optimal angle to the road with a negative camber during cornering.

In other words, the fact that the inside edge of the contact patch of the outer wheel will begin to lift during severe cornering due to the body roll will be minimized for outer tire by implementing a negative camber angle.

However, negative camber results in an adverse effect on the inner tire. The lateral force will be reduced, which is not significant due to the load transfer to outer wheel. On the other hand, when the maximum straight-line acceleration and braking is considered, the greatest longitudinal force is obtained with zero camber angle, since in this situation there is no body roll. As a result, tire will not experience the lifting effect due to body roll and the highest grip for the tire is obtained when the camber angle is zero.

The *toe angle* instead is the angle of the two front wheels or two rear wheels relative to each other when the vehicle is viewed from a top view. If the front of the wheels points inward towards the car so that the front of the wheels is closer together than the back of the wheels then the wheels are in the toe-in position. Instead the wheels are in the toe-out position when the front of the wheels points away from the car so that the front of the wheels is further apart than the back of the wheels. A toe-in is shown in *Figure 9*.



Figure 9 - Top view: toe-in
taken from: Eindhoven University of Technology Mechanical Engineering - Dynamics & Control
Dr. Ir. I.J.M. Besseling lecture notes 2015

A small amount of static toe-in is generally used to eliminate free-play in the suspension.

Toe angle also has an influence on the handling behaviour of a car on corner entry. It is harder for a vehicle to turn into a corner with more toe-in on a pair of wheels. Conversely, the more toe-out on a pair of wheels, the easier the vehicle will turn into a corner. This phenomenon can be explained by the fact that the radii of the arc of the inner and outer tires, which are traced during cornering, determine the easiness of the corner entry. For a pair of wheel with toe out, the inner tire will have a smaller radius of arc than the outer tire has. This provides easiness in corner entry. However, for a pair of wheel with toe-in, the inner tire will have a larger radius of arc than the outer tire has. In this situation, it is difficult to make the car turn since the inner tire is moving against the outer tire. When the car is already in a turn, weight transfers to the outer tire and the effect of the inner tire is reduced. Due to this load transfer, toe mainly affects corner entry.

Moreover, the understeer behaviour of the vehicle is affected by the toe-angle (*Figure 10 – Figure 11*). When the amount of toe-in is increased on a pair of wheels, the lateral force during cornering is also increased. If the lateral forces on the rear wheels are increased, the vehicle will have an understeer tendency, which means the stability is increased. Therefore, more toe-in on the rear wheels will result in a higher understeer tendency of the vehicle. Conversely, more toe-out on the rear wheels will result in less understeer tendency.

With a toe angle some lateral forces will occur during acceleration and braking. For braking and acceleration, it is important to have the highest possible longitudinal force but it is important to notice that more the lateral forces are high more the longitudinal ones that can be obtained are small.

Furthermore, toe increases tire wear since the tires are moving against each other and scrubbing over the ground. The outside edges of the tires will be deformed with toe-in and toe-out tends to increase tire wear on the inside edges of the tires. Therefore, if a negative camber angle is used on the wheels which causes the inside of the tires to wear more than normal, the implementation of toe-out to these wheels should be considered carefully since the combination of excessive negative camber and toe-out can quickly wear the inside of the tire.

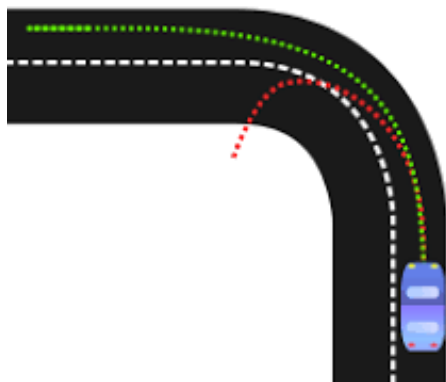


Figure 10 - Oversteer behaviour

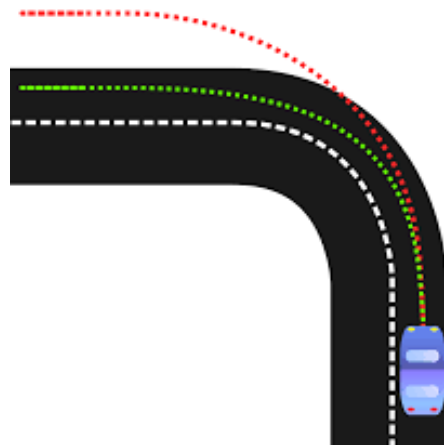


Figure 11 - Understeer behaviour

Retrieved January 20, 2018, from https://en.wikipedia.org/wiki/Understeer_and_oversteer

4. Characteristic parameters and their influence on vehicle dynamics

The biggest challenge for a designer is to establish the packaging parameters that once fixed cannot be changed and they determine the performance of the whole vehicle. To fix the kinematic characteristic of the suspension, the kingpin axis that affects the above characteristic wheel's angles, the centers of velocities and the passive system as the anti-dive, anti-lift and anti-squat must be defined.

4.1 Kingpin axis

By fixing the kinematic points of the suspension it is fixed the axis around which the wheel steers. Around this axis, called “*kingpin*”, act the forces that will be perceived by the driver.

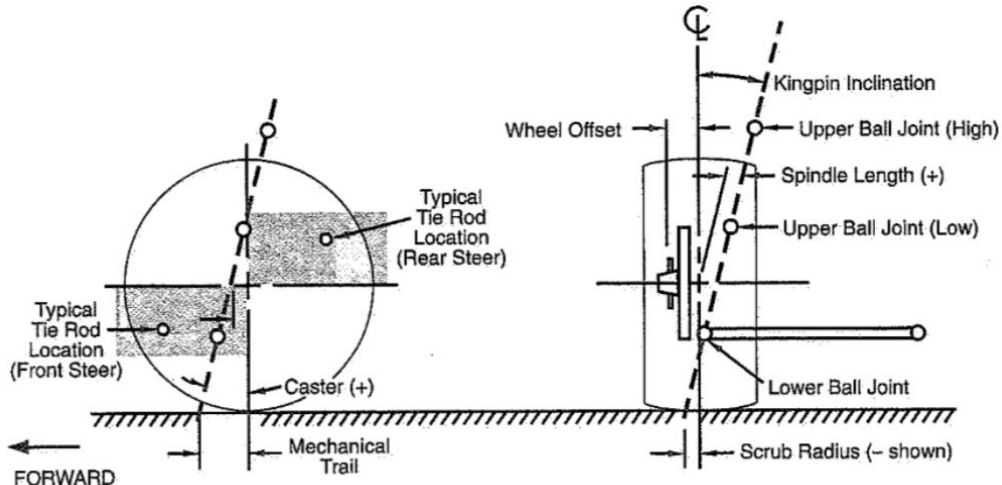


Figure 12 - Front suspension packaging
taken from: Milliken-Race Car Vehicle Dynamics (1997)

This axis is characterized by some geometric parameters that affect the performance of the car and what the driver feels.

The main parameters that are reported in *Figure 12* are:

- **Mechanical trail:** In lateral view is the distance between the intersection of the steering axis with the ground and the point of wheel contact. By convention it is positive when the point of the steering axis falls in front of the contact point as shown in *Figure 12*. The relevance of this parameter is clear in the vehicle while cornering: in this case the lateral force, that for simplicity is placed at the center of the wheel footprint, makes a moment that tends to realign the wheel if the mechanical trail is positive. This effect is called self-alignment and means that once the driver steers he feels an opposite force on the steering wheel to this perturbation. However, having positive mechanical trail values

too high is not good because otherwise the resistant moment generated is too big. Instead with a negative mechanical trail value any external perturbation that caused the wheel to turn around the steering axis would be automatically amplified, thus making the vehicle unstable. If the trail was null, the steering behaviour would be neutral (no self-alignment or misalignment). This situation would not be acceptable for the stability of the vehicle in a straight line.

- **Scrub radius:** it is the equivalent of the mechanical trail in the front view and it is conventionally positive when the point relating to the extension of the steering axis is inside the vehicle track. In *Figure 12* is shown its negative value. If the longitudinal forces are the same on the left and right tire, the moment governed by these around the steering axis is balanced, but there are cases in which the forces are different. It is the case when for example there is an unbalanced braking or traction, or there is a lack of grip of one of the two front or rear wheels. During these possible cases the vehicle will tend to maintain the direction, in fact the car's skidding in one direction will be contrasted by a greater moment on the steering in the opposite direction. It's better to have a small negative value of radius scrub to reduce the torque required to steer.

The values of the mechanical trail and the scrub radius can change while the suspension moves but it is necessary that not change their sign. If this happens the driver can have some difficulties to predict the change in behaviour of the vehicles.

In lateral view the necessity to have a positive mechanical trail it makes that the relative *caster angle* is positive. It is the angle between the kingpin axis and the perpendicular axis to the wheel that passes through the contact point with the ground. By convention it is positive when the axis parallel to the kingpin through the wheel center produced a positive mechanical trail. The caster angle produced an effect called pumping effect. This is a kinematic effect due to the fact that, if the suspensions and the chassis are considered fixed, when the wheel turns the distance between the contact point and the ground it is not constant. It cannot happen that there is an interpenetration or detachment between the tire and the ground, so the chassis is lowered or raised creating a pumping effect. The solution to have the same mechanical trail value but reducing the caster angle value is to introduce a *spindle length* in the side view. It is the distance between the center wheel and the kingpin axis. Its value is positive if the center wheel is behind the kingpin axis. It influences the sliding of the tire contact point with the ground during the steering and therefore the wear of the tire and the force necessary to steer in steady state.

The same considerations made for the caster angle and the kingpin offset can be done for the *kingpin inclination* and the *spindle length* in the front view. These two parameters characterized the scrub radius value. The *kingpin inclination* is positive when the kingpin axis is inclined

towards the inside of the vehicle. The *spindle length* instead is negative if the center wheel lies outside the kingpin axis with respect to the vehicle.

The importance of the *caster angle* and the *kingpin inclination* is more important for the front suspensions where there is a steering system. Instead in the rear suspensions where there is not the steering system the *spindle length* and the *spindle length* have more importance.

Furthermore, in the choice of values attributed to these parameters, the geometric constraints must always be considered. For example, the joints of the arms must be inside the wheel rim that for the regulation cannot be more than 13" or must be consider the space already occupied by the braking systems or wheel hub (Appendix C).

4.2 Centers of velocities

A study related to the position and the movement of the centers of instantaneous rotation is necessary to evaluate the position of the wheel during the suspension travel.

As the linkage is moved, the center moves, so proper geometric design not only establishes all the instant centers in their desired position at ride height, but also controls how fast and in what direction they move with suspension travel.

The real suspensions motion is defined in the space therefore speaking of centers of velocities would be wrong. A three-dimensional treatment, however, would be difficult to interpret so it is convenient to break down this three-dimensional problem into two, two-dimensional problems. It is possible with a projection of the suspensions points on the frontal and lateral plane.

The word "instant" means that the measure is about a particular position of the linkage. "Center" instead refers to a projected imaginary point that is effectively the pivot point of the linkage at that instant.

By projecting the suspension geometry in the front view the center of instantaneous rotation can be found by graphics through the intersection of the two suspension arms extensions (*Figure 13*).

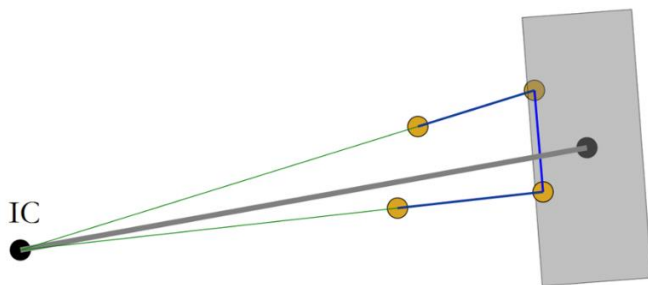


Figure 13 - Center of instantaneous rotation geometry construction

Figure 13 suggests how two short links can be replaced with one longer one.

It is possible thanks the *Chasles's theorem*: “if $\omega \neq 0$, the center C is on the normal line to the trajectory of any point P of the representative plane p , drawn through P ” (Figure 14). Chasles's theorem implies that C is geometrically determined by the trajectories of any two points P_1 and P_2 of the representative plane p . The normal lines to these trajectories drawn through $P_1(t)$ and $P_2(t)$ intersect at $C(t)$. If $\omega(t) = 0$, the center of instantaneous rotation $C(t)$ is not defined (where vector ω is the angular velocity). If ω is identically zero, the motion is a translation and the trajectories of any two points are parallel lined. In such a case C might be defined as the point at infinity of the normal bundle of such parallel lines.

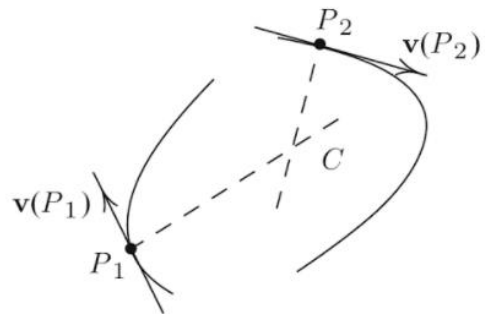


Figure 14 - Chasles's theorem
taken from: DiBenedetto – Classical Mechanics – Theory and Mathematical Modeling (2011)

The same thing done for the front view can be done for the side view by projecting the points of the suspension in this view. Once the arms are extended they will intersect in another center of instantaneous rotation in this view.

In the three-dimensional space the two instant centers are replaced by instant axes connected them together. This line shown in Figure 15 can be thought of as the instant axis of motion of the knuckle relative to the body.

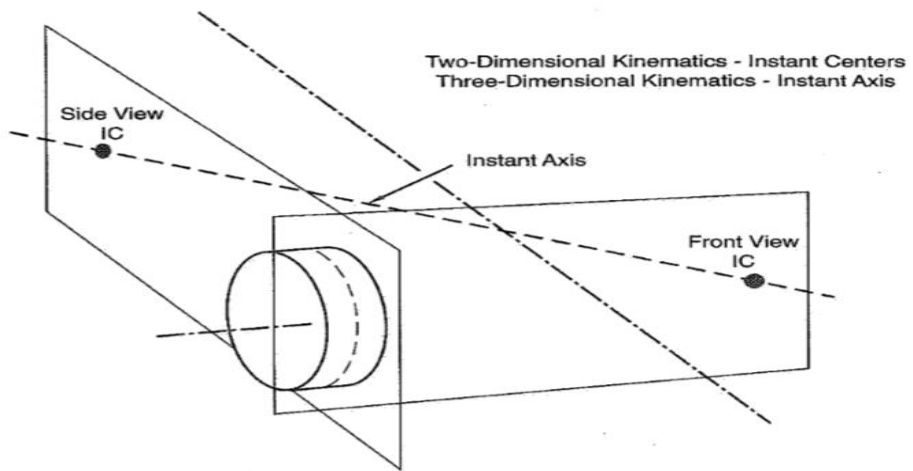


Figure 15 - Instant Axis
taken from: Milliken-Race Car Vehicle Dynamics (1997)

With these two centers of instantaneous rotation the properties of a particular suspension design are established. The positions of these instantaneous centers of rotation influence the kinematics

and dynamics of the suspension. The one in the front view is predominantly related to the wheel when it is subjected to lateral accelerations; while the second, in the lateral view, is predominantly in the case of longitudinal accelerations or decelerations.

4.2.1 Front view

The instant center in the front view defines the roll center height, the camber change rate, scrub motion and data needed to determine the steer characteristics.

The **roll center** is the point around which the chassis rotates in the front views.

Arnold Kennedy theorem of three centers states that “*if three bodies have plane motion relative to one another, then there are three instant centers, and the three instant centers all lie on the same line*”.

This theorem is exploited for the construction of the roll center. Considering the center of instantaneous rotation of the suspension found before in front view and the contact point of the wheel with the ground, the roll center must pass through the line that joins these two points. Repeating this procedure for the opposite side of the car can be found the roll center point as the intersection between the two lines (*Figure 16*).

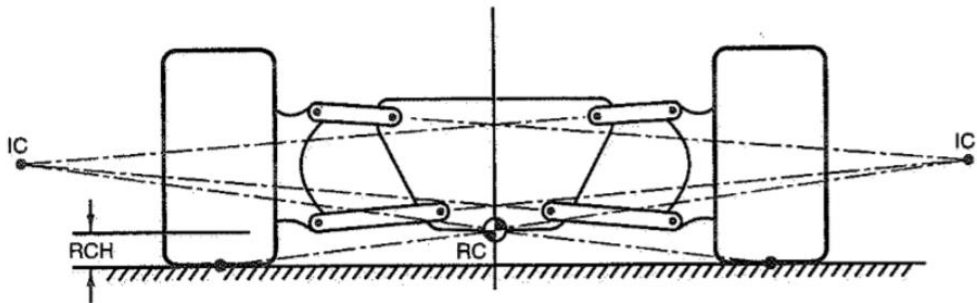


*Figure 16 - Roll center construction
taken from: Milliken-Race Car Vehicle Dynamics (1997)*

Usually the roll position is not exactly in the centerline of the car especially if the suspension geometry is asymmetric or once the car assumes a roll angle in a turn.

The roll center establishes the point at which the force coupling is calculated between the unsprung and sprung masses. When a car corners, the centrifugal force that acts at the center of gravity takes a moment with respect to the roll center. The higher the roll center the smaller the rolling moment about the roll center which must be resisted by the springs; the lower the roll center the larger the rolling moment. If the roll center is in the center of gravity the forces due to the load transfer pass through the suspension arms and there is not the roll car due to the compression of the shock absorbers. For this reason, usually, it takes the name of nonrolling center.

In other words, through an higher roll center (i.e. closer to the center of gravity) a lower roll is observed with the same stiffness.

Another factor to keep in mind associated to the eight of the roll center is the *Jacking moment* (*Figure 17*). If the roll center is above the ground level the lateral force on the tire generates a moment about the instant center. This moment pushes the wheel down and lifts the sprung mass. Instead if the roll center is below the ground level the force will push the sprung mass down.

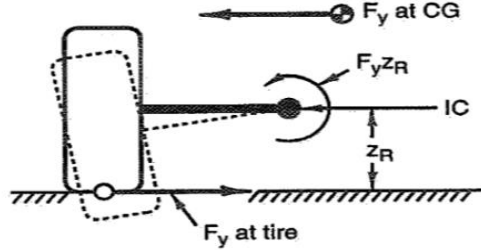


*Figure 17 - Jacking effect with a high roll center
taken from: Milliken-Race Car Vehicle Dynamics (1997)*

The position of the instant center on the horizontal axis, that connects it and the upright, determines the *camber change rate*. The amount of the camber change respect to the wheel travel, assuming to have the instant center fixed, is described by the following equation:

$$\gamma = \arctan\left(\frac{1}{D}\right) \left[\frac{\text{deg}}{\text{m}}\right]$$

where D is the distance between the instant center and the upright on the horizontal axis and more D is short more the camber gain is large (*Figure 18*).

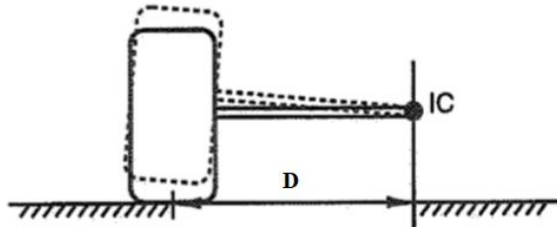


*Figure 18 - Geometrical representation of the Camber change rate
taken from: Milliken-Race Car Vehicle Dynamics (1997)*

The absolute height from ground of the front view instant center and the swing arm length control also the *tire scrub*. This is the lateral motion relative to the ground that results from vertical travel of the wheels.

As can be seen from *Figure 19* if the instant center is above ground and inboard, the tire will move outward as it rises; if it is below ground level and inboard, the tire will move inward with jounce travel.

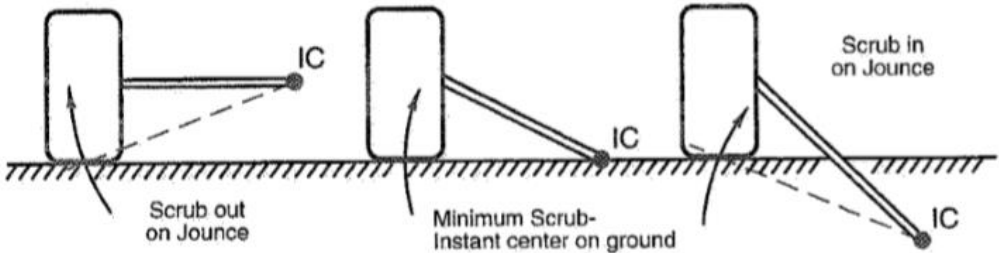


Figure 19 - Scrub respect to IC height
taken from: Milliken-Race Car Vehicle Dynamics (1997)

4.2.2 Side view

The instant center in the side view instead defines in the race cars mainly the anti-lift and anti-dive/squat information.

The position of the center of instantaneous rotation in this view is important to define the **pitch** of the vehicle.

In particular it is possible to obtain the anti-dive, anti-lift and anti-squat characteristics expressed in percentage terms. These properties determine respectively the sinking of the front and the raising of the rear car in case of braking or the sinking of the rear in case of acceleration. Suspension “anti’s” do not change the steady-state load transfer at the tire patch but they determine how much of the total force compresses the springs and how much stressed the arms. If a suspension has 100% anti, all the longitudinal load transfer is carried by the control arms that will be strongly stressed and none by the suspension springs, so the suspension does not deflect when braking or accelerating. If a suspension has 0% anti, then all the load transfer is reacted by the springs and the suspension will deflect proportional to the wheel rate.

The *Squat* is the dipping of a car's rear end that occurs due to the load transfer from the front to the rear suspensions during acceleration. Anti-squat in rear suspensions reduced the bump travel during forward acceleration on rear-wheel-drive cars only.

Instead the *Dive* is the dipping of a car's front end that occurs due to the load transfer from the rear to the front suspensions during braking. Anti-dive geometry in front suspensions reduces the bump deflection under forward braking.

Anti-lift instead can be found in front or rear suspensions. In the front suspensions occurs with front-wheel drive and it reduces the suspension droop deflection under forward acceleration. In the second case, rear suspensions, it reduces droop travel in forward braking.

To calculate these characteristics are used the following equations:

$$\% \text{Anti dive} = \frac{\tan \varphi_F}{h/l} * 100$$

$$\% \text{Anti squat} = \frac{\tan \varphi_R}{h/l} * 100$$

$$\%Anti\ lift = \frac{\tan \varphi}{h/l} * 100$$

The geometric meaning of the above equations is shown in *Figure 20*.

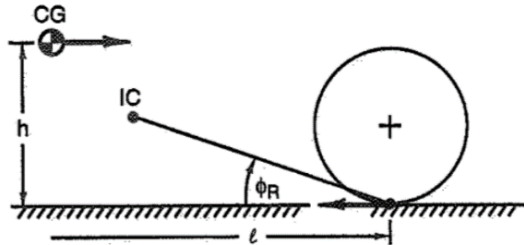


*Figure 20 - Calculation of the anti-squat percentage
taken from: Milliken-Race Car Vehicle Dynamics (1997)*

where φ is the angle between the side view instantaneous center of velocity and the contact point of the wheel with the ground (φ_R for the rear car and φ_F for the front car). The distance between the center of gravity and the wheel contact point with the ground is defined for the horizontal axis by the parameter “ l ” and for the vertical axis by the parameter “ h ” (*Figure 20*).

Each “anti” effect described above is assumed to be positive so it always working in such a way that the pitch deflections of the whole car would be reduced.

5. I OPTIMIZATION:

Camber and toe optimized curves using the “g-g” diagram

The characteristics required by the suspension generally come from the study of the dynamic behaviour of the vehicle and the analysis of the intrinsic characteristics of the tires.

In fact, from the tires data (*Pacejka coefficients*) and the vehicle dynamics equations it is possible to obtain what is called “*g-g*” diagram. It is a graph that shows all the states reachable from the vehicle in terms of longitudinal and lateral acceleration.

Through the various information obtained from the optimization of the “*g-g*” diagram it is possible to extract the specific one about the optimal behavior of the suspension.

5.1 Dynamic vehicle model

It is necessary to introduce the vehicle model to study the dynamic behaviour of the vehicle. Its dynamic equations are then used as closing equations during the “*g-g*” diagram optimization.

The dynamic model of the vehicle is based on the *roll axis vehicle model* (*Figure 21*).

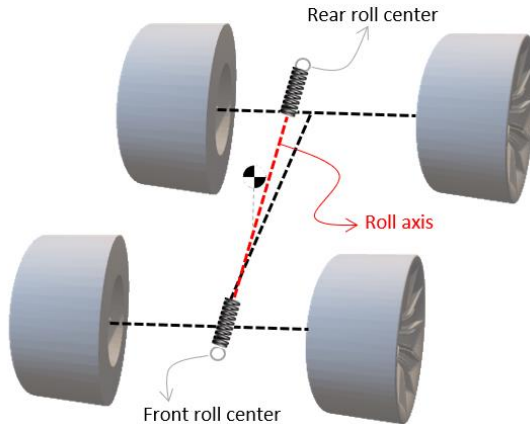


Figure 21 - Roll axis model

In the model of *Figure 21* the suspensions’ behaviour is simplified by introducing an axis that crosses the rear and the front roll center of the vehicle: the sprung mass is free to rotate around this axis called roll axis.

In each roll centers is positioned a torsion damped springs that simulates the opposition moment to the roll created by the combination of the left and right suspension and anti-roll bar (ARB) on the single axle.

In this model the pitching dynamics is not considered so the load transfer between front and back of the car is immediate.

5.1.1 Dynamic model equations

The dynamic equations of the model are the same used for the optimal control of the car that have been written previously by a FSAE colleague *Edoardo Pagot*.

The equations are written in Maple that is a symbolic and numeric computing environment that allows to write and manipulate them quickly. It is used also the MBSymba package to further simplify the process. MBSymba is a collection of methods and procedures for the automatic generation of the equations of motion of multibody systems.

The degrees of freedom of the system are the following:

- spin of the four tires masses;
- rotation around the z axis of the front wheels (steering);
- translation along the x and y axis and the rotation around the z axis (yaw) of the total mass of the vehicle;
- rotation of the sprung mass around the roll axis.

A sign convention used for the model is provided in *Figure 22* which is based on the international norm ISO 8855.

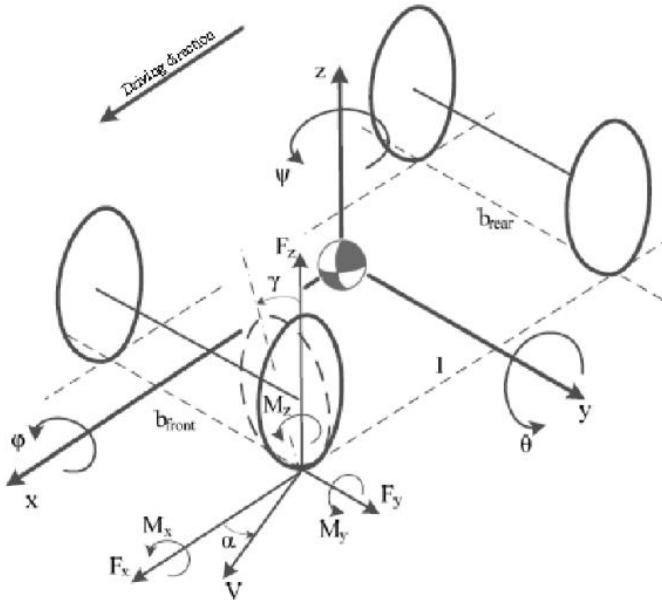


*Figure 22 - Sign convention
taken from: ISO 8855 Vocabulary*

As can be seen in *Figure 22* the z axis exits from the plane in the vehicle top view.

Finally, the dynamic equations are five:

1. Newton equation along the x axis.
2. Newton equation along the y axis.
3. Euler equation around the z axis.
4. Euler equation around the roll axis.

5. Equation to reduce the ODE system from the second to the first order. In the Euler equation around the roll axis in fact there are the second and the first derivative of the roll angle. To reduce the derivative order, it is necessary to introduce the variable of the roll velocity.

The starting multibody model then has been manipulated and expanded to generate the complete set of dynamic equations necessary for a complete and more realistic simulation of the vehicle behaviour.

5.1.2 Dynamics of vertical forces

In the dynamic equations there is not the Newton equation along the z axis. The *vertical loads* are calculated with the equilibrium equation between the reaction forces of the ground and the contributions related to the static load and the load transfer, which value can be defined by $F_{zSteadyState}$.

In fact the vertical force discharged to the ground has its own dynamics due to the elasticity of the tires and suspensions. However, this dynamic can be reduced to the first order because the aim of the shock absorbers is to avoid oscillations of the vertical load on the tires.

This implementation makes the simulation closer to the reality. Moreover it is also necessary to eliminate the algebraic loop between vertical loads on the tires and forces generated by the tires: one is a function of the others and vice versa.

The algebraic loop is iteratively solved by the Matlab *ODE Solver*, but it could generate problems and delays.

The equation for each of the four vertical forces is given by:

$$\tau_{F_z} \frac{dF_z}{dt} + F_z = F_{zSteadyState}$$

where τ_{F_z} is a constant.

5.1.3 Dynamics of tire drift angles

The tire drift angles are calculated from the multibody model according to the classic *Pacejka* definition.

The nonlinear characteristics of the tire forces are described by *Magic Formula* and they are better explained in Appendix A.

The curves generated by the *Magic Formula*, however, represent the values of the steady-state tire forces, so it is necessary to define the tire dynamics. It can be implemented through the formulation of the *Relaxation Length* of the tires. Relaxation length is a property of pneumatic tires that describes the delay between when a slip angle is introduced and when the cornering force reaches its steady-state value. The dynamics of tire forces is implemented only for lateral forces (side slip α) and not for the longitudinal slip k .

For each tire the following relation can be written:

$$\tau_\alpha \frac{d\alpha}{dt} + \alpha = \alpha_{SteadyState}$$

5.1.4 Steering dynamics

A dynamic of the first order governs the relationship between the steering required to do the corner and the one that is actually applied to the wheels. This dynamic derives from the fact that a "human" driver cannot start a steering input with a frequency higher than 1Hz. Therefore the equation acts as a low-pass filter of the steering inputs with the following expression:

$$\tau_\delta \frac{d\delta}{dt} + \delta = \delta_{Control}$$

Moreover the steering geometry is based on the articulated quadrilateral system known as *Ackerman quadrilateral*.

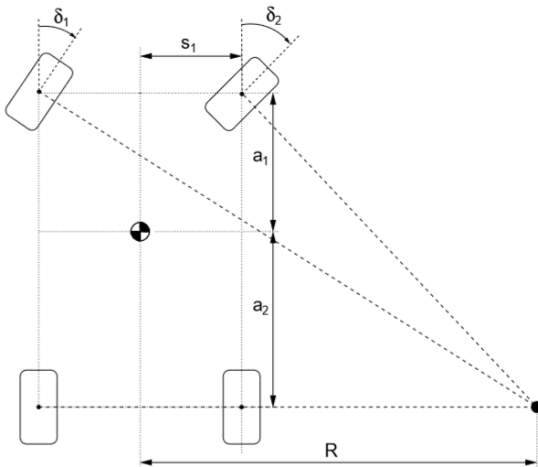


Figure 23 - Ackerman steering (chassis - top view)
taken from: Vehicle dynamics - Lecture notes 2015, Eindhoven University of Technology

The Ackerman steering equations are:

$$\tan \delta = \frac{a_1 + a_2}{R} ; \quad \tan \delta_1 = \frac{a_1 + a_2}{R + s_1} ; \quad \tan \delta_2 = \frac{a_1 + a_2}{R - s_1}$$

where $a_1 + a_2$ is the length of the wheelbase, s_1 is the half vehicle track, R the radius of curvature, δ_1 is the angle of the outer wheel and δ_2 the angle of the inside wheel respect to the curve.

5.1.5 Wheel dynamics (spin)

It has been said that the wheels can rotate around their axis y (spin) as rigid bodies. The Euler equations of each wheel around the y-axis are essential to calculate their angular velocity and therefore the longitudinal slip of each wheel. It can be seen how the acceleration of a single wheel is given by the algebraic sum of the applied brake/motor torque “T” and by the torque deriving from the longitudinal force “F” generated by the tire (which is a function of the longitudinal slip).

The equation for each wheel is:

$$I_f \frac{d\omega}{dt} = -r_f F + T$$

with I_f rotational inertia of the wheel and r_f radius of the wheel.

The front wheels have a further degree of freedom connected to the rotation around the z axis (steering movement). This generates an additional equation of motion, but it is neglected. Moreover, all the dynamic contributions deriving from the acceleration and speed of the steering (inertial forces and centrifugal forces due to the steering acting on the vehicle) are negligible, so that the first and second derivative of the steering has been set to zero in the first five dynamic equations.

5.1.6 Final dynamic equations set

The final obtained set of equations describing the vehicle dynamics is composed of 18 equations:

- 1 – Newton equation along the x axis;
 - 1 – Newton equation along the y axis;
 - 1 – Euler equation around the z axis;
 - 1 – Euler equation around the roll axis;
 - 1 – Equation to reduce the ODE system from the second to the first order;
 - 4 – Dynamics of vertical forces
 - 4 – Dynamics of tire drift angles
 - 1 – Steering dynamics
 - 4 – Wheel dynamics (spin)
-

18 equations

5.1.7 Matlab environment

The model is then export in a Matlab software in a way to use the optimization packages available in this environment. MATLAB (matrix laboratory) is a multi-paradigm numerical computing environment.

To export the model from Maple to Matlab is necessary to rewrite the equations in the format used in Matlab.

The first step is to rewrite the equation in explicit form:

$$\dot{X}(t) = F(X(t), U(t), P) \quad (5.1)$$

where $X(t)$ are the system state variables, $U(t)$ the controls and P the parameters.

This can be done in Maple using the *LinearAlgebra [GenerateMatrix]* command, which allows to collect the mass matrix and thanks its inversion it is possible to reach the equation form (5.1).

The next step is to change the form $\text{VariableName}(t)$ to VariableName , compatible with Matlab. It is convenient to rename the states as $X_1..X_{n_x}$ with n_x the number of states and control variables such as $U_1..U_{n_u}$ with n_u the number of control variables. It is important to note that in the “g-g” diagram optimization there is not a real distinction between the states and control variables because they are all considered as the inputs to optimized regardless of their origin. So from now on with the same variable X are indicated both the states and the control variables.

Moreover, in Maple it is possible to collect a list of all the parameters present in the equations renaming them in the form $P_1..P_{n_p}$ with n_p the number of parameters. The parameters represent all the variables that aren't function of time.

The last step is to convert the Maple code to Matlab code using the *CodeGeneration[Matlab]* command. The code will be printed on the screen and it can be copied and pasted in Matlab.

The *Magic Formula* expressions of the lateral and longitudinal forces, also considering their combined effect, are implemented directly in the Matlab software substituting the name of the variables with these expressions.

The tire data used in this FSAE race car model are the Hoosier 18×6-10” compound R25B. FSAE Tire Test Consortium(TTC) was held to provide low-charge tire test data for all FSAE teams around the world. Thanks to FSAE TTC, the tire test data of Hoosier 18×6-10 R25B is obtained, and the detail of tire test can be seen in reference [5].

Furthermore, the self-alignment torque and overturning moment are neglected (*Figure 24*).

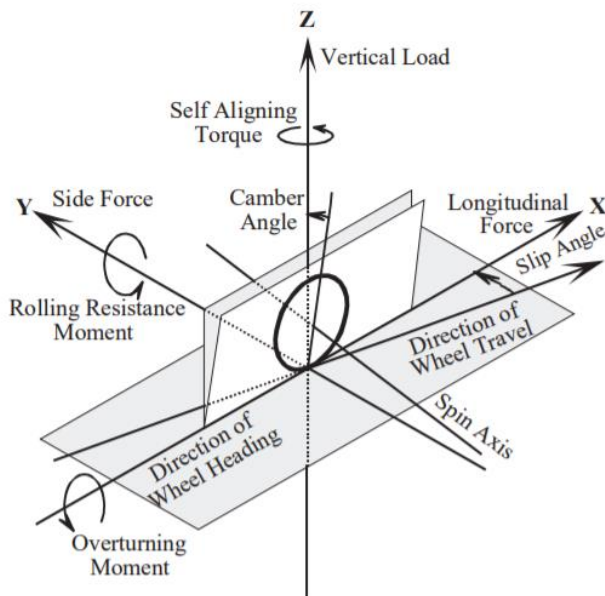


*Figure 24 - The tire coordinate system
taken from: Tire and Vehicle Dynamics (2012)*

The dynamic model also takes into consideration the *aerodynamic forces*: downforces, different from rear and front wheels, and the drag force (*Figure 25*). Aerodynamic forces, in fact, affect "g-g" maneuvering performance. The interaction of the aerodynamic and tire forces can have a large effect on lateral acceleration performance. For example, aerodynamic downforce (negative lift) increases the tire loads and this in turn increases the lateral force capability of the tires. Unlike the tire forces which are primarily independent of speed, the aerodynamic forces increase rapidly with speed. The equations for each of these aerodynamic forces are given by their relative coefficient multiplied by the squared speed.

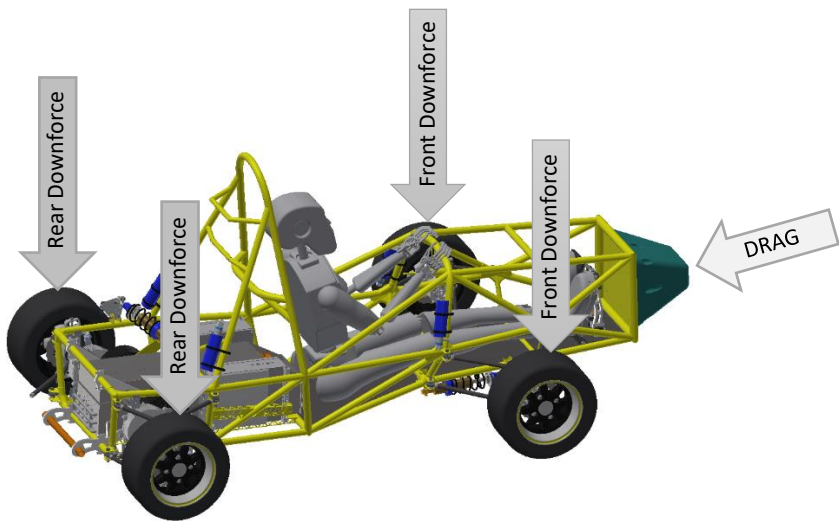


Figure 25 - Drag and downforces in dynamic model

5.2 The “g-g” diagram optimization

The “g-g” diagram defines the maximum performance of a vehicle in any combination of longitudinal and lateral acceleration. Its basic concept is to plot longitudinal versus lateral accelerations of a vehicle, scaled with respect to gravity.

The “g-g” diagrams are very used tools to find the physical limits of a vehicle also to characterize the racing driver's capabilities to push the vehicle to these limits.

The first published reference to the “g-g” diagram was in 1970. In a CAL Labs report it was suggested that the four tire friction circles could be collapsed into a single equivalent tire/road interface or ‘vehicle friction circle’. In fact, it is well known that the reason of this shape is due to the tire behaviour when combined longitudinal and lateral forces are present at the same time and the maximum values represent the tire lateral and longitudinal adherence or grip coefficients.

In general, the envelope of the maximum lateral and longitudinal accelerations is a sort of ellipse/circle that it is known as *ellipse of adherence*. Because the resultant force vector on a vehicle is simply the sum of the four resultant tire forces vectors the “g-g” diagram will look much like the friction circle for a single tire but with slight differences due to the longitudinal performance limits.

The main characteristic of the “g-g” curves is that they are curves of equilibrium. They are calculated from the *steady state* equations of the vehicle. The only equation that keeps its dynamics is the Newton equation along the x axis, whose state is therefore the longitudinal velocity of the vehicle and whose first derivative is the longitudinal acceleration. This is described in equations (5.2) and (5.3), where X_1 is the state associated to the longitudinal velocity.

$$\dot{X}_1(t) = F_1(X(t), P) \quad (5.2)$$

$$F_2(X(t), P) = 0 \\ \cdot \\ \vdots \\ F_{n_e}(X(t), P) = 0 \quad (5.3)$$

with n_e the total number of equations.

The only case in which the problem is really Steady State is when $a_x = 0$, ie the two points of the “g-g” diagram on the abscissa axis. In this case, in fact, all the equations are in the form:

$$F(X(t), P) = 0 \quad (5.4)$$

In the case where $a_x \neq 0$ the equations occur in the form (5.2) - (5.3) and are defined Quasi Steady State (QSS).

Any solution of the equations above (5.2)- (5.3) is an equilibrium point of the system. However, the goal of the “g-g” diagram is to find the points of maximum performance of the car, so an optimization is done.

The parameters P that remain constant during the optimization are thirty-three and represents by:

- ❖ P(1) = Drag coefficient (aerodynamic)
- ❖ P(2) = Down force coefficient front (aerodynamic)
- ❖ P(3) = Down force coefficient down (aerodynamic)
- ❖ P(4) = Front torsion spring damping
- ❖ P(5) = Rear torsion spring damping
- ❖ P(6) = Front spring stiffness
- ❖ P(7) = Rear spring stiffness
- ❖ P(8) = Center of gravity from distance from the front of vehicle
- ❖ P(9) = Center of gravity from distance from the rear of vehicle
- ❖ P(10) = Right wheel radius
- ❖ P(11) = Left wheel radius
- ❖ P(12) = Front track
- ❖ P(13) = Rear track
- ❖ P(14) = Gravity acceleration
- ❖ P(15) = Center of gravity height from ground
- ❖ P(16) = Rear center roll height
- ❖ P(17) = Front center roll height
- ❖ P(18) = Inertia I_{zz}
- ❖ P(19) = Inertia unsprung masses I_{xx}
- ❖ P(20) = Inertia unsprung masses I_{xz}
- ❖ P(21) = Inertia unsprung masses I_{yy}
- ❖ P(22) = Inertia unsprung masses I_{zz}
- ❖ P(23) = Inertia front wheel
- ❖ P(24) = Inertia rear wheel
- ❖ P(25) = Length tires longitudinal forces
- ❖ P(26) = Length tires lateral forces
- ❖ P(27) = Total mass
- ❖ P(28) = Mass front wheel
- ❖ P(29) = Mass rear wheel
- ❖ P(30) = Sprung mass
- ❖ P(31) = Reduction ratio steering wheel and wheel
- ❖ P(32) = Time constant steering wheel
- ❖ P(33) = Time constant vertical force

The state variables are forty and represents by:

- ❖ Lateral velocity
- ❖ Yaw velocity
- ❖ Roll angle
- ❖ Steering angle
- ❖ Side slip angle one for each wheel
- ❖ Longitudinal slip angle one for each wheel
- ❖ Vertical force for each wheel
- ❖ Roll acceleration
- ❖ Angular speed for each wheel
- ❖ Braking torque
- ❖ Engine torque
- ❖ Camber coefficients 3 for each wheel
- ❖ Toe coefficients 3 for each wheel

This optimization is obtained with a code implemented in Matlab program based on the 8DOF nonlinear dynamic model analysed at the beginning of this section. The equations obtained with this model are used as constraint equations to find the optimized “g-g” diagram.

In order to solve the optimization problem is used an open source software package for the solution of large scale non-linear optimization problems: **Ipopt** (InteriorPoint OPTimizer). It can be used to solve general nonlinear programming problems of the form:

$$\min_{x \in \mathbb{R}^n} f(x) \quad (5.5)$$

$$s.t. \quad g^L \leq g(x) \leq g^U \quad (5.6)$$

$$x^L \leq x \leq x^U \quad (5.7)$$

where $x \in \mathbb{R}^n$ are the optimization variables with lower and upper bounds, $x^L \in (\mathbb{R} \cup \{-\infty\})^n$ and $x^U \in (\mathbb{R} \cup \{+\infty\})^n$, $f: \mathbb{R}^n \rightarrow \mathbb{R}$ is the objective function, and $g: \mathbb{R}^n \rightarrow \mathbb{R}^m$ are the constraints. The functions $f(x)$ and $g(x)$ can be linear or nonlinear and convex or non-convex, but should be sufficiently smooth (at least once, ideally twice continuously differentiable). The constraints, $g(x)$, have lower and upper bounds, $g^L \in (\mathbb{R} \cup \{-\infty\})^m$ and $g^U \in (\mathbb{R} \cup \{+\infty\})^m$. Furthermore, the equality constraints of the form $g_i(x) = \bar{g}_i$ can be specified by setting $g_i^L = g_i^U = \bar{g}_i$.

Ipopt needs more information than just the problem formulation.

Matlab Syntax:

$$[x, info] = ipopt(x0, funcs, options)$$

where

$x0$ = initial guesses (one for each variables): the optimized problem solution is very sensitive to the choice of their values;

$funcs$ = it corresponds to objective and constraints functions with their Jacobian and Hessian functions;

$options$ = the mainly option is the one about the definition of the problem bounds (on variables and constraints).

In order to provide the information about the Jacobian and Hessian functions and their sparsity structure is used a useful Matlab toolbox for the symbolic differentiation: **ADiGator**.

ADiGator is an open source toolbox for the symbolic differentiation in Matlab.

Given a user defined function and a bunch of setup options, ADiGator generates a file containing the derivatives of the original functions. These functions are generated thanks the *adigatorGenFiles4Ipopt* function and They are then used as input for Ipopt.

A convenient by product of the file generation is the sparsity pattern of the derivative function. Moreover, as both the input and output to the algorithm are source codes, the algorithm may be applied recursively to generate derivatives of any order.

To explain how the “g-g” diagram optimized shape is found the one at a speed of 15 m/s (54 Km/h) is considered. It is used this velocity as example because it is the average speed of the vehicle for FSAE dynamic competition: autocross and endurance. (Appendix D).

The “g-g” diagram obtained after the optimizations is plotted in *Figure 26*.

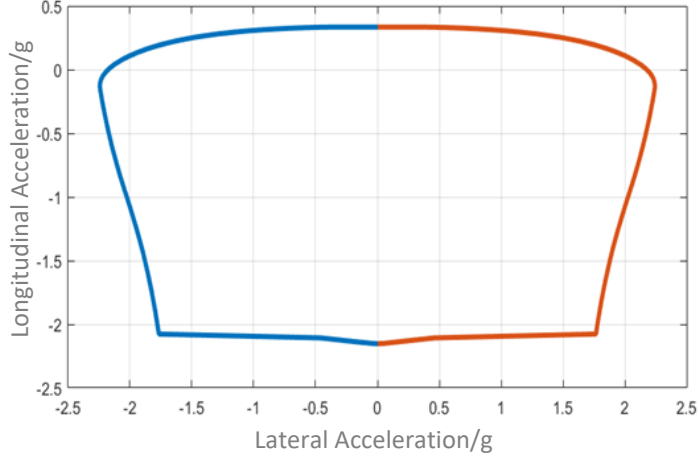


Figure 26 - The "g-g" diagram corresponds to the velocity of 15 [m/s]

It cannot be solved using a single optimization because in some points or areas a different objective function must be used to be able to make the problem converge. The optimization is done only for a half “g-g” diagram with negative lateral accelerations (*Figure 27*) and then it is mirrored with respect to the axis of longitudinal accelerations. It is possible because the race car is symmetrical along the longitudinal axis.

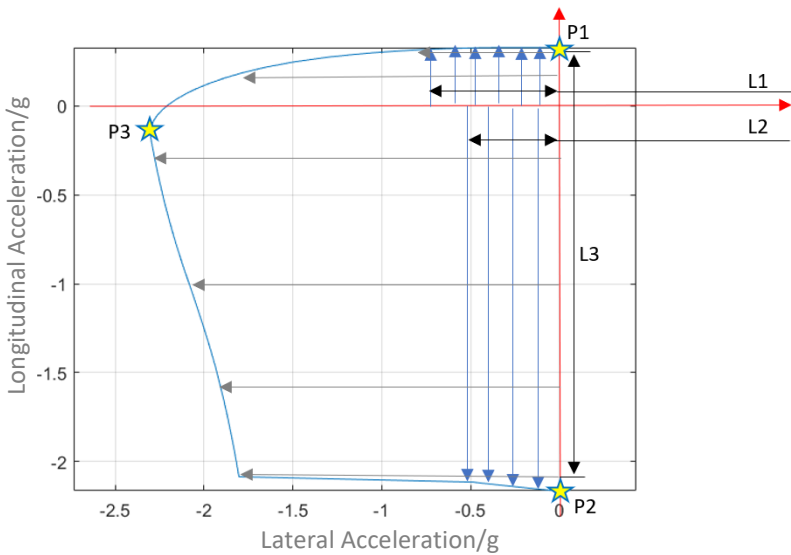


Figure 27 - Half "g-g" diagram optimization

where

P1 : Point of maximum longitudinal acceleration.

P2 : Point of minimum longitudinal acceleration.

P3 : Point of maximum lateral acceleration.

L1 : Length where is maximized the longitudinal accelerations.

L2 : Length where is minimized the longitudinal accelerations.

L3 : Length where is maximized the lateral accelerations.

In the sections below are described in detail how these points (P1,P2,P3) and the maximum acceleration values in the different areas (L1,L2,L3) are found.

5.2.1 Longitudinal acceleration and braking

The first boundaries to find are related to the performance envelope for straight-line operation: longitudinal acceleration and braking.

In the constraints to find these two optimized points is imposed that the yaw velocity (Ω) of the car is zero in order to consider only the longitudinal vehicle dynamic. The objective functions instead are related to the maximization and minimization of the longitudinal acceleration. Since Ipopt is a minimization software package the maximization is done by minimizing the negative value of the objective function.

To obtain the precise longitudinal acceleration the capacity of the motor traction force and the capacity of brake hydraulic system is taken into consideration.

5.2.1.1 Longitudinal acceleration

The optimal constrained problem has the following characteristics:

- objective function: longitudinal acceleration a_x , to be maximized (that is equal to the minimization of its negative value);
- constraints: equations of vehicle dynamics given by the Equations (5.2) - (5.3).

The key parameters affecting straight-line acceleration are engine torque, gear ratios, aerodynamic drag forces, and perhaps most importantly and relevant of all, the traction limit of the rear wheels.

The maximum acceleration that can be reached by the car is bounded by the traction limit or power limit. The approach used to define the longitudinal acceleration is first to consider the effect of the engine and gear ratio then to superimpose the effect of the traction limit and aerodynamic drag.

The configuration of the first Eagle's car, that is the same used in this optimization, is characterized by two rear motors (left wheel and right wheel). The motors used are the Emrax Motor 208 LC.

It is a brushless synchronus three phase AC high voltage motor liquid cooled.

The configuration of E-agle's kart allows the motor to have a maximum voltage of 302 V and a minimum voltage of 187 V; the resulting nominal voltage amount to 259 Vdc. The maximum power drawn by the battery is less than 80 kW and it is shared between the two rear motors.

The engine torque for each wheel couple has the results shows in *Figure 28*.

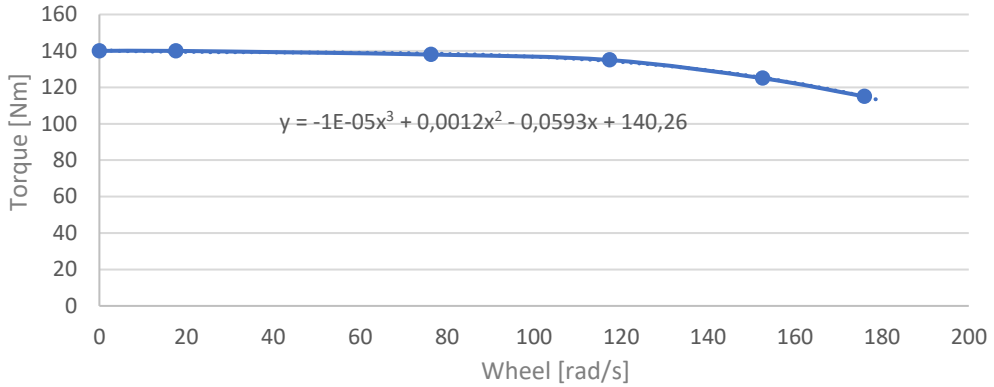


Figure 28 - Torque curve of Emrax 208 High Voltage CC

The gear ratio τ used in the above plot is 3,57 to find the resulting value to the wheels.

This is the maximum theoretical performance due to the engine. It will not be realised if the tires cannot transmit it to the road.

The traction limit is defined for rear-wheel-drive cars according to the *Pacejka* mathematical model.

Until the engine produces less force than the traction limit, the traction limit defines the maximum acceleration performance.

The other limiting factor is aerodynamic drag. The resultant force at each speed is found subtracting the drag force from the tractive force. Then if the force is divided by the mass of the car the resulting plot is the maximum acceleration versus velocity.

With the same objective function and constraints are found also the longitudinal maximum values near the maximum value with no lateral acceleration. Near the maximum longitudinal acceleration, the “g-g” diagram during the optimization may not converge. This is due the fact that near these points it assumes a flat shape that can generate problem during the optimization. These points are found by imposing the lateral acceleration values and maximizing the related maximum longitudinal acceleration (*Figure 29*). The discretization of these lateral accelerations points can be defined initially by the user. The final lateral acceleration value instead is found subtracting from the maximum longitudinal acceleration (with $a_x = 0$) a value of 0.5 [m/s²]. In the end a lateral optimization respect to this new point is done to find the related maximum lateral acceleration.

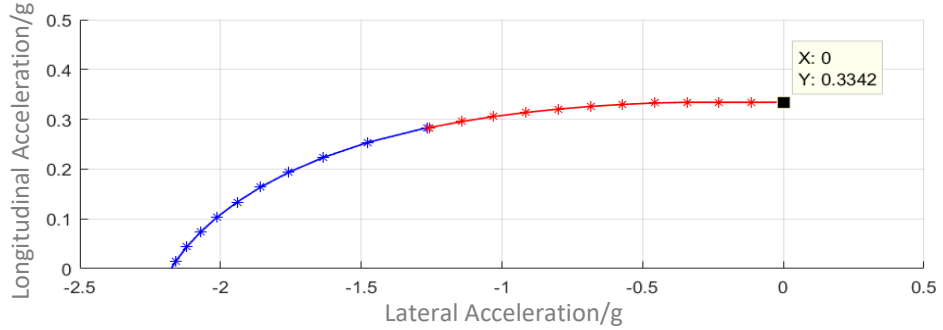


Figure 29 - Maximum longitudinal acceleration points

5.2.1.2 Braking

In case of braking the optimal constrained problem has the following characteristics:

- objective function: longitudinal acceleration a_x , to be minimized;
- constraints: equations of vehicle dynamics given by the Equations (5.2) - (5.3).

The minimum longitudinal value related to braking is more complicated to find because it is affected by all the four nonlinear tires models. There will be a theoretical value at zero velocity due to the static coefficient of friction and the static vehicle weight. The potential force will then increase parabolically due to aerodynamic drag adding to the friction force created by the tires.

A maximum braking torque limit for each tire is about 800 [N/m]. The tires can assume a value under this limit taken into account. Furthermore a braking balance coefficient is introduced to move forward the braking force respect to the rear of the car (≈ 0.75).

As seen for the longitudinal acceleration also in braking system the points near the minimum longitudinal braking are found with the same objective function and constraints of braking to guarantee the convergence (Figure 30). Also in this case the user can decide the interval of discretization.

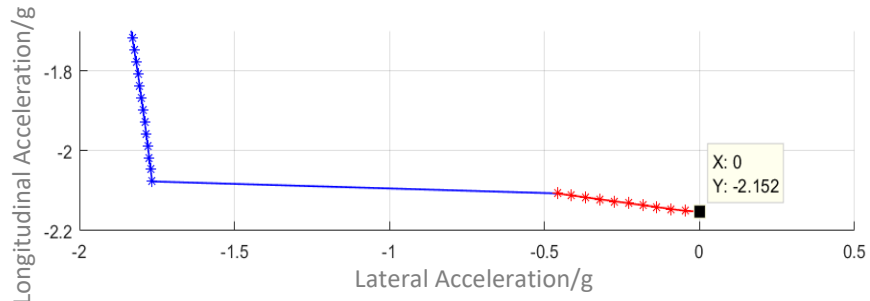


Figure 30 - Minimum longitudinal acceleration points

5.2.2 Lateral maximum acceleration

The next step is to find the optimized lateral accelerations for each possible longitudinal acceleration to complete the vehicle performance.

The longitudinal acceleration values are obtained dividing the interval between the points of maximum and minimum longitudinal acceleration where the upper and the lower optimization are arrived. The number of the divisions of equal length between these two points can be set by the user thanks to an initial interface.

The objective function is given by the following equation:

$$a_y = \Omega * u$$

where a_y is the lateral acceleration to minimize (because negative), Ω is the yaw velocity and u is the vehicle forward velocity that is the same for all the “g-g” diagram. In this case, taken as an example, the speed u is 15 [m/s].

It can happen that during the discretization of the longitudinal acceleration there is not the longitudinal acceleration value associated with the maximum absolute lateral acceleration point. So another optimization is done before to start the research of the optimized lateral acceleration points to find this longitudinal acceleration value. In conclusion it is added to the longitudinal acceleration discretized vector (*Figure 31*).

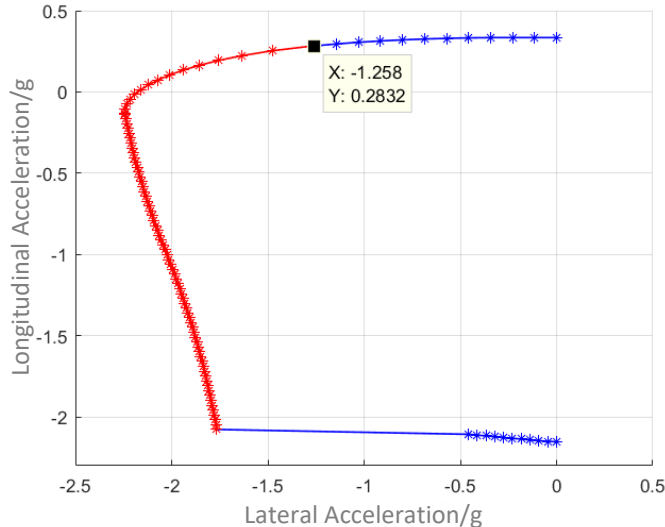


Figure 31 – Maximum lateral acceleration points

In all these optimizations, as initial guesses of the next step, the optimized solutions of the previous step are chosen. This allows to speed up the search of the optimized variables.

5.2.3 Considerations

Some considerations can be done about the final “g-g” diagram shape of *Figure 31*. The same things can be found also in other “g-g” diagrams at different velocities.

- The maximum lateral acceleration of the “g-g” diagram does not correspond to the longitudinal acceleration value of zero but to a lower value. It is due to the aerodynamic drag.
- During the optimization most of the time is taken to find the “g-g” diagram values about the point related to the maximum and minimum longitudinal acceleration and the one about the maximum lateral acceleration because the initial guesses are more general.
- The “g-g” diagram shape near the minimum longitudinal acceleration does not have a soft trend and it can be justified with the tires *ellipse of adherence* (APPENDIX A). It represents on a single graph forces that a tire can transmit to the ground for a given vertical load for all possible working points.

The one obtained with the tire Hoosier 18×6-10” compound R25B is shown in *Figure 32*. It is plotted only the first quadrant because in the others it is symmetrical.

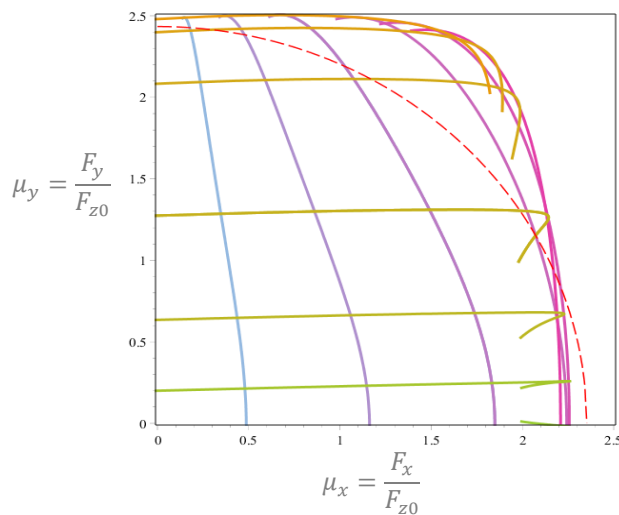


Figure 32 - Ellipse of adherence

The ellipse of adherence related to the tire used in *Figure 32* does not have a circular shape but is more squared. This shape is reflected in the final part of the “g-g” diagram’s shape near the minimum longitudinal acceleration.

- The time to find the optimized longitudinal acceleration values about the points near the maximum and minimum longitudinal acceleration are different in the case of acceleration and braking. This is due to the fact that in acceleration only the rear wheels are used. Instead during the braking there is the contribution of all the four dynamic nonlinear wheels models.

- The time to create a “g-g” diagram with the default parameters (*Figure 33*) to define the intervals of discretization for the lateral and longitudinal acceleration is about a minute and half.

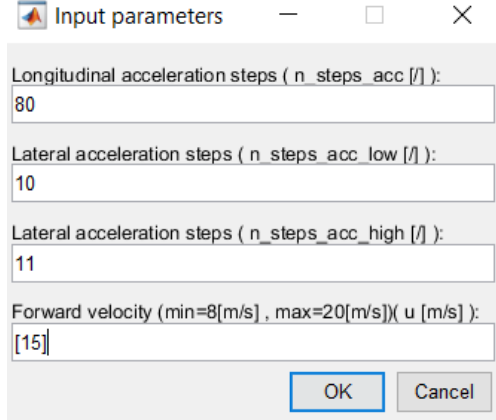


Figure 33 - Matlab user interface with default values

5.3 Camber and toe curves optimization

The lateral and longitudinal accelerations change with speed therefore by definition any “g-g” diagram is specific to one velocity. In *Figure 34* are plotted the optimized “g-g” diagrams for two velocities: 15 [m/s] and 20 [m/s]. The velocities taken into account are these two because during the dynamic FSAE test the average velocity are around 50-60 [km/h] (APPENDIX C).

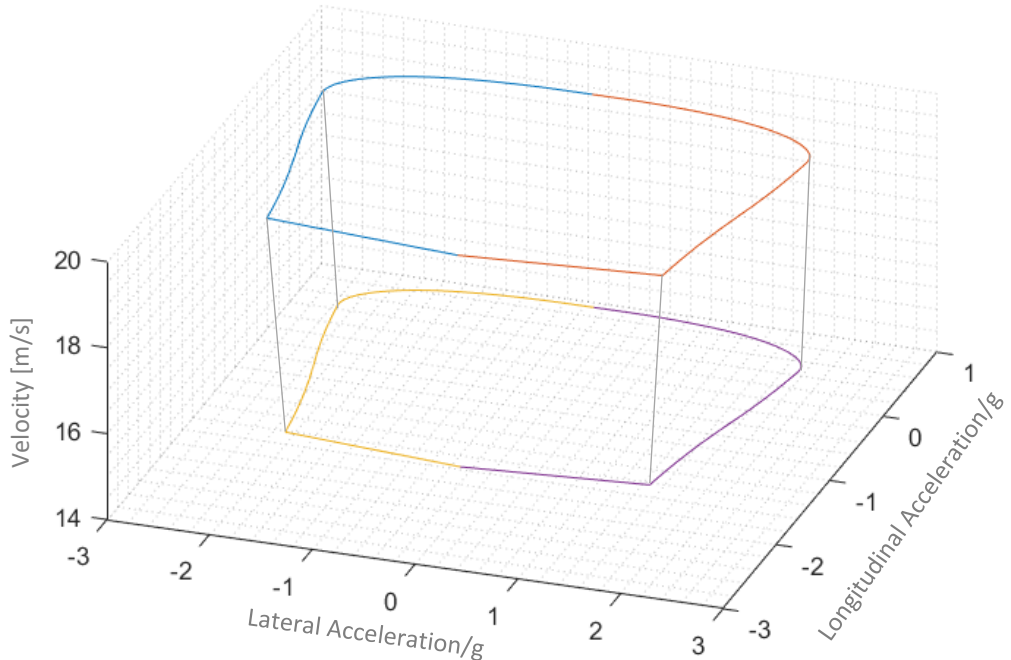


Figure 34 - Three-dimensional "g-g" diagrams at 15 [m/s] and 20 [m/s] velocity

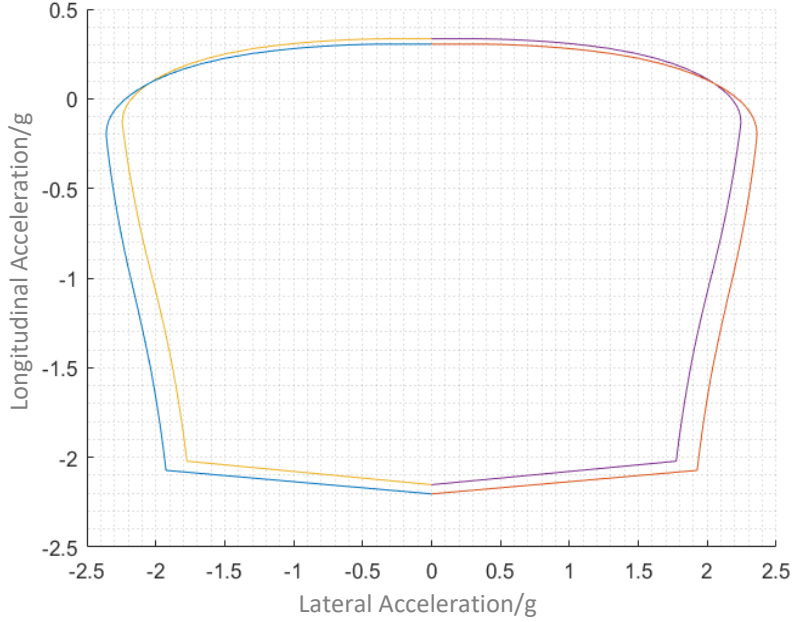


Figure 35 – Top view: "g-g" diagrams at 15 [m/s] and 20 [m/s] velocity

The top view of the above plot shows the increase in cornering and braking due to the increase in downforce and the decrease in acceleration as power limitations kick in with increasing speed (*Figure 35*).

Figure 35 shows that the difference in the "g-g" diagram changing the velocity it is not high. This is due to the fact that the vehicle speeds are low and so the difference it is not so relevant. Furthermore are considered only two velocities because decreasing the velocity under 15 [m/s] the difference in the "g-g" diagrams it is smaller. Using only two velocities the computational cost for the optimization is reduced.

A simplification is done during this optimization about the points near the lowest longitudinal acceleration. These points are simplified with a line between the lowest longitudinal point and the one found with an lateral optimization. The point with lateral acceleration is taken by rising 1 [m/s²] from the lowest longitudinal acceleration point to avoid the convergence problems. It is possible to do this simplification for the typical "g-g" diagrams flat shape in this area as explained in the previous considerations "g-g" diagram (*Figure 32*). It allows to reduce a lot the computational cost of the optimization without a relevant error.

Before we have seen how it is possible to find an optimized "g-g" diagram for different velocities. Another optimization that try to maximize the "g-g" diagram volume is done changing the camber and toe curves trend from the outside. By using the genetic algorithm this is done in Matlab environment.

5.3.1 Genetic algorithm

A **genetic algorithm** (ga) is a method for solving both constrained and unconstrained optimization problems based on a natural selection process that mimics biological evolution.

At each point on the “g-g” diagram corresponds a value of camber and toe that must be the same for every velocity because the suspension configuration remains the same.

A way can be to find each point of camber and toe on the “g-g” diagram and then interpolate them to find the curves. To overcome this step are optimized not each points but the coefficients of two second order equations: one equation for the camber and one for the toe.

These equations for the left rear group suspension are expressed as:

$$\text{Camber}_{rl} = \gamma_0_{c_{rl}} + \gamma_1_{c_{rl}} * \phi + \gamma_2_{c_{rl}} * \phi^2$$

$$\text{Toe}_{rl} = \gamma_0_{t_{rl}} + \gamma_1_{t_{rl}} * \phi + \gamma_2_{t_{rl}} * \phi^2$$

where $\gamma_0_{c_{rl}}, \gamma_1_{c_{rl}}, \gamma_2_{c_{rl}}$ are the coefficients of the camber equation and $\gamma_0_{t_{rl}}, \gamma_1_{t_{rl}}, \gamma_2_{t_{rl}}$ of the toe equation. The variable ϕ instead describes the vehicle roll and it is taken as the independent variable.

In the case of the right rear group suspension the equations are the same but reflected with respect to the axis of zero roll. This can be done because the vehicle is symmetric and the only suspension that respect the sign convention is the left one.

The lower and upper boundaries (*Table 1-Table 2*) of these coefficients are generated starting from the values of the *Chimera*’s vehicle model that are extracted thanks to the use of Maple software and then plotted in Matlab environment (*Figure 36 – Figure 37*).

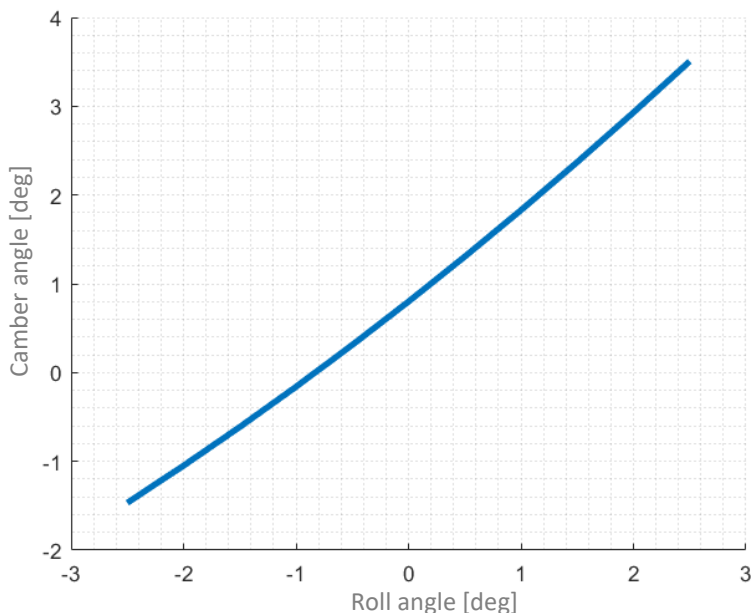


Figure 36 - Camber due to Roll angle

From the above Camber plot is obtained the corresponding equation with its coefficients:

$$Camber_{rl} = 0.0139 + 0.9944 * \phi + 2.0156 * \phi^2$$

The optimization boundaries imposed for the camber coefficients are:

	$\gamma 0_{c_{rl}}$	$\gamma 1_{c_{rl}}$	$\gamma 2_{c_{rl}}$
<i>lb</i>	0.012	0.7	1.3
<i>ub</i>	0.016	1	2.1

Table 1 - Lower and upper boundaries for each toe coefficient

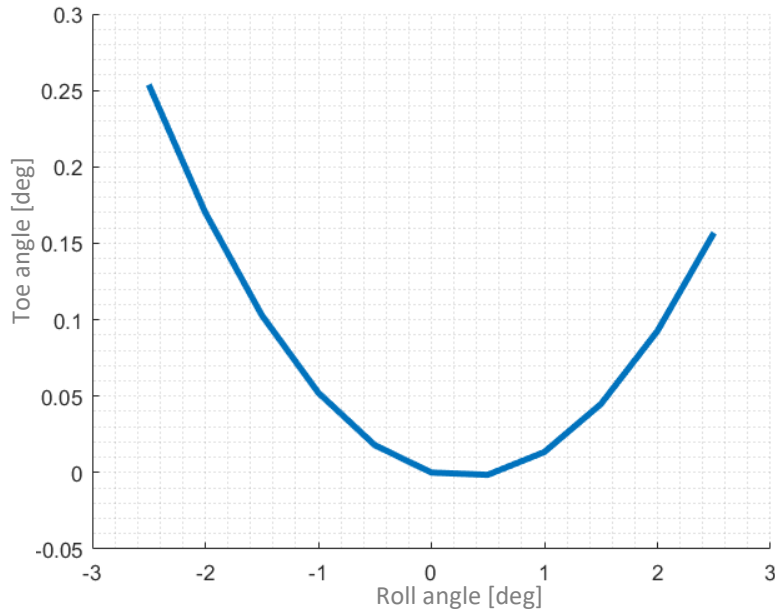


Figure 37 - Toe due to roll angle

From the toe plot instead is obtained:

$$Toe_{rl} = -0.1883 * 10^{-8} - 0.01937 * \phi + 1.8823 * \phi^2$$

The optimization boundaries imposed for the toe coefficient are:

	$\gamma 0_{t_{rl}}$	$\gamma 1_{t_{rl}}$	$\gamma 2_{t_{rl}}$
<i>lb</i>	-0.00001	-0.02	1.2
<i>ub</i>	0	-0.01	2.2

Table 2 - Lower and upper boundaries for each toe coefficient

The camber and toe curves with their coefficients and boundaries described above are used as inputs in the genetic algorithm to find their best values that maximizes the “g-g” diagram shape.

The following outline summarizes how the genetic algorithm works:

- the algorithm begins by creating a random initial population of camber and toe coefficients between their lower and upper boundaries (*Tables 1- Table 2*).

The number of individuals in a population can be changed with the Matlab command “*PopulationSize*”.

- The algorithm then creates a sequence of new populations. At each step, the algorithm uses the individuals in the current generation to create the next population. To create the new population, the algorithm performs the following steps:
 - a. Scores each member of the current population by computing its fitness value. These values are called the raw fitness scores.
 - b. Scales the raw fitness scores to convert them into a more usable range of values. These scaled values are called expectation values.
 - c. Selects members, called parents, based on their expectation.
 - d. Some of the individuals in the current population with the best fitness values are chosen as *elite*. These elite individuals automatically survive to the next generation (*Figure 38*).



Figure 38 - Elite child

- - e. Produces children from the parents. Children are produced either by combining the vector entries of a pair of parents (*crossover – Figure 39*) or by introducing random changes, or mutations, to a single parent (*mutation – Figure 40*).

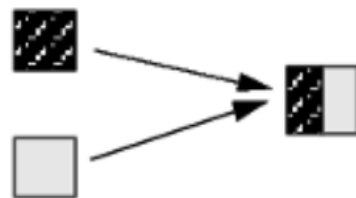


Figure 39 - Crossover child



Figure 40 – Mutation child

- - f. Replaces the current population with the children to form the next generation.
 - The algorithm stops when one of the stopping criteria is met. The one used in this optimization is the maximum number of generations (*Maxgenerations*) imposed at thirty.

The evolution of the optimization is described by the following Matlab interface:

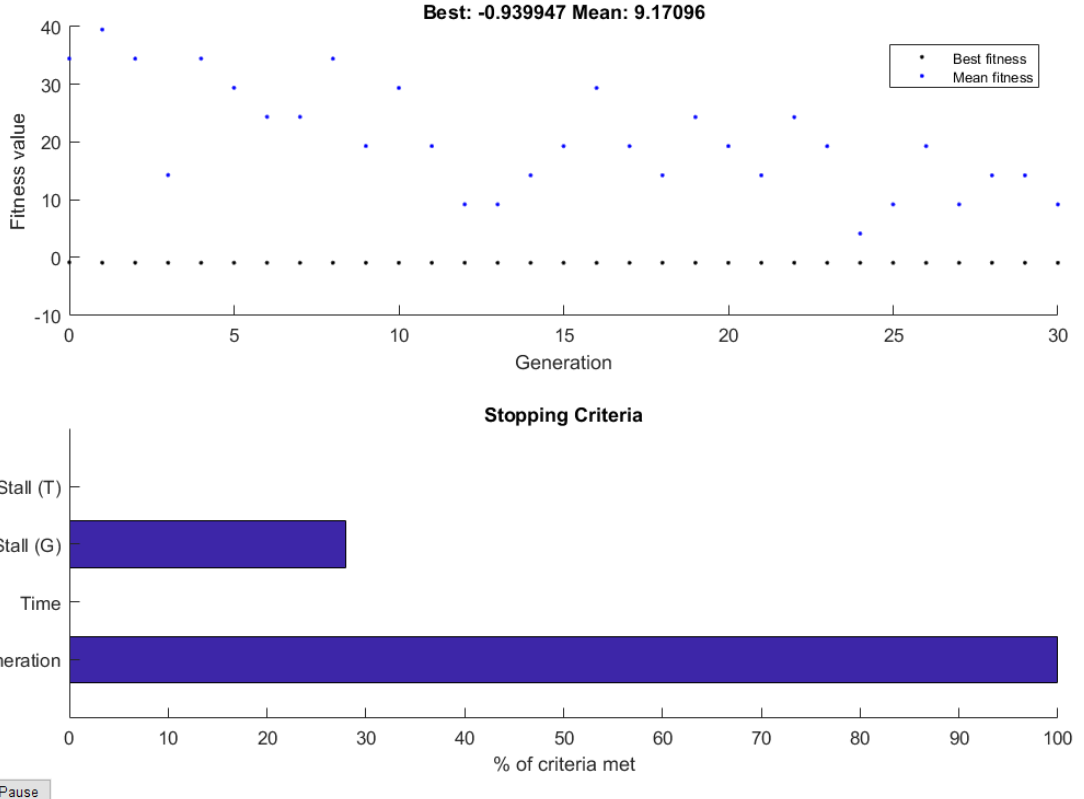


Figure 41 – Genetic algorithm optimization interface

After the thirtieth generation the algorithm stops. The convergence is reached before the thirtieth generation and it can be seen from the Stall (G) band. (Figure 41)

The stall band increases if there is no improvement in the objective function. This is a default stopping criteria in fact the algorithm stops if the average relative change in the best fitness function value over *MaxStallGenerations* generations is less than or equal to *FunctionTolerance*. In the case of “ga” algorithm the positive scalar of the *FunctionTolerance* is 1e-6.

In the interface in Figure 41 are plotted the Best and Mean fitness points at each generation. The value of the mean fitness points is high because during the “g-g” diagram optimization if in a point does not converge the function return a value of the volume of 100. Instead the best fitness points represent the best normalized volume values of the “g-g” diagrams at each generation. Their value is always better from generation to generation but due to the high value of the mean fitness their improvement cannot be easily seen in Figure 41.

5.3.2 Results

The final optimized coefficients values of the camber and toe equations are:

	$\gamma_0_{c_{rl}}$	$\gamma_1_{c_{rl}}$	$\gamma_2_{c_{rl}}$	$\gamma_0_{t_{rl}}$	$\gamma_1_{t_{rl}}$	$\gamma_2_{t_{rl}}$
Optimized value	0.0147	0.7657	1.8602	-0.0000	-0.0165	2.0434

Table 3 - Coefficients final results

With these new coefficients is now possible to find the optimized camber and toe curves. Plotting on the same graph also the *Chimera* vehicle curves, their different trends after and before the optimization can be visualized (Figure 42 - Figure 43).

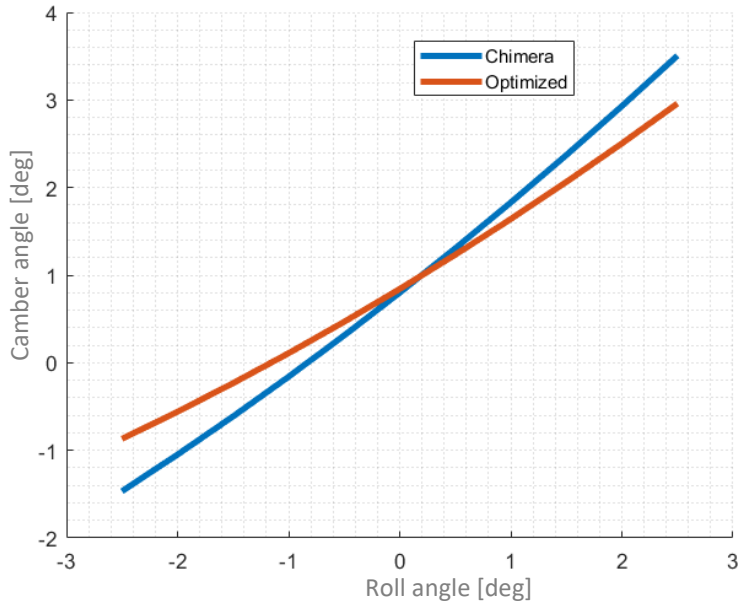


Figure 42 - Camber and Roll angle (Chimera vs Optimized)

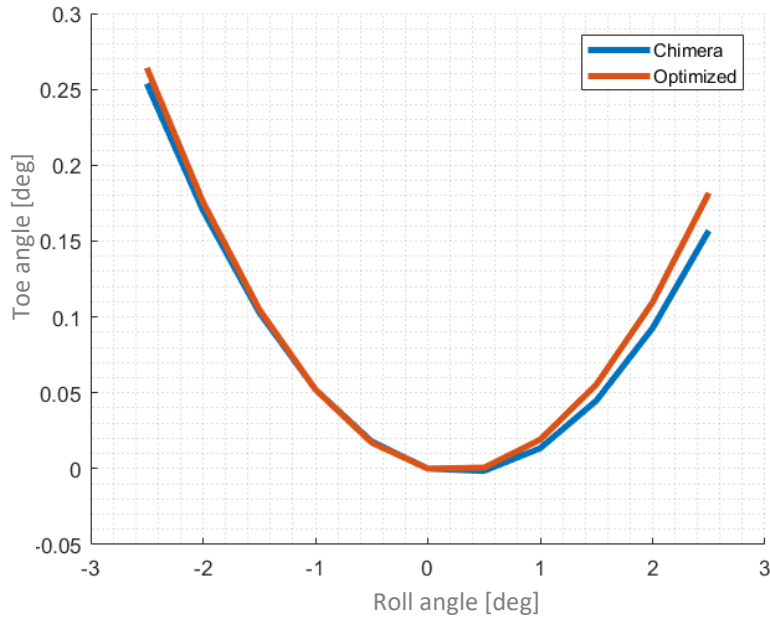


Figure 43 - Toe and Roll angle (Chimera vs Optimized)

In *Figure 42* it can be seen that the trend of the optimized camber curve respect to the initial one (*Chimera*) is the same but with a minor slope. At zero roll angle the value of the optimized camber angle is greater: 0.84 [deg] for the optimized and 0.79 [deg] for the initial one. The behaviour of the toe curves can be assumed equal due to the small variation of the toe angle during the chassis roll angle oscillation (*Figure 43*). The meaning of this plot in *Figure 43* is to maintain the toe angle as constant as possible and near zero during the suspension motion.

The toe value at the initial configuration, zero roll angle, is zero for the rear suspensions configuration because the vehicle analysed is a rear wheel drive car and the maximum grip there is when the toe angle is near zero. This is the same reason why the optimized camber curve has a lower slope than the starting one.

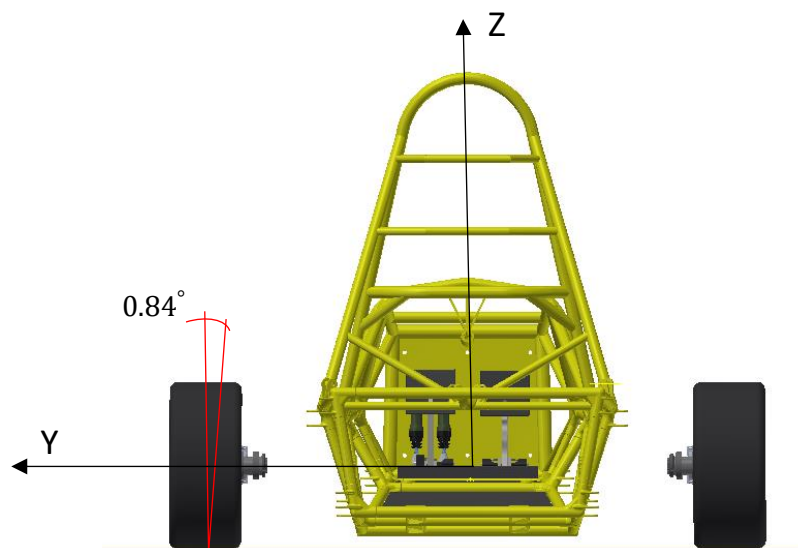


Figure 44 - Initial camber angle with zero roll angle

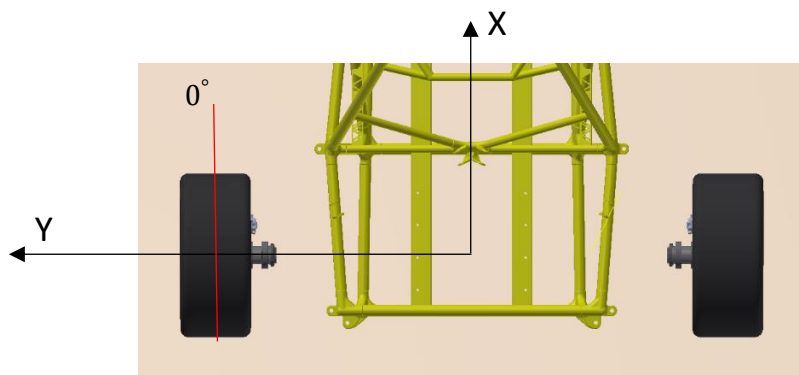
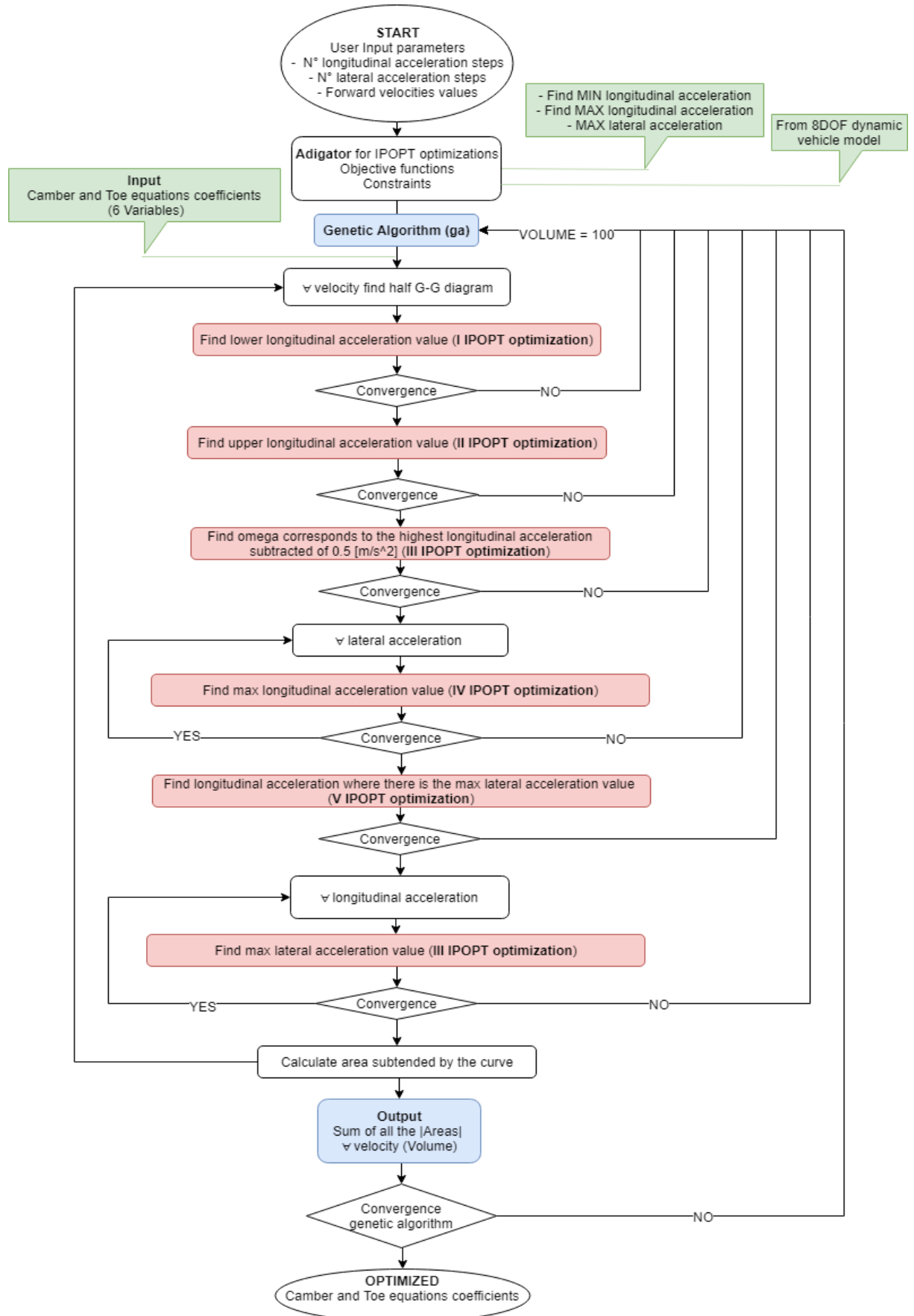


Figure 45 - Initial toe angle with zero roll angle

All the steps to find the optimized camber and toe coefficients equations from the “g-g” diagram optimization can be summarized with the following flow chart:



Starting from top to bottom of the previous flow chart in the first step there is the user Matlab interface where some input parameters used during the optimizations steps can be initialized (*Figure 46*).

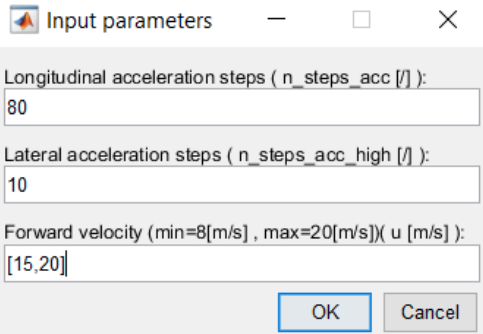


Figure 46 - Matlab user interface with initial default values

In the next step thanks to the ADiGator toolbox a file containing the derivatives of each objective and constraint functions is generated.

The genetic algorithm then generates the first individual that corresponds to the coefficients of the camber and toe curves with which to find the “g-g” diagrams volume. This volume corresponds to the sum of the subtended areas by the “g-g” diagrams at each velocity initially set (*Figure 46*). The optimized shape of the “g-g” diagram is built with all the optimizations steps seen previously in this section. For each “g-g” diagram optimization a convergence control is done. During an optimization step, in fact, if it does not converge the optimization exits returning a higher value set at 100 if compared to the normalized one. If that occurs the genetic algorithm generates a new individual. Otherwise if all the optimizations to find the “g-g” diagram converge at the following longitudinal velocity, the corresponding normalized area is found. If the “g-g” diagram converge for a velocity the same steps are done for the other velocities always checking the convergence during the optimizations. Once that the “g-g” diagram areas at each velocity are found they are summed to each other to obtain the final volume. At this point the genetic algorithm generates a new individual and performs the same steps.

When the number of individuals reaches a fixed number, the genetic algorithm can proceed with the creation of a new generation using its properties.

After the thirtieth generation is evaluated the convergence of the genetic algorithm and the optimized individual, that contains the best camber and toe coefficients, is found.

The time for all this optimization is about sixteen hours considering that the time to generate a single “g-g” diagram is less than one minute.

6. II OPTIMIZATION:

Kinematic suspension optimization

Thanks to the optimized curves of the camber and toe angle obtained in the previous section is now possible to find the better suspension configuration that approximates these curves. To find it, another optimization in Matlab environment using the same software package Ipopt is done. The constraints related to the suspension motion are found using the software Maple, with MBSymba package. These equations are then exported in Matlab using the same steps seen in the previous section to export the equations of the dynamic vehicle model.

6.1 Objective function

The objective function for the optimisation is formulated to reduce the difference between the attained variation of a given wheel parameter respect to the corresponding desired variation of the same. This wheel parameter can be the camber γ or the toe angle δ evaluated over some region of suspension operation which is parametrised by the roll of the vehicle $\Phi = [\Phi_{min}, \Phi_{max}]$. The range of variation in Φ is given by the maximum roll angles values achieved during a race. In *Figure 47* is shown the simulated roll angle behaviour during the Varano de Melegari track by the *Chimera* vehicle.

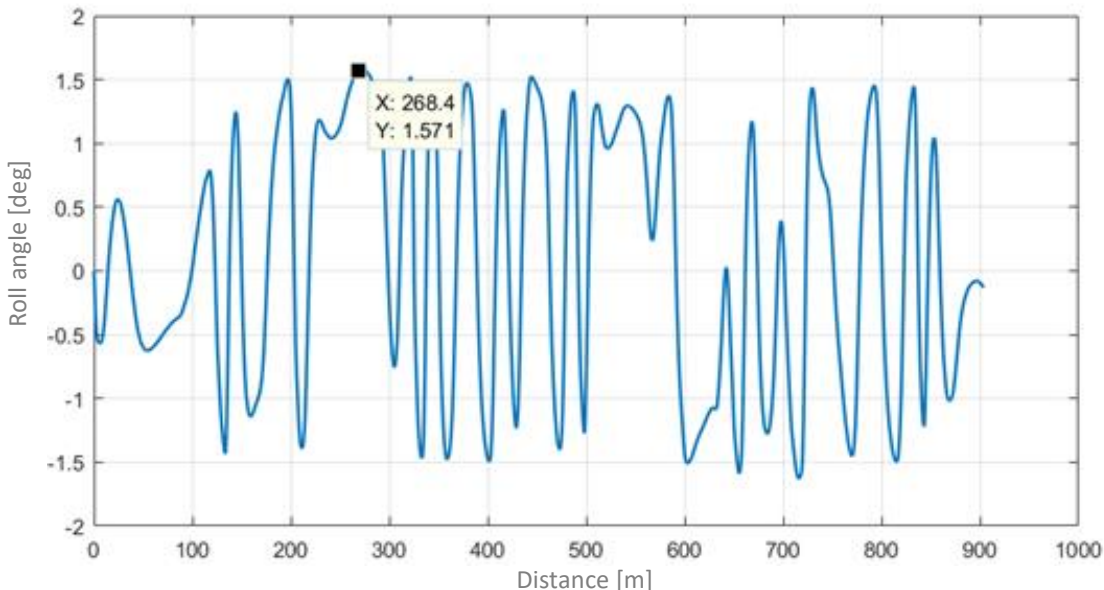


Figure 47 - Roll angle values during the Varano the Melegari track

The optimization must be guaranteed inside the roll angle range of *Figure 47*: ± 1.57 [deg]. However, the roll angle boundaries used in the optimization are ± 2.54 [deg]. That is done because this interval is the minimum suspension travel allowed by the FSAE regulation (Appendix C), even if the range that the car reaches during the race remains between ± 1.57

[deg]. Respect to this range the user can decide, thanks to an interface, the level of discretization for the optimization.

The individual objectives functions for camber and toe are combined to form a single one expressed as:

$$f(x) = \frac{1}{N} \sum_{i=1}^N \frac{(\gamma_a(X, \Phi) - \gamma_d(\Phi))^2}{\Delta_\gamma} + \frac{(\delta_a(X, \Phi) - \delta_d(\Phi))^2}{\Delta_\delta}$$

where N is the number of the samples obtained by dividing the domain $[\Phi_{min}, \Phi_{max}]$ uniformly by the user; $\gamma_a(X, \Phi)$ is the attained value of the camber for a given value of the roll angle Φ and for a given vector of design variables X ; $\gamma_d(\Phi)$ instead is the desired camber value given by the optimal curve of *Figure 42* for each possible roll value; The same thing can be said for the attained toe angle $\delta_a(X, \Phi)$ and the desired one $\delta_d(\Phi)$ of *Figure 43*; At conclusion the Δ_γ for the camber and Δ_δ for the toe are the maximum variations of the respective angles and they are used to normalize the Euclidean distance between the attained and desired angle values.

6.2 Constraints

With the software Maple the kinematic model of the rear suspension is built in order to obtain the constraints used in the optimization. To optimize the camber and toe angle it is not used the total kinematic model of the suspension but only those kinematic components that affect these angles: lower and upper wishbone and the steering axis that in the case of rear suspensions is fixed and it is used only to regulate the convergence. To visualize the model, the components dimensions and configuration of the first vehicle *Chimera* are used. This configuration is used as the initial guess in the optimization.

To visualize the final plot (*Figure 48*) are used some procedures previously implemented in Maple.

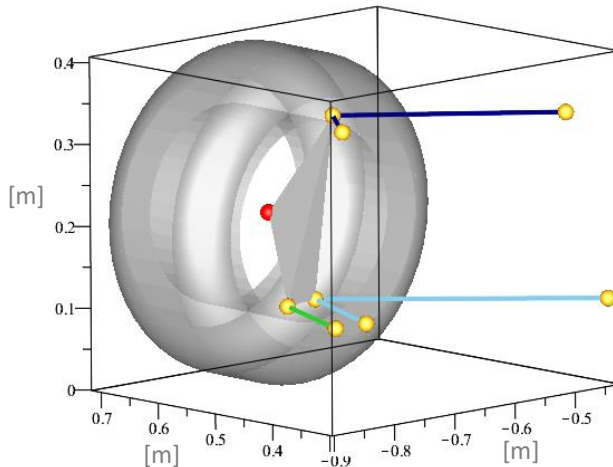


Figure 48 - Rear left suspension model with Chimera vehicle initial values

Different reference frames (RF) are then associated to the kinematic Maple model. They are plotted in different views (Rear-Top-Lateral) presented in *Figure 49*, *Figure 50*, *Figure 51*.

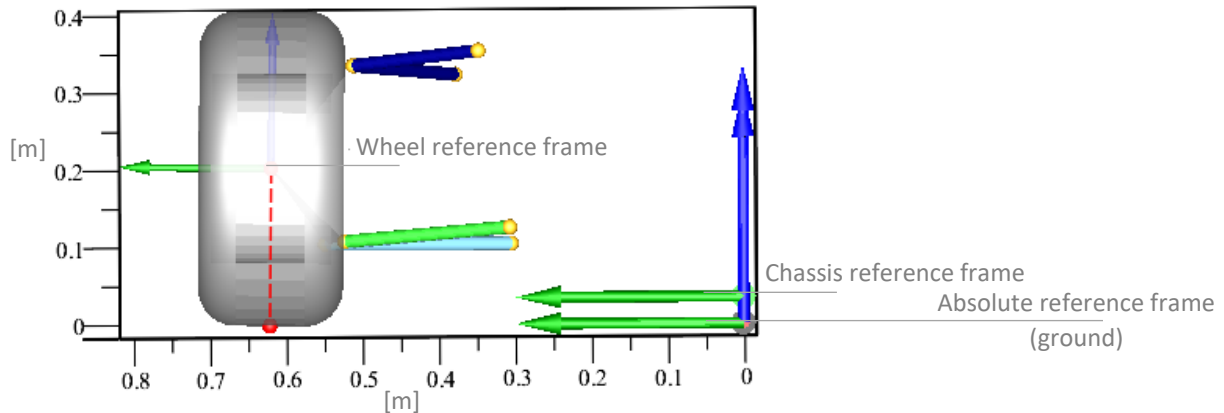


Figure 49 – Rear-view

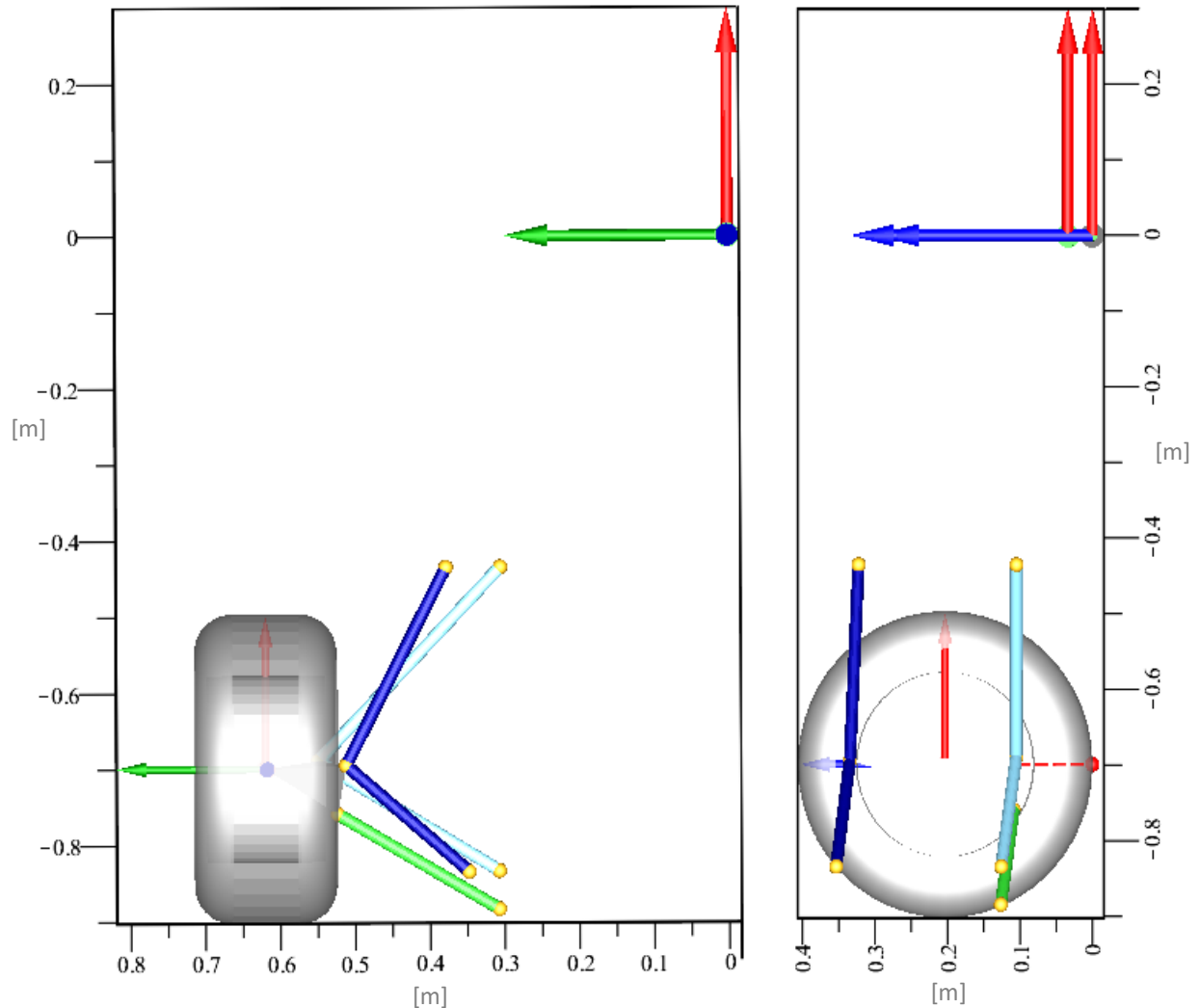


Figure 50 - Top-view

Figure 51 - Lateral-view

For each mechanical joint is defined a base point with a name to define it (*Figure 52*). Three coordinates (natural coordinates) are associated for each of these points in their reference frames.

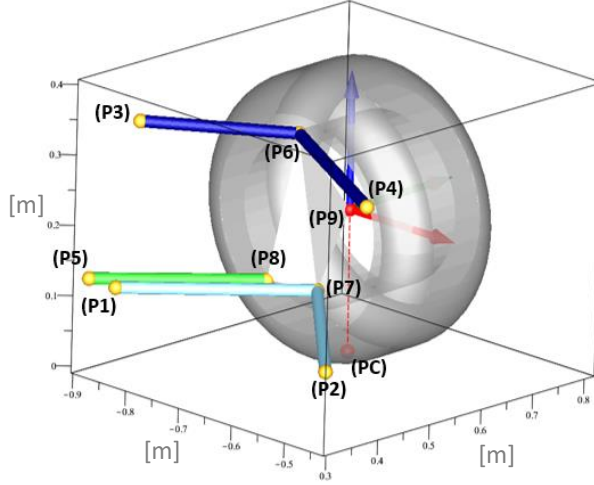


Figure 52 – Suspension model with points name

The absolute reference frame with respect to which it is built is the same used in the previous dynamic model (*Figure 22*).

In addition to the reference frame of the ground are defined other two reference frames: one for the wheel and the other for the chassis.

The reference frame of the wheel (*Figure 53*) has the same orientation of the absolute RF and it is fixed in the center of the wheel.

The coordinates of the points related to the wishbones, to the steering, on the side of the upright, and to the contact point of the tire with the ground are determined respect to this RF ($P_6-P_7-P_8-PC$). The origin of this RF (P_9) is free to move in all the three possible directions ($x_9(t), y_9(t), z_9(t)$). The same thing for the RF rotations ($\gamma_w(t), \theta_w(t), \delta_w(t)$) respect to the absolute reference frame (*Figure 53*).

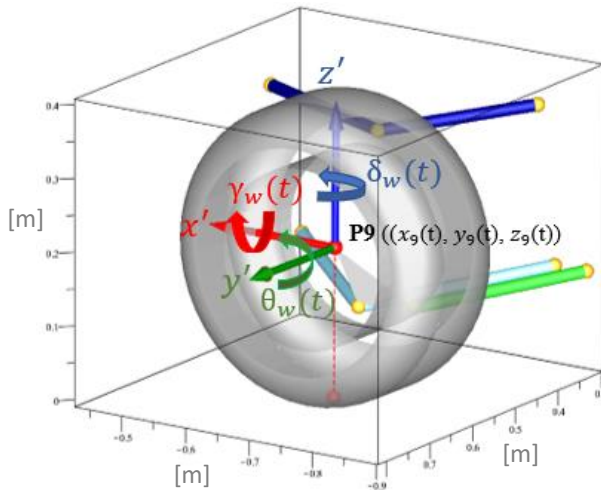


Figure 53 - Wheel RF degrees of freedom

The rotation around the axis z' characterizes the toe angle variation $\delta_w(t)$ instead the rotation around the axis x' characterizes the variation of the camber angle $\gamma_w(t)$. Only the angles of the rear left suspension group respect the sign convention in *Figure 22*, for the other ones must be adopted some sign corrections.

The other reference frame introduced in the model is the one related to the chassis. It is added because the suspensions positions in 3D CAD model are found respect to this one. It has the same orientation of the absolute reference system with the difference that its origin is translated along z axis of a quantity equal at least of 0.3 [m] (minimum distance of the chassis from the ground: Appendix C).

The independent variable used during the optimization to simulate the vehicle roll is given by the rotation ($\Phi(t)$) of the chassis vehicle around the x axis of the absolute RF.

The points that are defined respect to this RF are the ones related to the wishbones and to the steering, on the side of the chassis ($P1-P2-P3-P4-P5$).

The length of the suspensions arms and of the steering axis are initially fixed and starting from these values they can be longer or shorter. The initial values of the suspension lengths are assumed to be equal to the dimensions of the *Chimera* vehicle arms. Respect to these arms lengths are used some variables ($\Delta_{L_{36}}, \Delta_{L_{46}}, \Delta_{L_{58}}, \Delta_{L_{17}}, \Delta_{L_{27}}$) to allow their possible change in length (*Figure 54*).

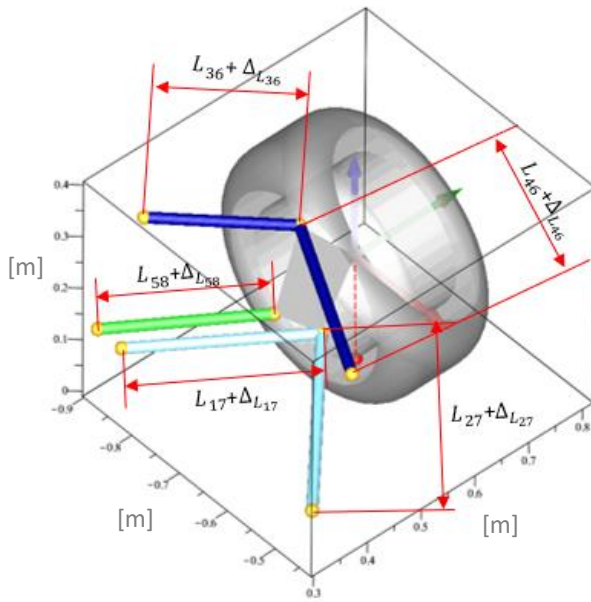


Figure 54 - Arms lengths with their variables

The constraints allow to fix the correct number of degrees of freedom to simulate the suspension behaviour.

To describe the positions of each mechanical joint, the natural coordinates in their respective reference frames are used. To constrain the problem, it is imposed that the bodies are rigid.

Therefore, the distance between the points must be constant: the scalar product between the vector that connects two points (P_A, P_B) with itself must be equal to the length of the distance between the two points (l_A). The following constraint can be expressed as:

$$l_A \cdot l_A - l_A^2 = 0, \text{ where } l_A = P_A - P_B$$

Each of the five lengths of the wishbone and steering arms, in fact, are constrained in this way. These constraints allow the free rotations around the extreme points fixing only their relative distance.

The sixth constraint is that the contact point between the wheel and the ground is fixed during the vehicle roll. The rotations around this point are allowed, only the translations are fixed.

6.3 Variables

The independent variable that changes during the optimization is the chassis roll angle $\Phi(t)$. The roll angle of the chassis change keeping the wheel contact with the ground fixed. The same thing could be done by fixing the roll angle and using as independent variable the wheel vertical motion.

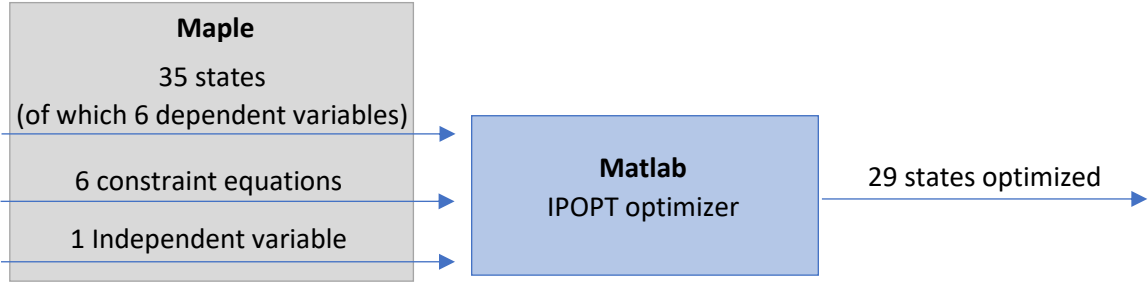
The dependent variables of the system represent the six possible wheel motions: $x_9(t), y_9(t), z_9(t), \gamma_w(t), \theta_w(t), \delta_w(t)$. They are related to the independent variable thanks to the above constraints. Among them do not appear the variable connected to the roll's height. This is due to the fact that it is fixed during this optimization to not increase the system complexity. It is possible to do this assumption because the real roll angle variation is so small to not cause a relevant effect on the variation of the roll height. Moreover it is guaranteed also with other possible suspension components as for example with the anti-roll bar. This component, in fact, tries to maintain the roll angle and its height as constant as possible during the race. Another variable that for the rear left suspension group is fixed and set to zero is the one related to the steering system $s(t)$.

These last two variables, even if for this optimization are set to zero, can be unlocked. This aspect makes the model adaptable to any type of suspension.

The parameters related to the tire radius and the initial arms lengths ($L_{36}, L_{46}, L_{58}, L_{17}, L_{27}$) are imposed and replaced directly in the Maple model.

The variables that must be optimized and that compared as states in the Matlab optimizer are the twenty-four coordinates xyz of the joint points ($P1-P2-P3-P4-P5-P6-P7-P8$) expressed in their reference frames and the five related to the arms lengths ($\Delta_{L_{36}}, \Delta_{L_{46}}, \Delta_{L_{58}}, \Delta_{L_{17}}, \Delta_{L_{27}}$).

Summing up the whole optimization process we have:



For each value of the roll angle the optimizer could found a suspension configuration that better approximate the desired curves. In reality it is not possible because once that the configuration is chosen it can change with the roll angle variation. To obtain a unique optimized configuration the total possible roll angle configurations, that can be defined by the user, are put in an unique vector. The Ipopt algorithm, in fact, tries to find the configuration that minimizes the objective function for all the possible values of the roll angle.

If the level of roll angle discretization increases more constraints are added to the optimization: six for each new roll angle value. The number of states also increases each time of six components to guarantee the possibility of free variation to the dependent variables.

The default roll angle discretization, that can be changed by the user, is given by eight values between the minimum and maximum (*Table 4*).

	<i>Min</i>							<i>Max</i>
<i>Roll angle</i> [rad]	-0.0436	-0.0312	-0.0187	-0.0062	0.0062	0.0187	0.0312	0.0436

Table 4 - Roll angle default discretized values

6.4 Results

The total time taken for this optimization is about two minute and half: a minute and half to generate the functions derivatives with Adigator toolbox and a minute to find the optimized values with Ipopt.

The values of the twenty-nine optimized states are:

	<i>Reference Frame</i>			
<i>P1</i>	$x1_0 = -0.48$ [m]	$y1_0 = 0.30$ [m]	$z1_0 = 0.1$ [m]	Absolute (ground)
<i>P2</i>	$x2_0 = -0.75$ [m]	$y2_0 = 0.33$ [m]	$z2_0 = 0.1$ [m]	Absolute (ground)
<i>P3</i>	$x3_0 = -0.48$ [m]	$y3_0 = 0.4$ [m]	$z3_0 = 0.33$ [m]	Absolute (ground)
<i>P4</i>	$x4_0 = -0.88$ [m]	$y4_0 = 0.38$ [m]	$z4_0 = 0.33$ [m]	Absolute (ground)
<i>P5</i>	$x5_0 = -0.81$ [m]	$y5_0 = 0.3130$ [m]	$z5_0 = 0.1151$ [m]	Absolute (ground)
<i>P6</i>	$x6_0 = 0.001$ [m]	$y6_0 = -0.11$ [m]	$z6_0 = 0.140$ [m]	Wheel
<i>P7</i>	$x7_0 = 0.0055$ [m]	$y7_0 = -0.08$ [m]	$z7_0 = -0.0985$ [m]	Wheel
<i>P8</i>	$x8_0 = -0.058$ [m]	$y8_0 = -0.13$ [m]	$z8_0 = -0.08$ [m]	Wheel

$\Delta_{L_{17}} = -0.0482 [m]$	
$\Delta_{L_{27}} = -0.0829 [m]$	
$\Delta_{L_{36}} = -0.0540 [m]$	
$\Delta_{L_{46}} = -0.0079 [m]$	
$\Delta_{L_{58}} = -0.0806 [m]$	

Table 5 - Optimization results

To associate at each state of *Table 5* the related variable on suspension configuration can be seen the previous *Figure 52* and *Figure 54*.

Once that the optimized states values are found they are imposed in the initial Maple model used to find the constraint equations. The related result of the suspension configuration can be seen in *Figure 55*.

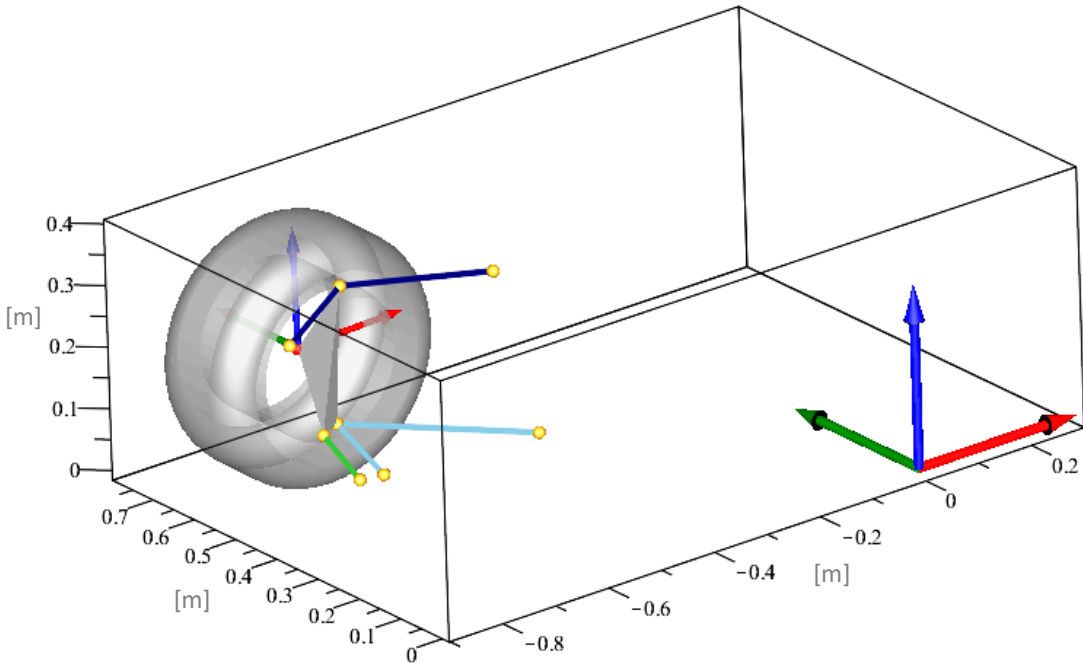


Figure 55 - Rear left suspension configuration with optimized results

The Maple model is then used to reach the suspension motion results for each value of the discretized roll angle value (*Figure 56*).

$\{x9(t) = -0.6988348206, y9(t) = 0.6048741326, z9(t) = 0.2031839095, \delta_w(t) = 0.003547503585, \gamma_w(t) = -0.01258463639, \theta_w(t) = -0.02802835482\}$
$\{x9(t) = -0.6987161203, y9(t) = 0.6035812942, z9(t) = 0.2031960828, \delta_w(t) = 0.002370632985, \gamma_w(t) = -0.006209319826, \theta_w(t) = -0.02882350314\}$
$\{x9(t) = -0.6986201604, y9(t) = 0.6020250117, z9(t) = 0.2031998444, \delta_w(t) = 0.001378593493, \gamma_w(t) = 0.001237370401, \theta_w(t) = -0.02940911861\}$
$\{x9(t) = -0.6985587164, y9(t) = 0.6002005061, z9(t) = 0.2031903916, \delta_w(t) = 0.0006935917187, \gamma_w(t) = 0.009724793794, \theta_w(t) = -0.02979816522\}$
$\{x9(t) = -0.6985433931, y9(t) = 0.5981007766, z9(t) = 0.2031623844, \delta_w(t) = 0.0004370190038, \gamma_w(t) = 0.01924172944, \theta_w(t) = -0.03000845791\}$
$\{x9(t) = -0.6985864143, y9(t) = 0.5957159665, z9(t) = 0.2031097884, \delta_w(t) = 0.0007381928811, \gamma_w(t) = 0.02979891372, \theta_w(t) = -0.03006476780\}$
$\{x9(t) = -0.6987016709, y9(t) = 0.5930324014, z9(t) = 0.2030256052, \delta_w(t) = 0.001746075198, \gamma_w(t) = 0.04143343906, \theta_w(t) = -0.03000199385\}$
$\{x9(t) = -0.6989062438, y9(t) = 0.5900310811, z9(t) = 0.2029014312, \delta_w(t) = 0.003646432387, \gamma_w(t) = 0.05421613226, \theta_w(t) = -0.02987035410\}$

Figure 56 - Dependent variables results during the eight roll angle steps

In *Figure 56*: $x_9(t), y_9(t), z_9(t)$ are the coordinates of center of wheel, $\delta_w(t)$ is the toe angle, $\gamma_w(t)$ is the camber angle, $\theta_w(t)$ is the wheel spin angle. Each line in *Figure 56* represents one of the eight roll angle steps.

The discretized camber and toe points for each of eight roll angle possible configurations are interpolated to find the related curves.

In conclusion, in Matlab environment the ideal camber curve found with the “g-g” diagram and the one found after this optimization are plotted together (*Figure 57*). The same thing is done for the toe curve (*Figure 58*).

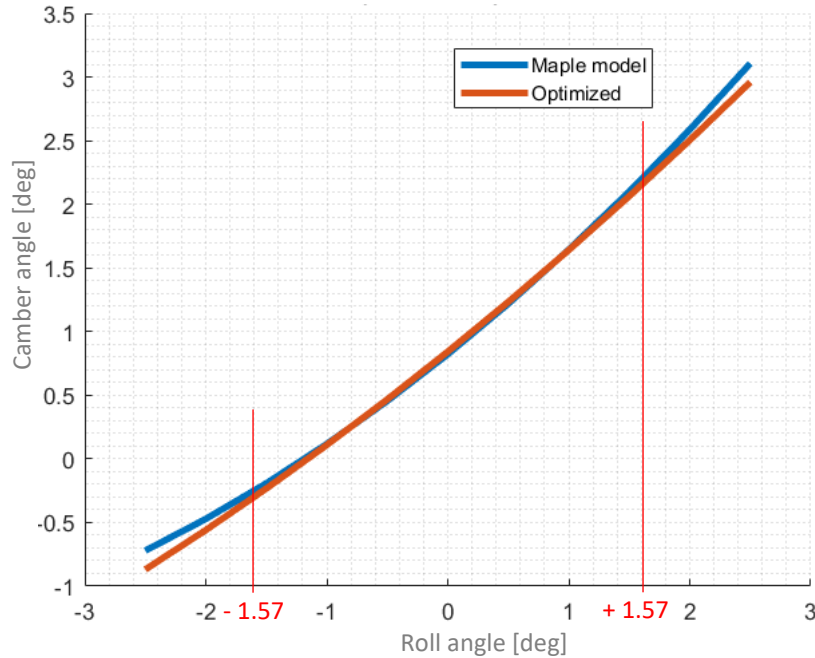


Figure 57 – Optimized and Maple model Camber Vs Roll angle

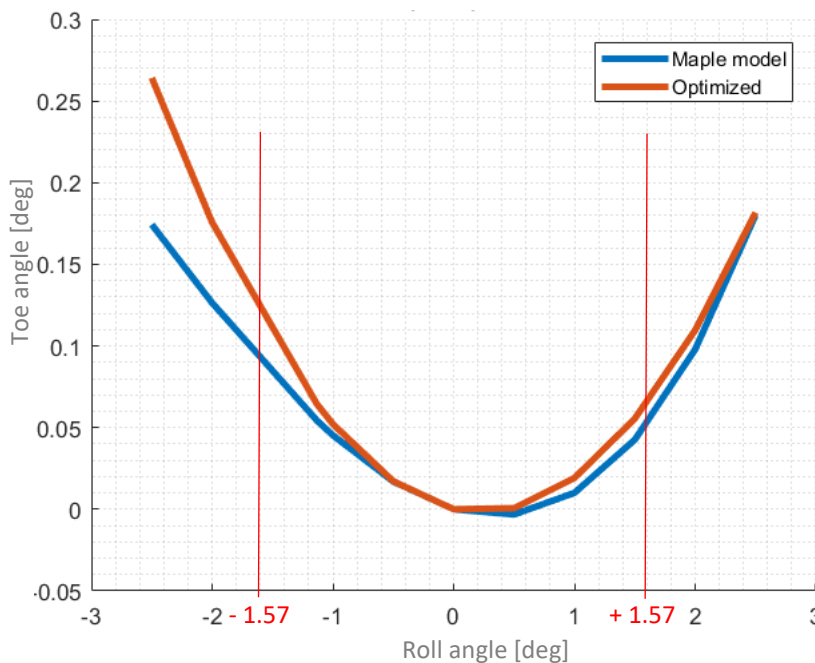


Figure 58 - Optimized and Maple model Toe Vs Roll angle

The camber curves in *Figure 57* between the two roll angle limits ± 1.57 [deg] (*Figure 47*) can be assumed overlapped; less overlapped outside this roll angle range. Instead for the toe (*Figure 58*) the difference between the optimized and the Maple curves could seem different. In fact, by looking at the axis of the ordinates the toe angle variation in degrees is very small. Furthermore, the toe variation with the Maple model is lower than the optimized one and it is good because for the toe angle it is important that its variation changes as little as possible during the suspension motion.

The camber and toe curves of the plots above are not exactly the same because It is important not only that they are as close as possible to the optimized values but also that the suspension is geometrical achievable and that some characteristic parameters seen in the initial sections of this thesis are in a correct range. This has reduced the possible ranges values of each state.

Geometrically speaking the suspension connections to the wheel group must be contained in the dimensions of the wheel rim guaranteeing the positioning of the braking system, hub and upright (*Figure 59*).



Figure 59 - Wheel group

Other main parameters that must be kept under control are the *kingpin inclination* and the *caster angle* (*Figure 60*). Their values are much more important for frontal suspensions because the steering system is present.

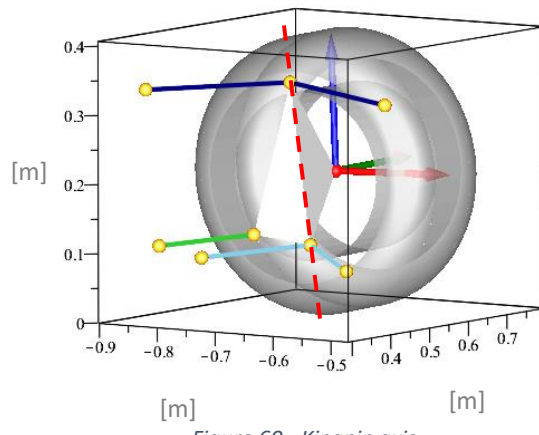


Figure 60 - Kingpin axis

For the model found these values are:

- Caster angle: +2.79 [deg].
- Kingpin inclination: - 8 [deg].

The signs of these angles are in agreement with what is explained in the above section about the “Characteristic parameters and their influence on vehicle dynamics”. Also their values are contained in the typical FSAE vehicles ranges (*Table 6*).

<i>Characteristic parameter</i>	<i>Minimum value</i>	<i>Maximum value</i>
<i>Caster</i>	+1 [deg]	+9 [deg]
<i>Kingpin</i>	- 9 [deg]	- 1[deg]

Table 6 - Typical FSAE parameters ranges

The rear *vehicle model track* is 1,20 [m]. Usually for the FSAE vehicles it is contained between 1,1 [m] and 1,4 [m] for rear and between 1,1 [m] and 1,5 [m] for the front one.

Another important parameter is the *roll center* position. It is implemented a function in Maple software to find it (*Figure 61*). Starting from the intersection between the two planes generated by the upper and lower wishbones, the coordinates y-z of the point with the coordinate x of the wheel center are found. Then a line between this point and the contact ground point of the symmetric rear right wheel is drawn. The z component of this line at y=0 is the roll center eight. It is possible because the car is symmetrical.

In the specific model the z coordinate of the roll center position is + 0.015 [m]. It is sufficiently above ground, so a good lateral stability of the vehicle is guaranteed.

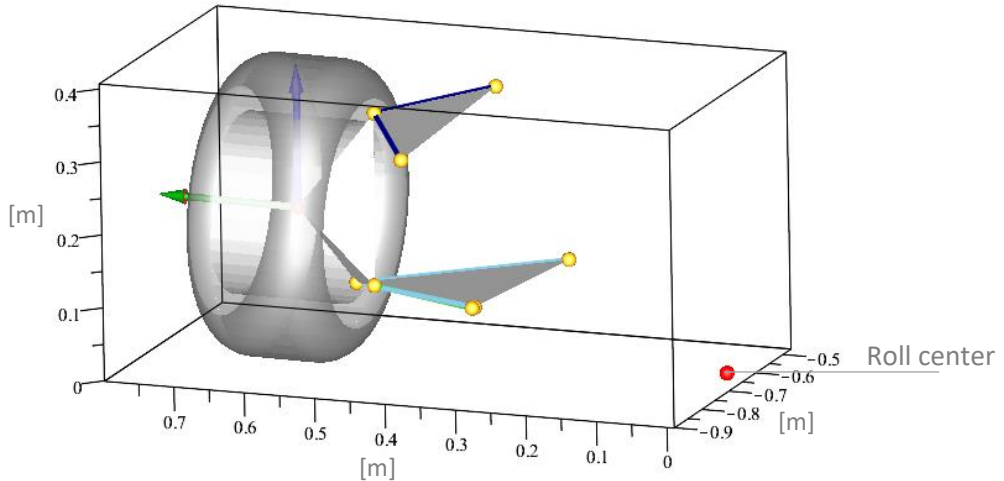


Figure 61 - Roll center geometric construction

Furthermore, the suspension usually must have the following geometrical characteristics:

- Lower wishbone parallel to the ground;
- Tie rod parallel to the lower wishbone arm;
- Upper wishbone smaller than the lower one.

The model found has these characteristics and thanks to them the suspension guarantees also a better structural response.

7. III Optimization: Suspension Motion ratio

7.1 Motion ratio theory

The motion ratio (MR) is the ratio of the spring or damper displacement to the wheel displacement. Since almost all FSAE cars use spring over dampers, the ratios are usually the same.

The motion ratios are described by the following equations:

$$\text{Spring motion ratio} = \frac{\text{Spring displacement}}{\text{Wheel displacement}}$$

$$\text{Damper motion ratio} = \frac{\text{Damper displacement}}{\text{Wheel displacement}}$$

For FSAE cars a motion ratio close to one and constant is recommended for better ride. This means to meet the FSAE requirement of 50.8 mm (2 inches) of wheel travel, a damper must have at least 63.5mm (2.5 inches) of travel. At a 1.0 motion ratio, this will allow for 50.8mm (2 inches) of wheel travel and 12.7mm (0.5 inches) of jounce bumper travel.

The basic component in motion ratio evaluation is the rocker, or lever (*Figure 62*).



Figure 62 – Rockers of Chimera vehicle

In most FSAE vehicles a rocker is included to link the basic suspension to the spring and damper. It translates the bump force from push-rod, or pull-rod, to the shock absorber according to the suspension configuration. Including a push-rod, or pull-rod, and rocker allows to position better the spring and damper. It can be placed vertically inside the body, or, as it is common nowadays, laid down horizontally on top of the body or along the upper sides of the gearbox. This improves the aerodynamics by removing the spring-damper unit from the high-speed airflow, and the inclusion of a rocker in the system makes it very easy to change the motion ratio and rising rate simply by changing the geometry of the rocker.

The *total bump motion ratio* between the movement of the wheel and shock absorber can be divided into the pull rod motion ratio and the rocker one which their sum gives the final motion ratio (*Figure 63*).

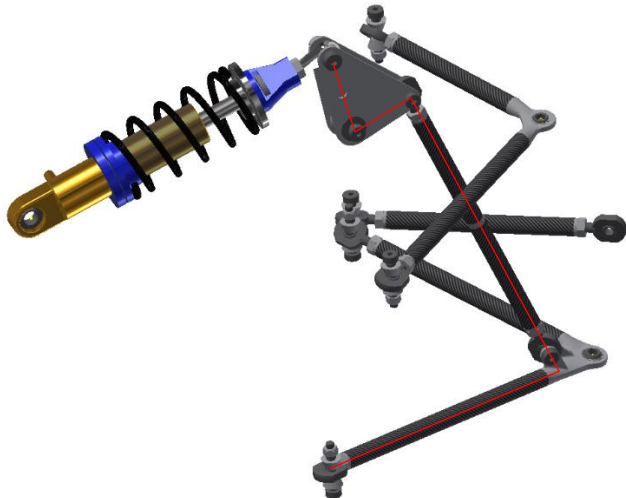


Figure 63 - Total motion ratio

The *pull rod motion ration* is about the rod movement to the wheel movement. The movement is not equal due to the angle at which the rod is mounted (theta) and also the distance at which it is mounted (A) from the total moving distance (B) between the chassis and the upright mount. These geometrical parameters are represented in *Figure 64*.

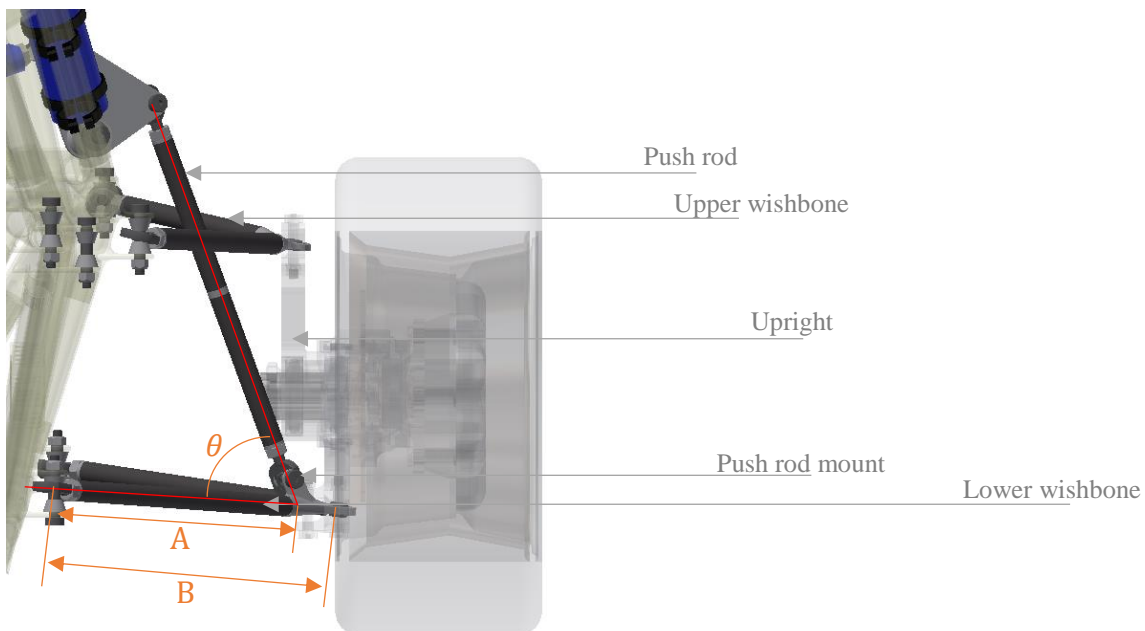


Figure 64 - Push rod motion ratio dimensions

The equation used to find the following motion ratio is:

$$\text{Motion ratio} = \frac{A}{B} * \sin \theta$$

If the ratio is not 1:1 the lost ratio with the pushrod dimensions can be regained with the rocker dimensions. The *rocker* is characterized by an acute angle (θ) and long rocker arms (A,B) that are visible in *Figure 65*. The equation to calculate the new motion ratio is the same of the above equation.

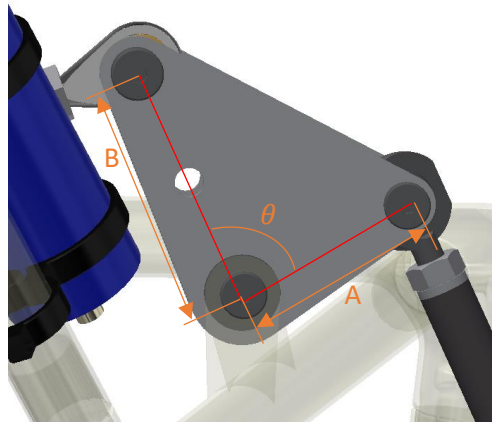


Figure 65 - Rear rocker motion ratio dimensions

The suspension configuration with the rocker allow to reach the desired motion ratio. Another solution adopted by some FSAE teams is to use the shock absorber directly as a push-rod, or pull-rod, not using the rocker component. This solution has the advantage of being simpler and lighter than the other one. On the other hand this configuration loses in flexibility and it not guarantees a constant motion ratio due to the rotation and shortening of the shock absorber. This solution adopted by a German team can be seen in *Figure 66*.



Figure 66 - E-Motion Rennteam Aalen vehicle
Retrieved February 5, 2018, from <https://www.emotion-rennteam.de/>

This solution without the rocker is not considered among the possible suspension configurations in the optimization due to the related disadvantages described above.

There are several reasons for using motion ratios equal or greater than one. The first is that higher motion ratio requires lower spring rates for the same wheel rates.

The *spring rate*, that is the stiffness of the actual spring [N/mm], is defined with the following expression:

$$\text{Spring rate} = \frac{\text{Wheel rate}}{MR^2}$$

Lower spring rates are also lighter, and result in less spring and shock friction as well as lower component loads. The other reason is greater damper travel and higher shock velocities. Since dampers perform better at higher velocities, and the wheel displacements are quite small on a FSAE car, higher motion ratios produce better shock performance.

The amount of force transmitted to the vehicle chassis reduces with increase in motion ratio. The force in the spring, in fact, is (roughly) the vertical force at the contact patch divided by the motion ratio.

Furthermore, it is kept as close as possible to one to make it robust to the internal games. Otherwise the wheel or shock absorber games can be amplified if the motion is not close to one.

In *Table 7* are compared typical travels, velocities and spring preload changing the motion ratios value.

<i>Motion Ratio</i>	<i>1:1</i>	<i>0.75:1</i>	<i>0.5:1</i>
<i>Wheel Travel</i>	25 [mm]	25 [mm]	25 [mm]
<i>Shock/Spring Travel</i>	25 [mm]	18.8 [mm]	12.5 [mm]
<i>Wheel velocity</i>	50 [mm/s]	50 [mm/s]	50 [mm/s]
<i>Shock Velocity</i>	50 [mm/s]	37.5 [mm/s]	25 [mm/s]
<i>Wheel Rate</i>	25 [N/mm]	25 [N/mm]	25 [N/mm]
<i>Spring Rate Required</i>	25 [N/mm]	44 [N/mm]	100 [N/mm]
<i>Spring Preload</i>	50 [Kg]	67 [Kg]	100 [Kg]

Table 7 - Motion ratio comparison
Retrieved February 5, 2018, from <http://www.kaztechnologies.com>

7.2 Motion ratio optimization

Also the motion ratio optimization is modular and can be done for different types of suspension's configurations: push-rod or pull-rod.

In the specific case the suspension configuration analysed and optimized is a push-rod one for the rear left suspension group.

7.2.1 Objective function

The objective function imposed in this optimization is that the final Motion ratio during the suspension travel is as close as possible to one. It means that the vertical displacement of the wheel is the same to the one of the shock absorber (*Figure 67*).

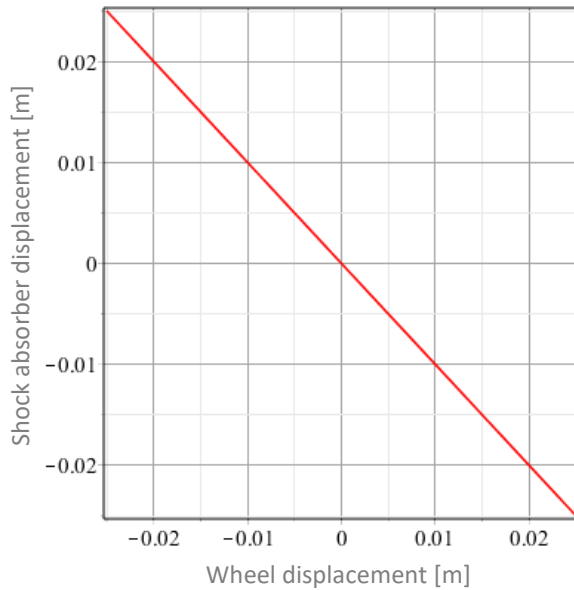


Figure 67 - Desired Motion ratio 1:1

This Motion ratio value is chosen equal to one for its good properties explained in the first part of this section where are illustrated the advantages and disadvantages about different Motion ratio values.

The objective function is expressed by the following equation:

$$f(x) = \frac{1}{N} \sum_{i=1}^N (\delta_w + \delta_s(X))^2 \quad (7.1)$$

where N is the number of the samples obtained by dividing uniformly the independent variable δ_w related to the wheel vertical displacement. The user can decide the number of optimization points with an interface at the beginning of the optimization. The wheel displacement range is fixed between -0.0254 [m] and +0.0254 [m] that must be guaranteed by the FSAE regulation (Appendix C). $\delta_s(X)$ instead is the Shock absorber displacement that depends to the X states among which there are also the variables to optimize.

The sign “+” between the two displacements in the expression (7.1) is due to the fact that their signs are reversed: an increase in the wheel displacement corresponds to a compression of the shock absorber vice versa a wheel droop corresponds to an extension of the shock absorber.

The linear trend of the output between the two displacements (*Figure 67*) allows not to use many samples reducing a lot the computational cost of the optimization.

To find the optimized states are used three steps for the wheel displacement (*Table 8*).

	Min	Max
<i>Wheel displacement [m]</i>	-0.0254	0

Table 8 - Wheel displacement optimization steps

The vertical wheel displacement values in *Table 8* are defined respect to the absolute reference system (ground) of the suspension model.

7.2.2 Constraints and variables

The constraint equations are obtained in Maple environment. Some new points to simulate the push-rod, the rocker and the shock absorber are added to the previous Maple model used for the camber and toe optimization (*Figure 68*).

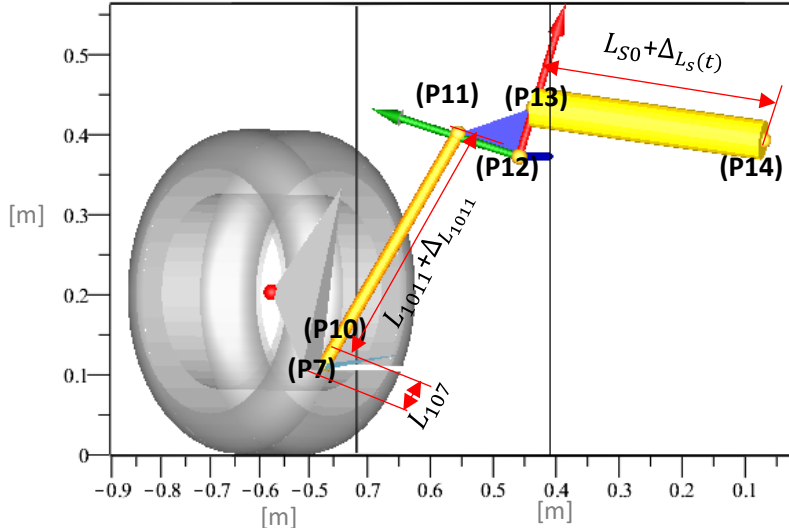


Figure 68 - Suspension model with the new components that affect the motion ratio

In this model all the states used in the previous camber and toe optimization are fixed with their optimized values. It is necessary to add all the kinematic suspension model, even if the motion ratio is not affected by the suspension wishbones or by the tie rod, to simulate the wheel displacement during the suspension travel (*Figure 69*).

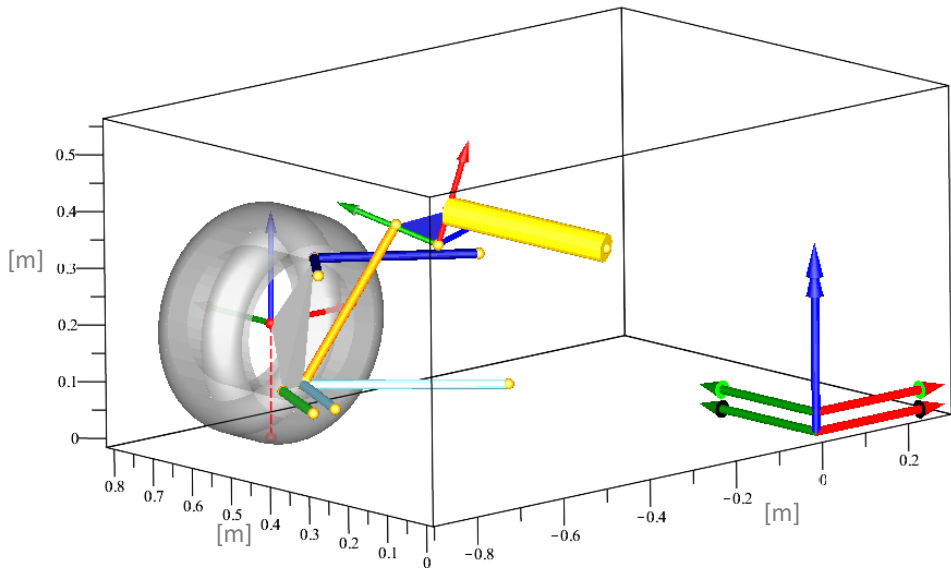


Figure 69 - Total final model

Furthermore, from the experience of the first vehicle it has been seen that if the forces of the pushrod do not discharge to the point P7 that represents the center of the 3D joint (*Figure 70*) some bending moments are generated.

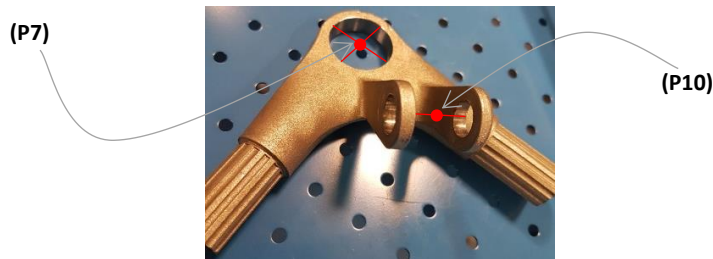


Figure 70 - 3D Chimera metal joint with non-aligned points

In *Figure 71*, in fact, are presented the stresses [Mpa] on the *Chimera*'s suspension lower arm due to the load coming from the non-aligned push-rod and the one coming from the upright. The push-rod force in the simulation is about 3500 [N] with a maximum stress in red of 200 [Mpa].

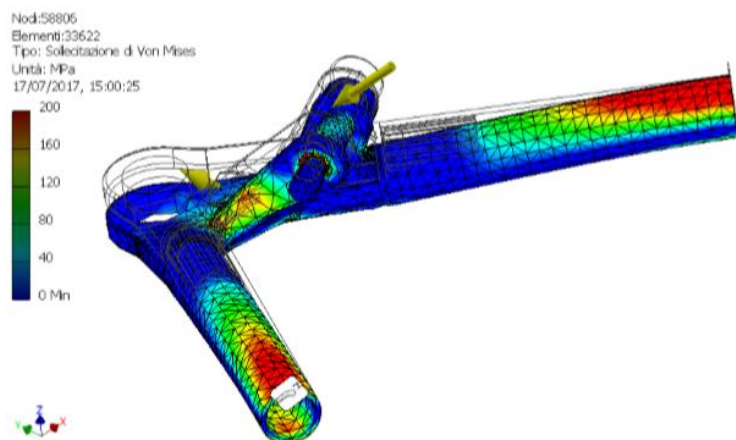


Figure 71 - Stresses of the Chimera vehicle's lower arm

To avoid this problem in the new suspension configuration is imposed that the position of the 3D joint's point P10 is on the line that connect the point P7 and P11 and all the components that affect the motion ratio are bounded on a plane. This plane connected the point P7 of the lower wishbone, the point P7v that has the same coordinate of P7 but translated respect z axis and finally the point P14 that connects the shock absorber with the chassis.

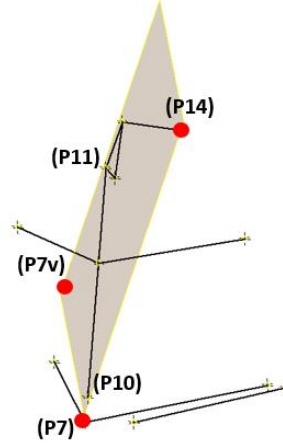


Figure 72 - Alignment plane of points

The constraint of keeping the points P10,P11,P12,P13 on this plane (*Figure 72*) is imposed directly in the Maple suspension model.

This new implementation increases a lot the computational cost of the optimization, but it is necessary to obtain a correct result in the suspension configuration also from a structural point of view.

In the Maple model of *Figure 73* and *Figure 74* can be seen in red the constraint plane generated as shown above.

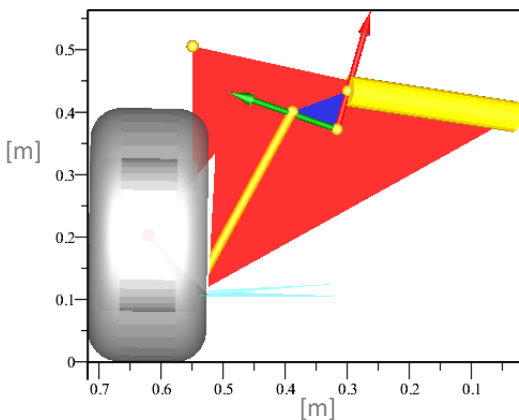


Figure 73 – Rear view of rear left suspension

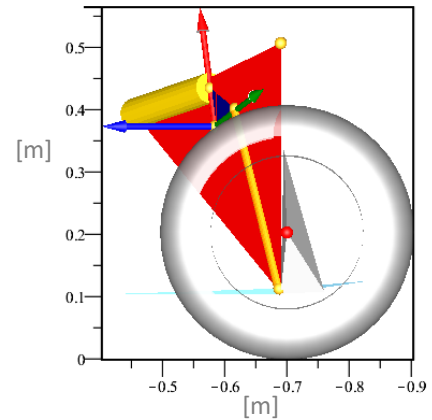


Figure 74 - Side view of rear left suspension

Another Reference system is put in the center of the roker's pivot point with the z axis perpendicular to the red plane of *Figure 73* and *Figure 74*. To find the direction of the z axis of this new reference frame is done a cross product between the two versors of the vectors that connect the points P7-P7v and P7-P14. This axis is then translated in the roker's pivot point P12.

The rocker rotations around this axis z is defined by the $\alpha(t)$ angle.

The angle between the two initial vectors, which vectors connect the point P7-P7v and P7-P14, is not 90 [deg] so another cross product between one of them and the new z vector is done.

The rocker's dimensions are the lengths l_{11} between P12 and P11 points and l_{13} between the points P12 and P13; another rocker's parameter is the angle between these two lengths expressed by η (Figure 75).

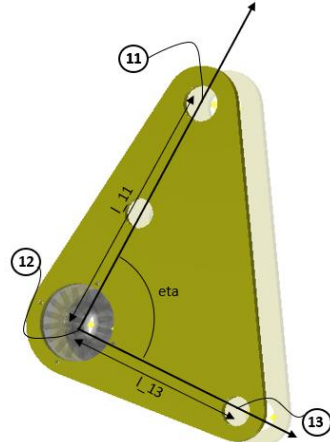


Figure 75 – Rocker's dimensions

Respect to the rocker's reference frame one of the two lengths l_{13} lies on its axis y. Instead the other one l_{11} is decomposed along the x and y axes of this reference frame. This is due to the fact that the η angle between the two rocker lengths can be different from 90 [deg] (Figure 76).

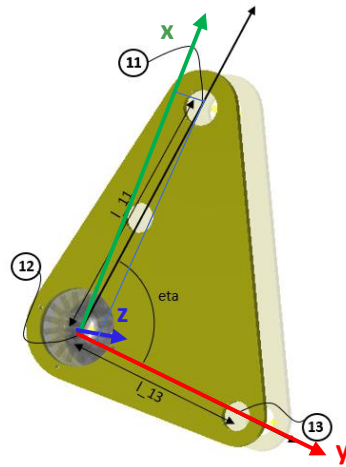


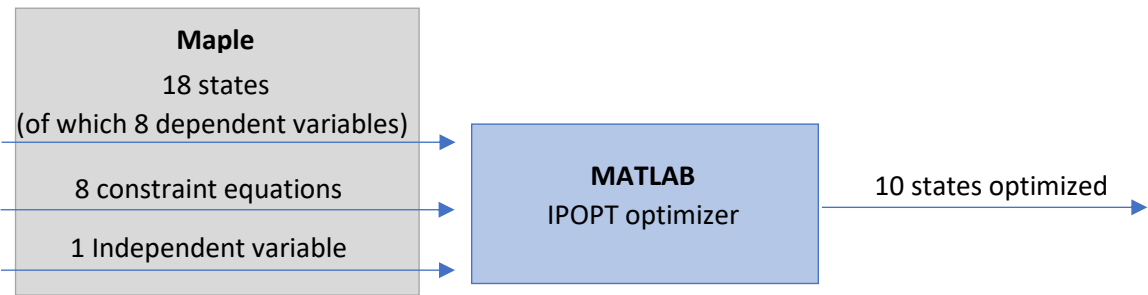
Figure 76 – Rocker's dimensions in their reference frame

At the six constraint equations are now added other two constraints for the new dependent variables. These two variables are $\Delta L_s(t)$ that simulates the shock absorber travel and the angle $\alpha(t)$ for the rockers roll around its pivot point P12. The two new constraints are added imposing that the distance between the points P10-P11 and P13-P14 must be constant (rigid bodies). These constraints allow the free rotation around the points P10, P11, P12, P13 and P14.

The new dependent variables as for the previous camber and toe optimization can change during the suspension travel. Instead the optimized states related to the suspension configuration must be the same during the motion because the suspension cannot change its configuration when it moves. As in the previous section to optimized only a single configuration the variables are taken as vectors.

The variables and constraints are then imported in Matlab environment where is done an optimization with the Ipopt software package.

The whole optimization process can be split in this form:



The optimized states are:

- L_{107} is the distance between the two points P10 and P7 of the 3D joint;
- $\Delta_{L_{1011}}$ is the variation of the push-rod length respect its initial value before the optimization;
- x_{12}, z_{12} are the coordinates of the rocker pivot; there is not the coordinate y_{12} because it is self-calculated in such a way this point lies on the plane (*Figure 72*);
- x_{14}, y_{14}, z_{14} are the coordinates of the shock absorber connection with the chassis;
- l_{13}, l_{11} the two lengths of the rocker and η the angle between them.

The initial length of the shock absorber is assumed to be constant because usually it is bought and its dimensions are standard. For this optimization it is taken as length the one of the shock absorber used in the *Chimera* vehicle: 0.308 [m], length at rest (*Figure 77*).



Figure 77 - Chimera's shock absorber

The state L_{107} to be optimized usually the smaller, the better. The limits related to this dimension are geometric: if it is too small it does not allow the positioning of the bolt to connect the 3D joint with the push rod (*Figure 78*).



Figure 78 – Assembly of the 3D printed joint with the push rod

Its values during the optimization can be assumed fixed and set at about 40 [mm]. This length allows a correct assembly of the bolt as can be seen in *Figure 78*.

Furthermore, must be noticed that the position of the connections of the rocker (P12) and the shock absorber (P14) with the chassis in this optimization are assumed to be near the positions of the ones of the *Chimera* vehicle. These two points for the future optimizations of any other vehicle depend a lot on the chassis shape.

As independent variable it is assumed the wheel displacement δ_w .

7.2.3 Results

The time spent to do this optimization is about three hours: forty-five minutes to generate the functions derivatives with Adigator toolbox and two hours and fifteen minutes to find the optimized values with Ipopt.

The high value of the time is given due to the complexity of the constrains implemented to guarantee a correct suspension motion and the structural points positions.

The values of the ten optimized states found with the motion ratio optimization can be seen in *Table 9*.

	Reference Frame		
P12	$x_{12} = -0.5811$ [m]	$z_{12} = 0.3693$ [m]	Absolute (ground)
P14	$x_{14} = -0.4496$ [m]	$y_{14} = 0.0253$ [m]	$z_{14} = 0.3501$ [m]
	$\Delta_{L_{1011}} = -0.036$ [m]	$L_{107} = 0.04$ [m]	
	$L_{13} = -0.09$ [m]	$L_{11} = -0.0745$ [m]	

$$\mu = 1.4 \text{ [rad]}$$

Table 9 - Optimization motion ratio results

The point P12 in *Table 10* does not have the “y” coordinate because it is automatically calculated by the implemented Maple code. The distance L_{107} respects the previous considerations of *Figure 78*.

The graphical meaning of the states in *Table 9* can be graphically displayed from *Figure 68*.

These states values are than used in the Maple suspension model to derive the Motion ratio curve (*Figure 79*).

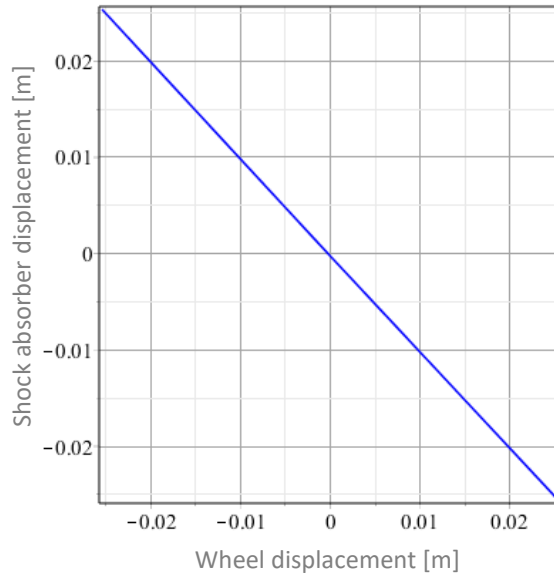


Figure 79 - Motion ratio curve with optimized points

Plotting the curve found with the desired one in Matlab environment is obtained:

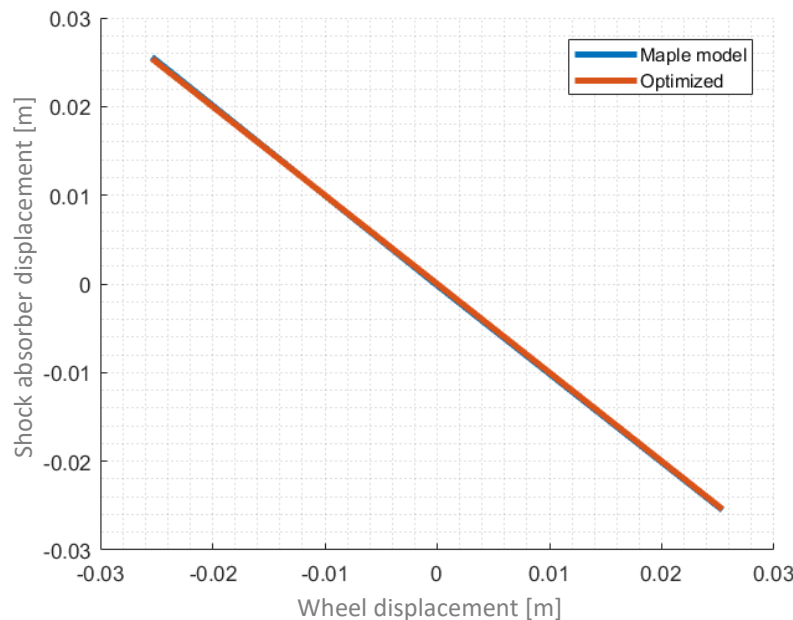


Figure 80 - Optimized and Maple model motion ratio

From *Figure 80* can be seen that the two Motion ratio curves, the ideal and the model one, are overlapping.

During the wheel displacement the rocker rotation $\alpha(t)$ around its pivot point (P12) is plotted in *Figure 81*. All the angle values are evaluated with respect to the absolute reference system.

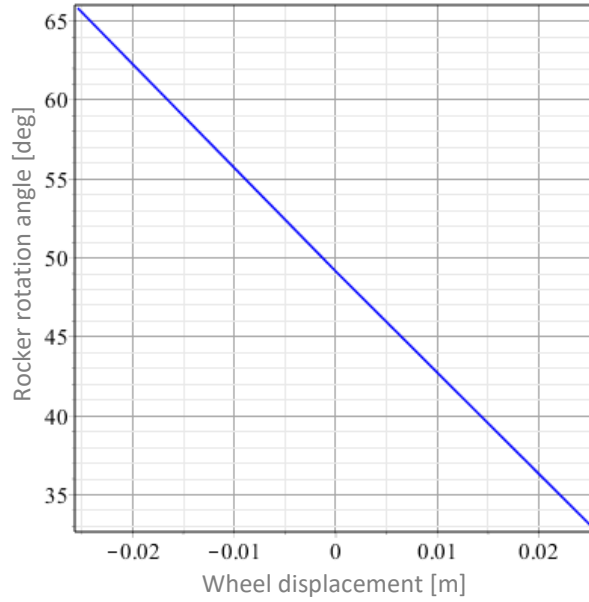


Figure 81 - Rocker rotation angle

Starting from the value of the 32.84 [deg] when the wheel displacement is at the negative limit of -0.0254 [m] the rocker angle increases its value up to 65.77 [deg]. The value of 65.77 [deg] is reached when the wheel displacement is +0.0254 [m]. The rocker total rotation around its pivot point between the two extreme limits of the wheel is 32.93 [deg].

When the wheel displacement is zero (initial configuration) the rocker angle is 49.14 [deg] respect to the absolute reference frame (*Figure 82*).

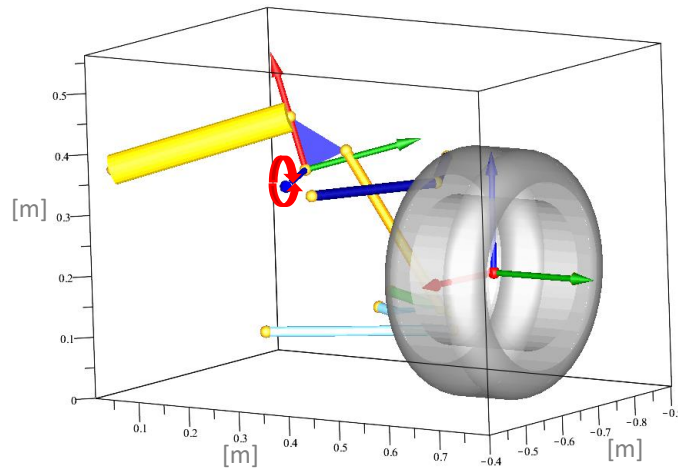


Figure 82 - Initial rocker configuration (wheel displacement set at zero)

The optimized points of the components that affect the motion ratio with the final suspension configuration are plotted in *Figure 83*.

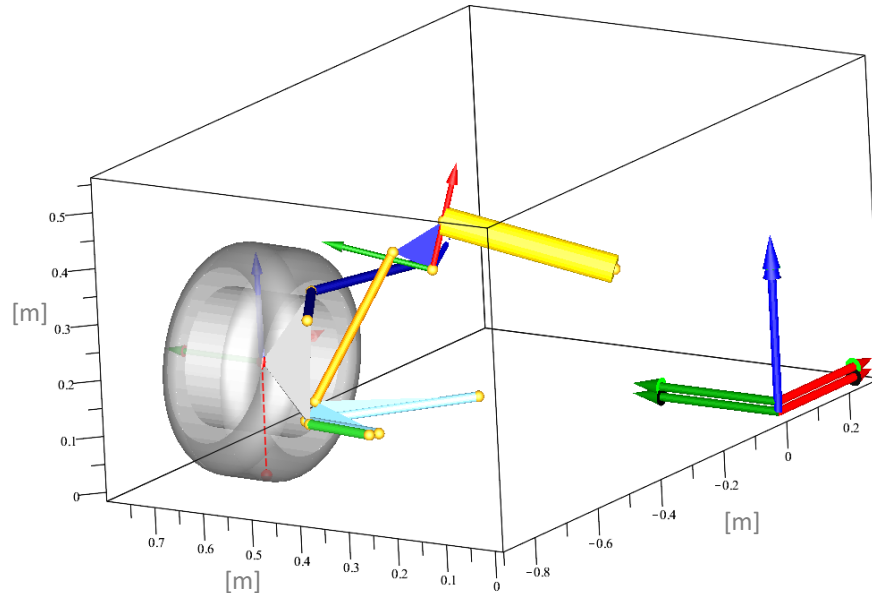


Figure 83 - Final optimized suspension hardpoints

After all this optimizations work, adding the rear right suspension to the model, the final model of the rear suspensions configuration is plotted in *Figure 84*. The rear right suspension is obtained given the symmetry of the vehicle.

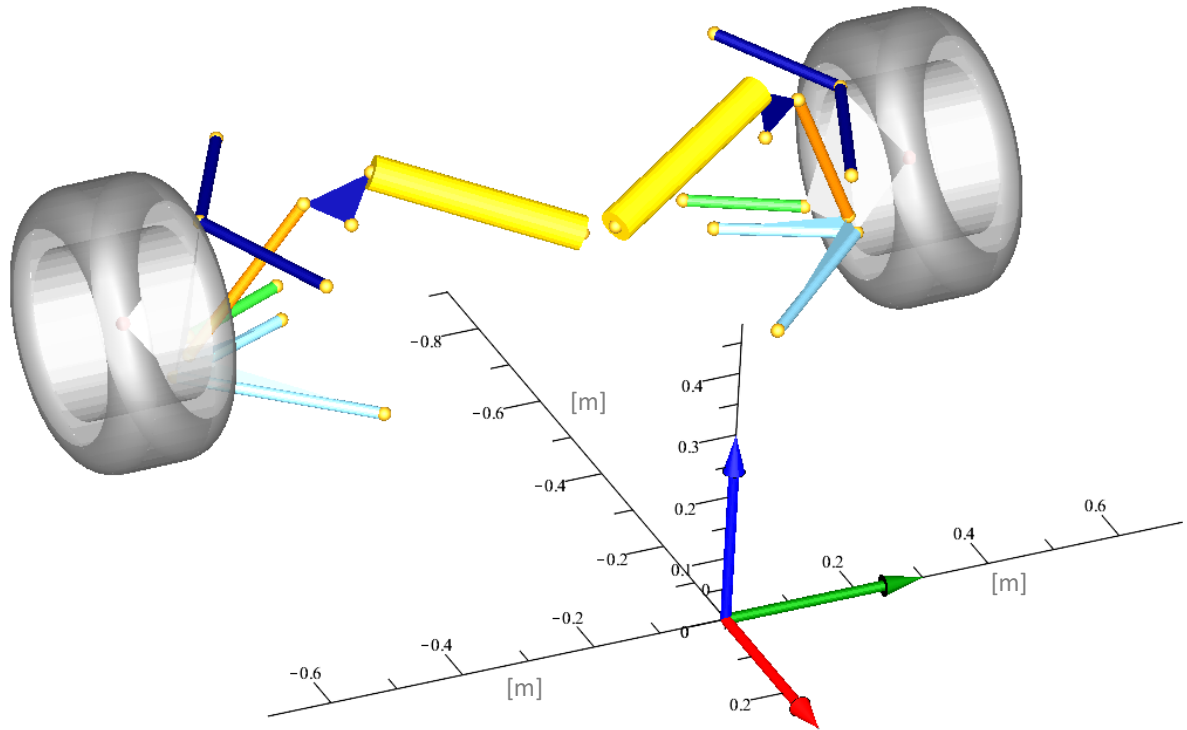


Figure 84 - Optimized rear suspensions configuration

7.3 Validation Model with Motion ratio

To validate the Maple model of the suspension is calculated the behaviour of the motion ratio between the wheel and the shock absorber of the rear left suspension configuration. The suspension takes in exam is the one built in the first vehicle “*Chimera*”. Finally, the motion ratio found is compared with the ideal one obtained from the Maple software.

The precision of this validation test is in the order of tenth of millimeter. To have a significant change in the motion ratio target this precision is enough.

This is a pure kinematic test where all the forces necessary to generate the suspension motion are not considered because the only data compared to obtain the motion ratio behaviour are the wheel and the shock absorber displacements.

In *Figure 85* is shown the work stations to make the test measurements.

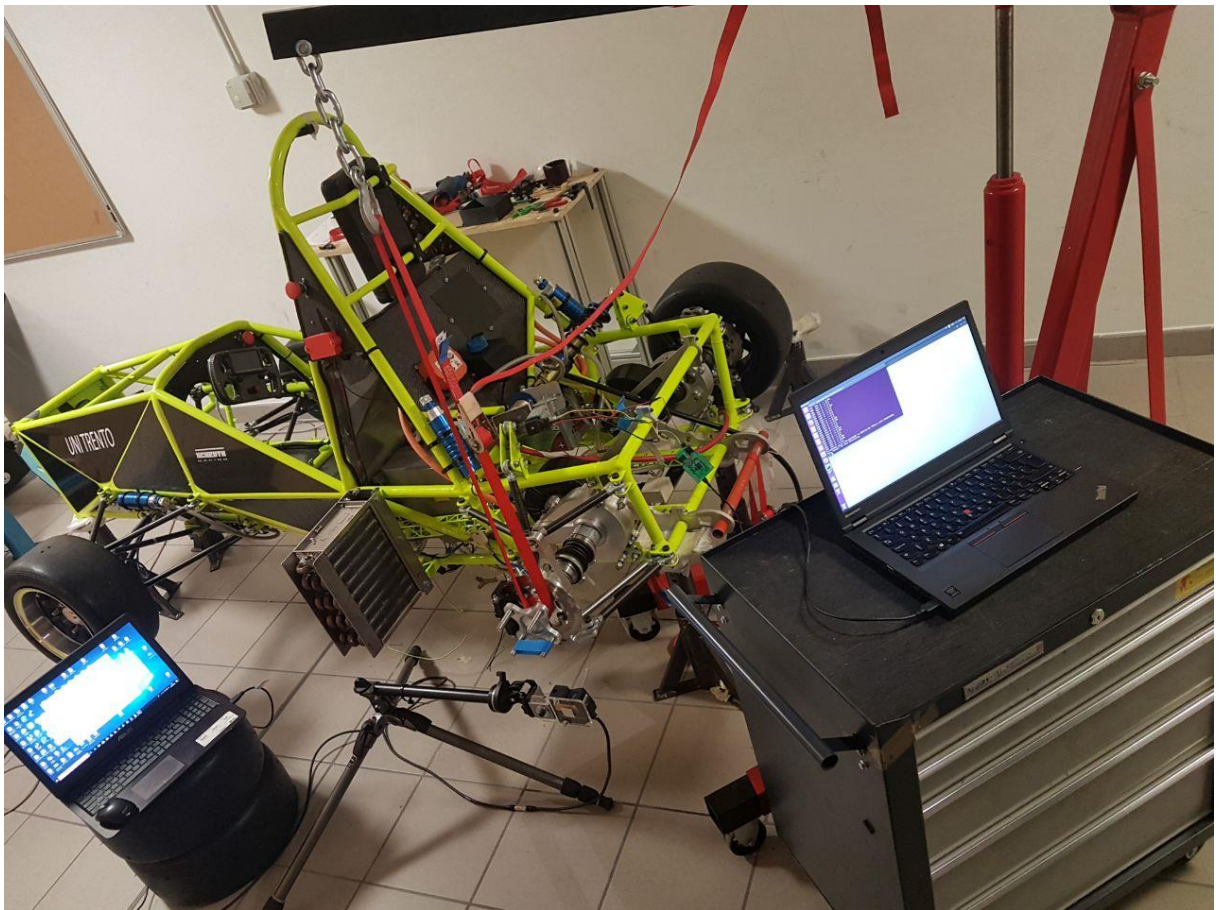


Figure 85 - Instruments layout for the motion ratio validation

7.3.1 Sensors

The sensors used in this validation are used to measure the wheel and shock absorber displacements during the suspension motion.

The sensor used to measure the wheel displacement is:

- KEYENCE LK-G157: It is an high resolution laser that can capture a distance variation in the order of microns. It is however used in this validation even if this precision it is not necessary for the final goal. Its reference distance is about 150 [mm] with a measuring range of ± 40 [mm] (*Figure 86*).

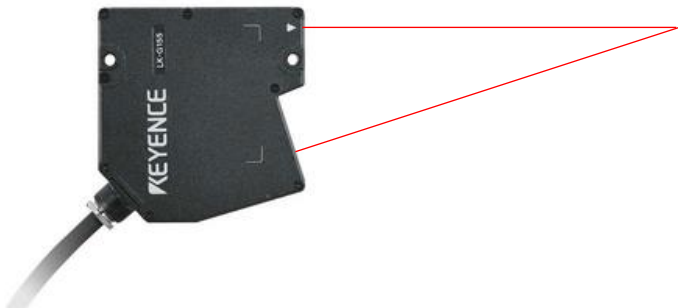


Figure 86 - Keyence LK-G157
Retrieved February 10, 2018, from <https://www.keyence.it/>

It is used the software LK-Navigator to make the optimal settings of the LK-G and to collect data from a PC. This software gives also the possibility to initialize the first reading as the zero distance and to choose the sampling frequency.

How can be seen from *Figure 87* during the test the tire was disassembled from the hub to allow a better measure. The laser, in fact, makes the triangulation with the plane given by the scotch appropriately placed on the hub.



Figure 87 - Laser station

Instead the sensor used to measure the shock absorber displacement is:

- WAYSEAR KTC 150: it is a potentiometer with a maximum range of 150 mm.

The acquisition (ADC reading: Analog to Digital Conversion) and its relative calibration is done thanks to a microPython and the laser sensor (*Figure 86*). During the calibration the sensor and the laser used to calibrate it are fixed on the same plane given by a ground steel plate. Furthermore, the laser is placed perpendicular to the potentiometer plane (*Figure 88*).

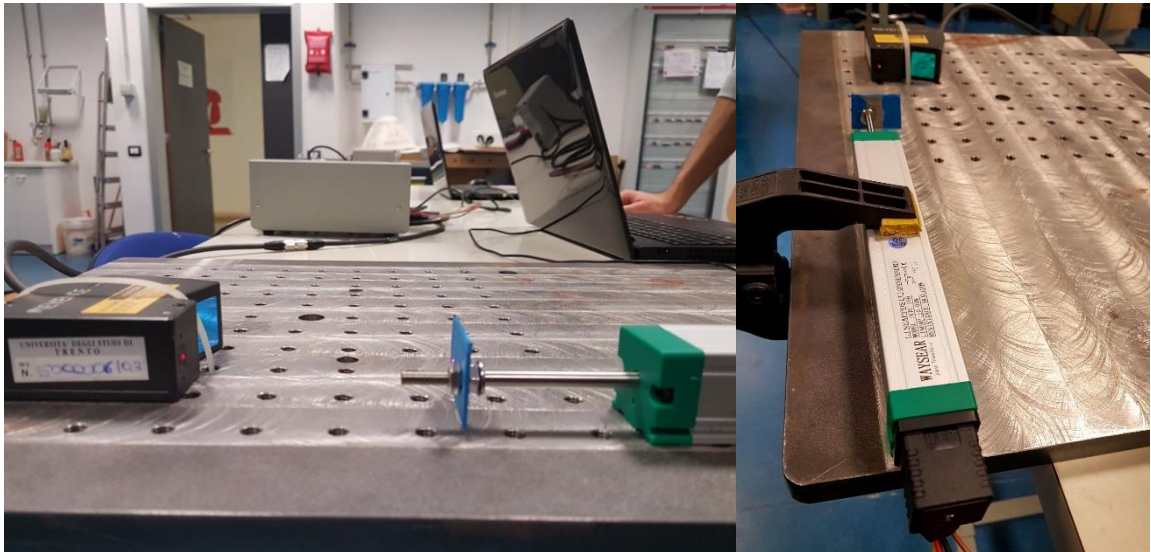


Figure 88 - Displacement sensor calibration

Once the acquisitions are performed a regression model is used to find the coefficient to convert the analogue reading in a distance.

The linear regression is done in matlab using the *polyfit* command (*Figure 89*).

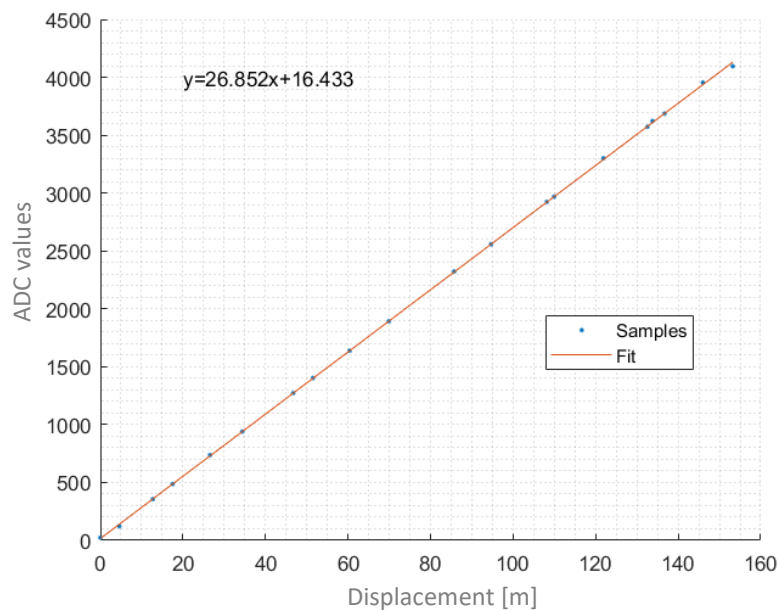


Figure 89 - Linear regression

From the equation derived from the previous regression (*Figure 89*) can be extracted the coefficient used to find the distances values from the fit equation $y = 26.852x + 16.433$. Therefore to convert a ADC value in a displacement one is done dividing the value for the regression coefficient 26.852.

In the Phyton code is also implemented the function that keeps the first ADC reading as the initial zero value distance.

7.3.2 Assumptions

The ends of the sensor displacement (WAYSEAR KTC 150) are considered fixed to the shock absorber during the suspension motion without any possible displacement. This is possible because to fix this sensor are used steel plates with a thickness of 4 [mm] that guarantee the stiffness in the connection (*Figure 90*).

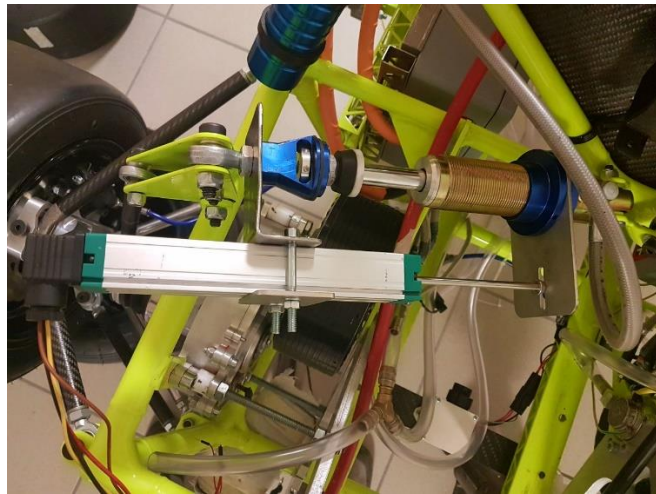


Figure 90 - WAYSEAR KTC 150 / Shock absorber connection

The bearings used in the suspensions group were bought by the SKF company. The producer for the series that are used in this vehicle guarantees a tolerance that not allow games of the order of magnitude of 1/10 [mm] so it is assumed that their influence is null. Furthermore, to reduce their influence in the displacement value of the shock absorber of its two bearings, they are not considered in this measure. It is possible connecting the WAYSEAR KTC 150 instrument between them.

The rockers and the 3D printed joints are realized respectively with the laser cutting machine and with the steel 3D printer. Both two machines guarantee a precision less than one tenth of a millimeter. Therefore, their dimensions are assumed the same to the ideal ones.

The *spring* on the shock absorber is removed because the forces during the test are not considered (*Figure 90*).

7.3.3 Lengths check

The components that can be affected to some lengths error are the suspensions carbon arms and the shock absorber. Their lengths are measured to see if their values are the same to the ideal ones in the Maple and CAD model (*Figure 91*). Some variations respect the built suspensions (*Figure 92*) could be relative to their production or assembly process.

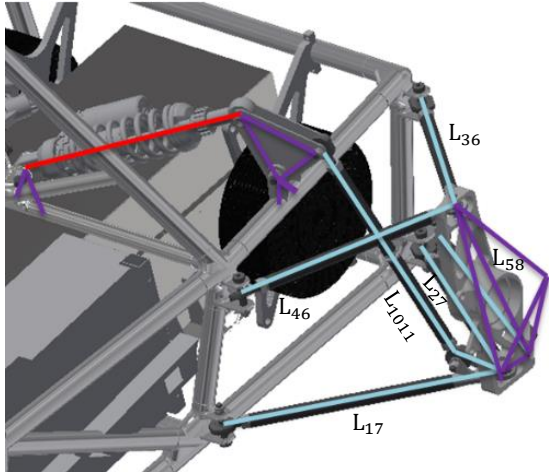


Figure 91 - CAD model rear left suspension



Figure 92 - Built model rear left suspension

	IDEAL	BUILT
L_{17}	35,28	35,4
L_{27}	28,27	28,3
L_{36}	29,24	29,2
L_{46}	21,63	21,7
L_{58}	25,02	24,02
L_{1011}	33,52	33,3

Table 10 - Arms lengths

The ideal and built lengths are not very different (*Table 10*) but to have a more accurate comparison the maple model is modified using the actual built lengths values. The dimensions of the shock absorber are respected.

The working range of the shock absorber is between the 281,69 [mm] (fully compressed) and 334,62 [mm] (fully extended). The Δ distance interval between these two extreme positions is 52,93 where the initial shock absorber working position is 308,08 [mm]. Respect to this position the shock absorber can change its length about \pm 26 [mm].

The suspension travel between the full compression of the shock absorber and the position when it is fully extended is the same to the one obtained inverting its motion.

To find the motion ratio between the displacement of the wheel and the shock absorber is done by compressing the shock absorber and moving it respect its fully extended position.

7.3.4 Results

The simulation of *Figure 93* shows the shock absorber travel measured with the sensor displacement (WAYSEAR KTC 150).

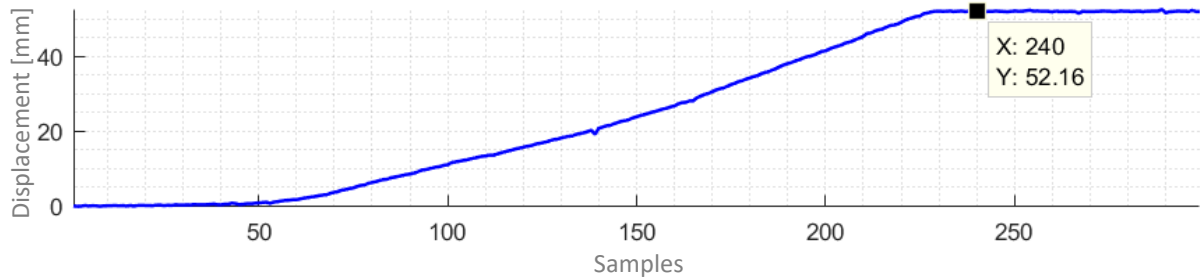


Figure 93 - Shock absorber travel

The trend of the curve is not linear because it is done moving down the wheel thanks to a folding hydraulic crane that not guarantee a linear motion.

The sampling rate is 100 Hz but the samples that were selected were separated up to three units, and then an average is made to reduce the noise. Nevertheless some noise in the measure remains.

Different thing for the measure done with the more accurate laser sensor (KEYENCE LK-G157) (*Figure 94*) with a sample rate of 300 Hz.

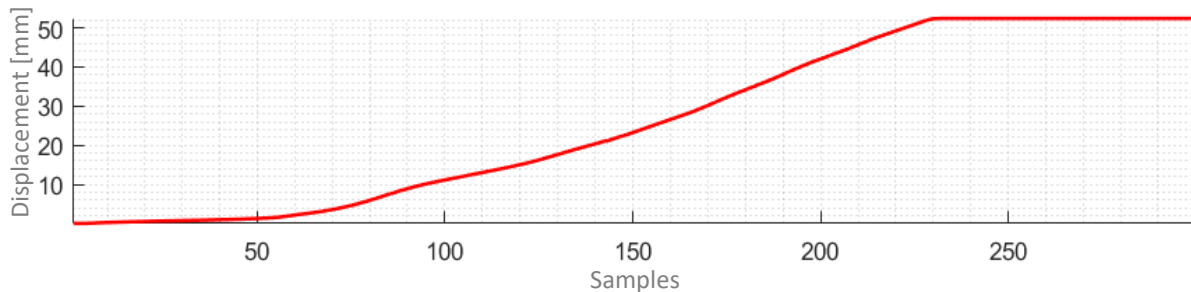


Figure 94 - Wheel travel

Once that the two curves with the two different instruments are found, they are synchronized and plotted in the same graph (*Figure 95*).

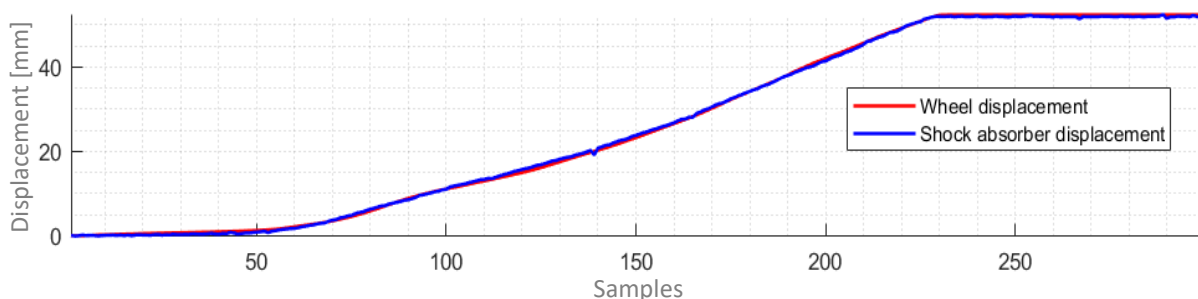


Figure 95 - Wheel and shock absorber displacement

In conclusion the wheel displacement vs shock absorber one is plotted to be compared with the one obtained with the Maple model. (*Figure 96*)

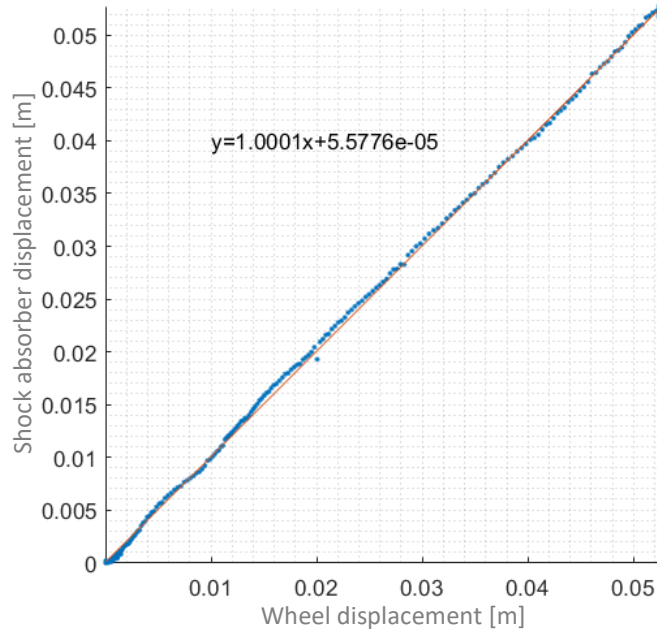


Figure 96 - Motion ratio measured

The same graph obtained with the maple model, where are used the new lengths of *Table 10*, is plotted in *Figure 97*.



Figure 97 - Motion ratio from ideal Maple model

The curve equation of *Figure 97* is:

$$y = 1.0113x + 4.8225 * 10^{-5}$$

The wheel displacement in the plots of *Figure 96* goes from 0 to 52 [mm] where 0 is the shock absorber fully compressed configuration; instead in the plot of *Figure 97* the wheel displacement goes from -26 [mm] to +26 [mm] because the 0 corresponds to the shock absorber initial working configuration.

The Motion ratios of *Figure 96* and *Figure 97* are then plotted on the same graph from 0 to 52 [mm] (*Figure 98*).

The behaviour and the final value of the measured Motion ratio and the ideal one from the Maple model can be assumed to be the same because the difference between them is negligible (*Figure 98*).

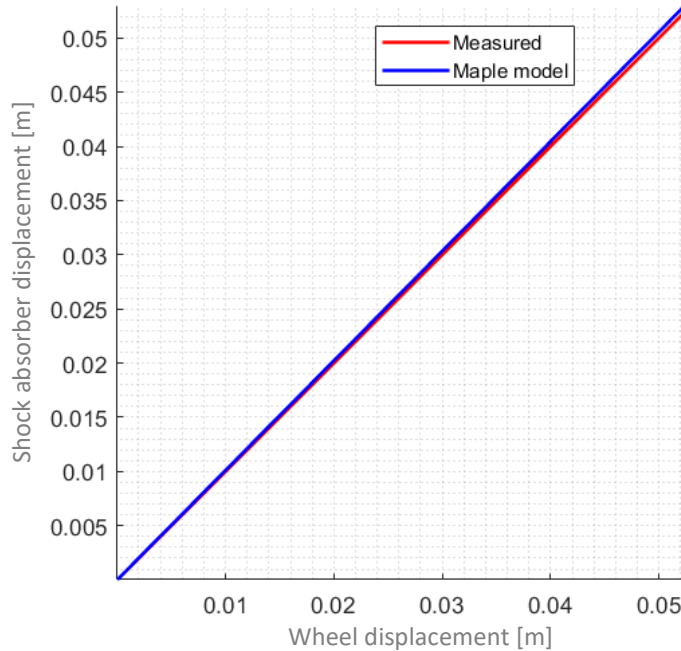


Figure 98 - Motion ratio measured and the one from Maple model

With this validation it is verified that the suspensions built of the *Chimera* vehicle respect the design characteristic about the Motion ratio.

CONCLUSIONS AND FUTURE WORK

Conclusions

The final results of this thesis work, related to the kinematic optimization of a racing car suspension, show all the potential of the implemented work methodology.

In fact, thanks to this optimization instrument, it is possible to find the optimal kinematic points of any suspension configuration, starting from the “g-g” diagram optimized curves.

The key points of this thesis can be summarized in the following points:

- the obtained results are related to the optimization of a rear left suspension for a FSAE car but can be used for every other type of suspension;
- the optimized camber and toe curves of this thesis are not the ones of a general racing car but are specific of the UniTn FSAE car, and are obtained from its “g-g diagram”;
- thanks to the user-friendly interfaces, at the beginning of each optimization the user is free to set the values of different optimization parameters;
- the suspension model that better approximates the optimal camber and toe curves are automatically calculated from the software, as well as the position of the suspension components that affect the Motion ratio parameters, according to the desired value;
- the Maple model goodness is demonstrated through its validation, that comes from the comparison between the calculated Motion ratio and the real one, measured on the first FSAE car built by the team of University of Trento.

The results obtained for every optimization are influenced by the initial guesses of the input parameters; e.g., in the case of the “g-g” diagrams, the main factors that can change their shapes are the ones related to the tires.

The advantage to have used the Ipopt software package lies on its calculation power and the possibilities to manage a lot of input variables. The Adigator toolbox has allowed to save time in the calculation of the function derivatives.

Despite this, the time spent for the whole activity is high, because of the complexity of the multiple optimizations. The longer step consists in finding the optimal camber and toe coefficients equations using the “g-g” diagram.

Future work

A future work, already planned, will be to use the optimization instrument described in this thesis in order to design the new suspensions' vehicle of the E-Agle Trento racing team.

During each optimization process it will be important to share the work with colleagues that works on the wheel group and the vehicle chassis; in fact, optimal solutions for the suspensions may not be the same for the other components groups.

One further future development could be the validation of the “g-g” diagram shape comparing the simulation results with the data collected during the races.

REFERENCES

- [1] Formula Student Rules 2018. Available at:
https://www.formulastudent.de/fileadmin/user_upload/all/2018/rules/FS-Rules_2018_V1.0.pdf (1 January 2018)
- [2] William F. Milliken and Douglas L. Milliken, *Race car vehicle dynamics*, Society of Automotive Engineers, USA, 1995.
- [3] Massimo Guiggiani, *The Science of Vehicle Dynamics*, Springer, 2014
- [4] Emmanuele DiBenedetto, *Classical Mechanics – Theory and Mathematical Modeling*, Birkhäuser, USA, 2011
- [5] Kasprzak, E. and Gentz, D., "The Formula SAE Tire Test Consortium-Tire Testing and Data Handling," SAE Technical Paper 2006-01-3606, 2006, doi:10.4271/2006-01-3606.
- [6] Hans Pacejka, *Tire and Vehicle Dynamics*, Butterworth-Heinemann, 2012
- [7] Dr, F. Biral, *Dynamics and control of vehicle and robots* – lecture notes 2017-2018, University of Trento
- [8] Dr. Ir. I.J.M. Besselink, *Vehicle Dynamics* - lecture notes 2015, Eindhoven University of Technology
- [9] Giovanni Naldi and Lorenzo Pareschi, *Matlab Concetti e progetti*, Apogeo, Second edition 2012
- [10] Andreas Wächter and Lorenz T. Biegler, *On the implementation of an interior-point filter line-search algorithm for large-scale nonlinear programming*, Available at: <http://cepac.cheme.cmu.edu/pasilectures/biegler/Ipopt.pdf> (25 January 2018)
- [11] Andreas Wächter, *Short Tutorial: Getting Started With Ipopt in 90 Minutes*, USA. Available at:
<http://citeseerx.ist.psu.edu/viewdoc/download?doi=10.1.1.210.3547&rep=rep1&type=pdf> (15 January 2018)
- [12] Matthew J. Weinstein, *Algorithm: ADiGator, a Toolbox for the Algorithmic Differentiation of Mathematical Functions in MATLAB Using Source Transformation via Operator Overloading*, University of Florida. Available at:
<http://www.anilvrao.com/Publications/SubmittedJournalPublications/adigator-CALGO.pdf> (15 January 2018)

APPENDIX A: Magic Formula

The vehicle dynamics depends on the forces and moments developed by the contact between the tire and the ground (*Figure A.1*):

- longitudinal force F_x ;
- lateral force F_y ;
- the self-aligning moment of the wheel M_z .

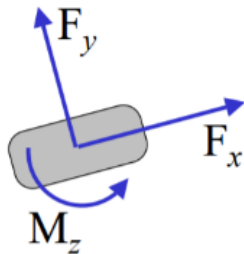


Figure A. 1 -Tire forces and moments

All the tire forces arise as a result of slip within the contact patch. Slip can be either lateral or longitudinal.

The Magic formula can be seen as a box with the following inputs and outputs:

Inputs:

- Longitudinal slip k
- Side slip angle α
- Camber angle γ
- Vertical load F_z

Outputs:

- Longitudinal force F_x
- Lateral force F_y
- Self aligning moment M_z

The sign conventions for forces, moments and wheel slips are represented by the following configurations:

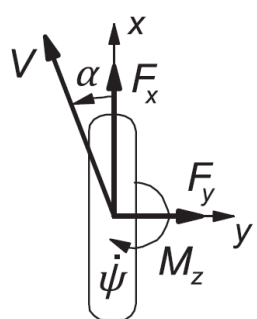


Figure A. 2 - Side angle (top view)

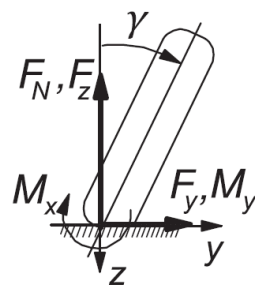


Figure A. 3 - Inclination/camber angle (rear view)

taken from: Tire and Vehicle Dynamics (2012)

The wheel slip convention is the following: for the side slip ($\tan\alpha = -\frac{V_{sy}}{V_x}$) and for the longitudinal slip or slip ratio ($k = -\frac{V_{sx}}{V_x}$).

The *side slip angle* is the difference between the direction the tire is facing, and its velocity. "0" means that the tire is going straight ahead (no slip). It is a result of the tire being forced in a different direction to the vehicle it is attached to. A good way of visualising this is to consider a car travelling in a straight line and then to apply a steering angle. The result is shown in *Figure A.4*. Can be seen that the rubber is distorted and slips back as it leaves the contact patch. The elastic forces generated in this region have equal and opposite reactions with the road and this is the origin of lateral tire force (*Figure A.4*).

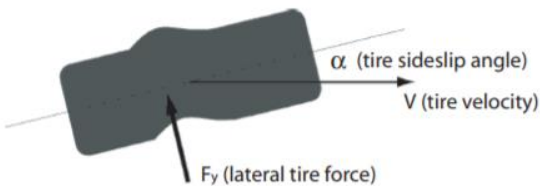


Figure A. 4 - Lateral tire deformation
taken from: Tire and Vehicle Dynamics (2012)

The *slip ratio* is the spin velocity divided by its actual world velocity. A slip ratio of -1 means full braking lock; a ratio of 0 means the tire is spinning at the exact same rate as the road is disappearing below it. A slip ratio of 1 means it is spinning. That is caused by the torque from the engine trying to rotate the tire faster than it would in a free-rolling condition. This compresses the tread as it enters the contact patch and this rubber must slip back as it leaves the contact patch (*Figure A.5*). As with lateral force, this slip causes a resultant force. Braking is obviously the same process but in reverse (*Figure A.6*).

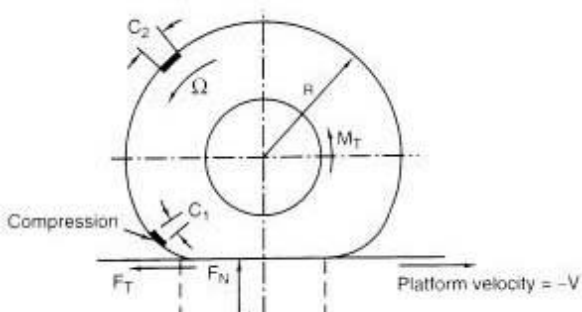


Figure A. 5 – Tire traction

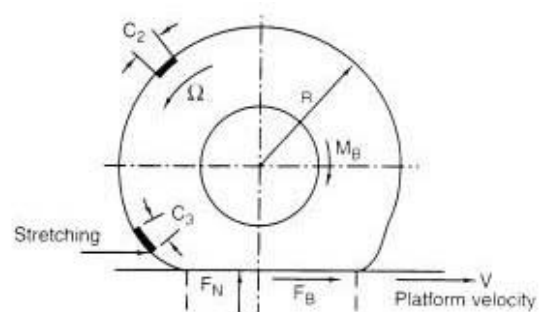


Figure A. 6 - Tire braking

taken from: Tire and Vehicle Dynamics (2012)

The tire forces, both the longitudinal and lateral force, increase almost proportionally with the vertical load F_z .

A tire model is necessary to allow to find the dynamic calculation of these forces and moments. A widely used semi-empirical tire model to calculate steady-state tire force and moment characteristics for use in vehicle dynamics studies is based on the so called *Magic formula*.

Although, over the years, several versions of the Magic formula have been developed, they are all based on the following function:

$$y = D \sin[C \arctan\{Bx - E(Bx - \arctan Bx)\}] \quad (\text{A.1})$$

with

$$Y(X) = y(x) + S_V \quad (\text{A.2})$$

$$x = X + S_H \quad (\text{A.3})$$

where Y is the output variable F_x , F_y or possibly M_z and X the input variable $\tan\alpha$ or k , and B is the stiffness factor, C the shape factor, D the peak value, E the curvature factor, S_H the horizontal shift, and S_V the vertical shift.

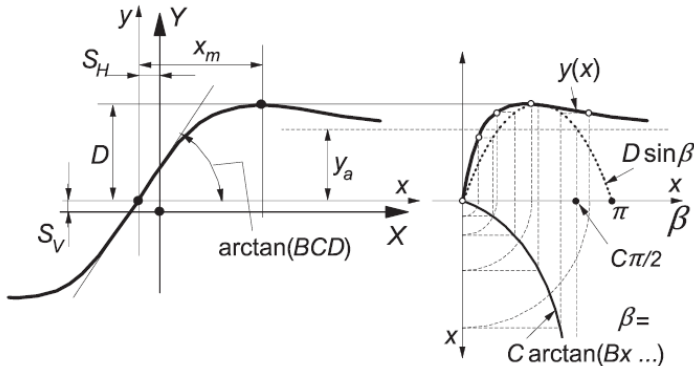


Figure A. 7 - Curve produced by the original sine version of the Magic Formula, Eqn (A.1)
taken from: Tire and Vehicle Dynamics (2012)

The *Magic Formula* $y(x)$ typically produces a curve that passes through the origin $x = y = 0$, reaches a maximum, and subsequently tends to a horizontal asymptote. For given values of the coefficients B , C , D , and E , the curve shows an anti-symmetric shape with respect to the origin. To allow the curve to have an offset with respect to the origin, two shifts S_H and S_V have been introduced. A new set of coordinates $Y(X)$ arises as shown in *Figure A.7*. The formula is capable of producing characteristics that closely match measured curves for the side force F_y (and if desired also for the aligning torque M_z) and for the fore-and-aft force F_x as functions of their respective slip quantities: the slip angle α and the longitudinal slip k with the effect of load F_z and camber angle γ included in the parameters.

Figure A.7 illustrates the meaning of some of the factors by means of a typical side force characteristic. Obviously, coefficient D represents the peak value (with respect to the central x -

axis and for $C \geq 1$) and the product BCD corresponds to the slope at the origin ($x=y=0$). The shape factor C controls the limits of the range of the sine function appearing in formula (A.1) and thereby determines the shape of the resulting curve. The factor B is left to determine the slope at the origin and is called the stiffness factor. The factor E is introduced to control the curvature at the peak and, at the same time, the horizontal position of the peak.

The curves produced by the Magic Formula with the *Chimera* tire data are plotted in *Figure A.8* and *Figure A.9*. They have as inputs once the longitudinal slip k and once the side slip angle α with the outputs respectively the pure longitudinal F_{x0} and the lateral forces F_{y0} divided by the nominal load F_z .

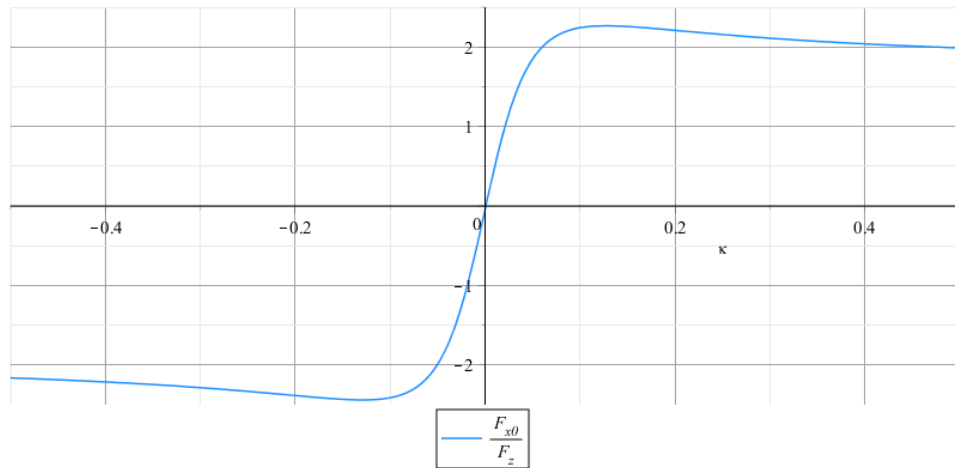


Figure A. 8 - Magic formula model: longitudinal slip ratio vs longitudinal force/nominal load

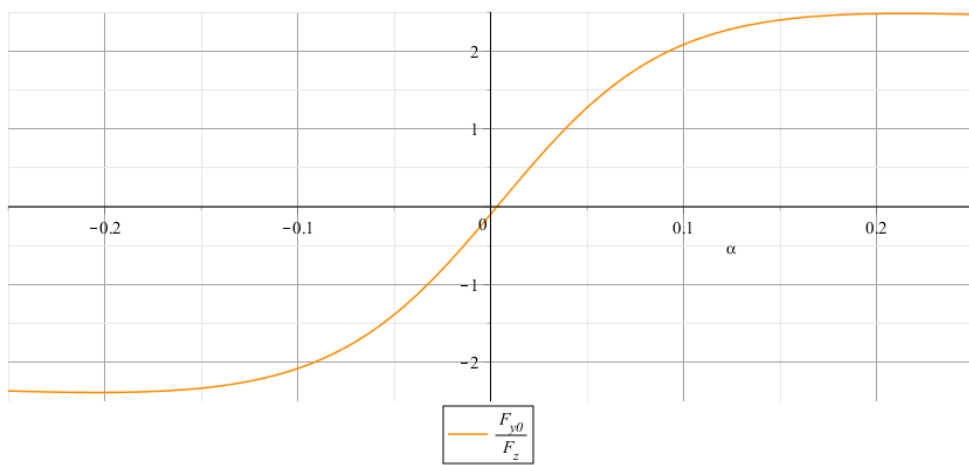


Figure A. 9 - Magic formula model: lateral slip angle vs lateral force/nominal load

The effect of the load F_z and the camber angle γ on the previous Magic formula curves based on *Chimera* tire data are shown below.

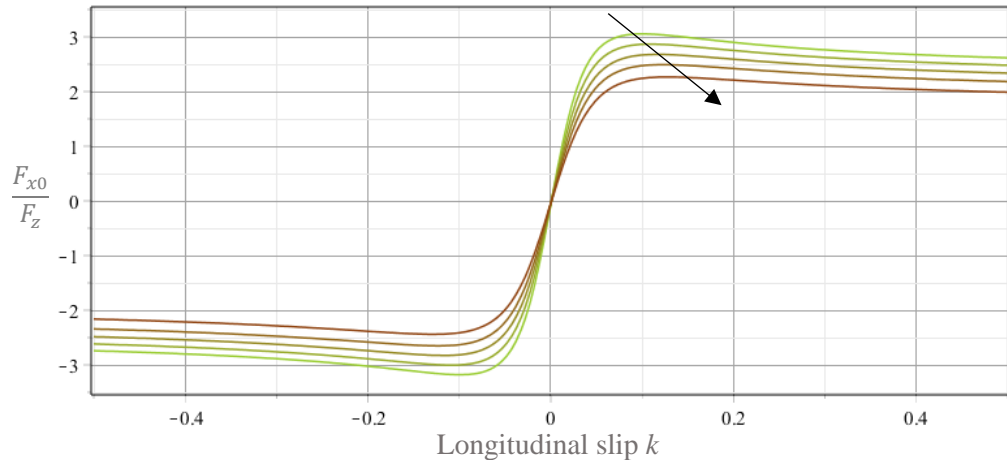


Figure A. 10 - Vertical load effect on longitudinal slip ratio vs longitudinal force/nominal load curve

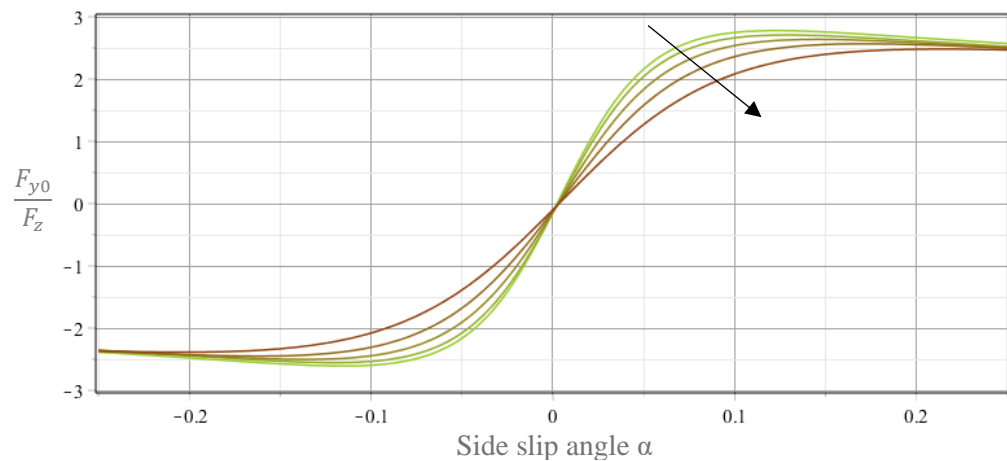


Figure A. 11 - Vertical load effect on lateral slip angle vs lateral force/nominal load curve

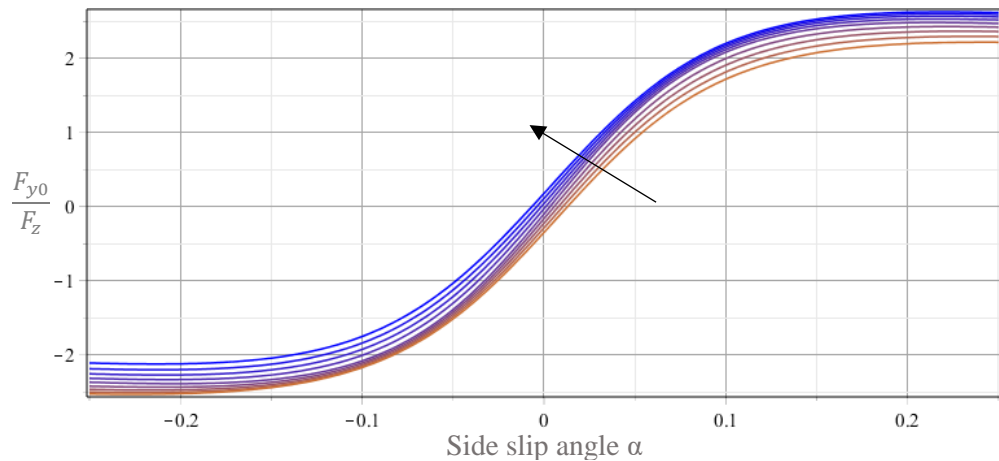


Figure A. 12 - Camber effect on lateral slip angle vs lateral force/nominal load curve

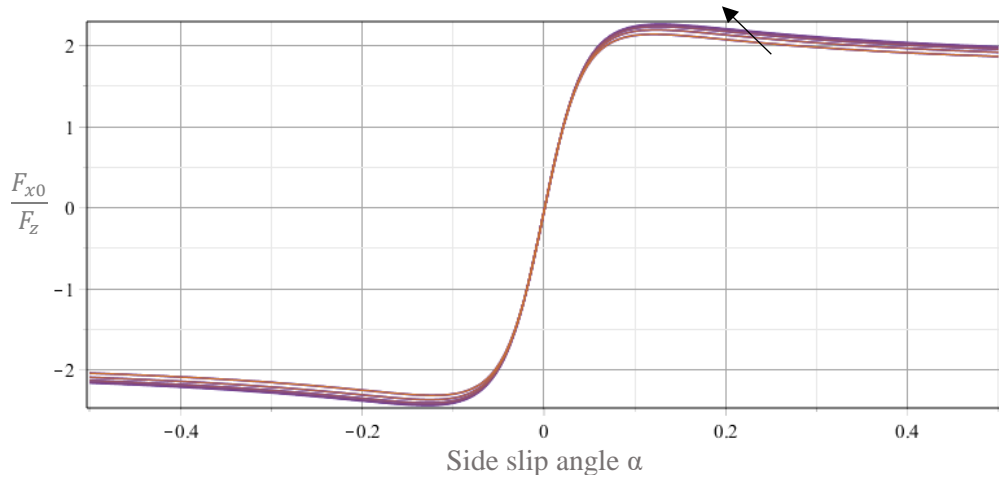


Figure A. 13 - Camber effect on longitudinal slip ratio vs longitudinal force/nominal load curve

The arrows in *Figure A.10* and *Figure A.11* show the variation of the vertical load from 50 [N] to 889 [N]. Instead the arrow in *Figure A.12* and *Figure A.13* represents the camber angle variation from +4 [deg] to -4 [deg]. In *Figure A.12* is evident how the wheel camber may give rise to a considerable offset of the F_y vs α curves.

In the magic formula tire model are considered not only the pure longitudinal and lateral slip but also the *combined slip*. The reduction of longitudinal forces and lateral forces for combined slip conditions is considered by applying a weighting function to the “pure” characteristic.

In *Figure A.14*, a three-dimensional graph is shown indicating the variation of F_x and F_y with both α and k . The initial ‘S’ shape of the F_y vs k curves (at small α) due to the vertical shift function is clearly visible.

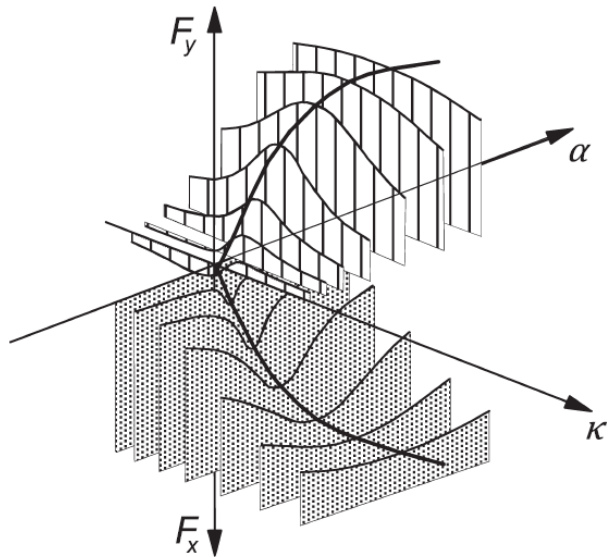


Figure A. 14 - Three-dimensional graph of combined slip force characteristics
taken from: Tire and Vehicle Dynamics (2012)

Plotting the lateral and longitudinal force together with both α and k variables is obtained the ellipse of adherence in a two-dimensional plane. In *Figure A.15* it is plotted normalized respect the vertical load F_z . It widens almost proportionally with the vertical load. Increasing the load by 10% the ellipsis of adherence widens less than 10%.

Some other considerations are done below to explain better its meaning (*Figure A.15*).

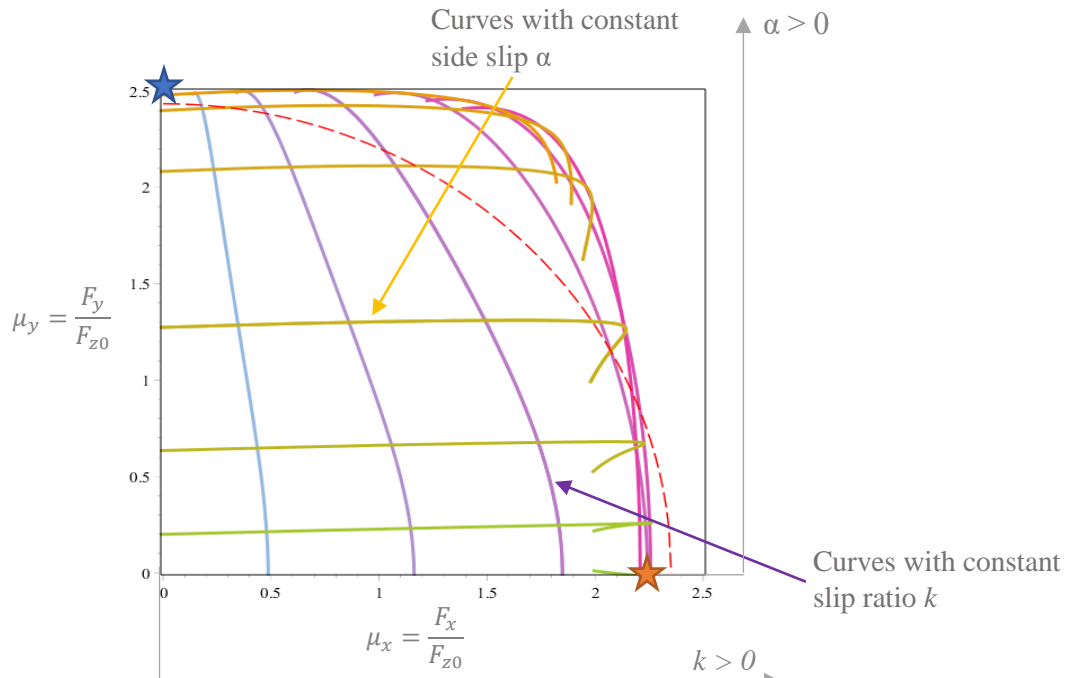


Figure A. 15 - Ellipse of adherence

★ : The maximum and minimum values for the lateral force there are for $k = 0$ therefore without traction on the wheels.

★ : The maximum and minimum values for longitudinal force there are for $\alpha = 0$ therefore with wheels aligned with the direction of the vehicle

APPENDIX B: IPOPT algorithm

Ipopt implements an interior point line search filter method that aims to find a local solution of (5.5)-(5.7). This algorithm only tries to find a local minimum of the problem so if it is necessary an maximization must be convert the problem minimizing the negative objective function. Moreover if the problem is nonconvex, many stationary points with different objective function values might exist, and the value at which it converges depends mainly on the starting point.

Internally, Ipopt replaces any inequality constraint in (5.6) by an equality constraint introducing a new bounded *slack variable* (e.g., $g_i(x) - s_i = 0$ with $g_i^L \leq s_i \leq g_i^U$), so that bound constraints are the only inequality constraints.

To simplify the notation it is assumed that all variables have only lower bound of zero, so the equations (5.5)-(5.7) become:

$$\min_{x \in \mathbb{R}^n} f(x) \quad (\text{B.1})$$

$$s.t. \quad c(x) = 0 \quad (\text{B.2})$$

$$x \geq 0 \quad (\text{B.3})$$

As an interior point (or “barrier”) method, Ipopt considers the auxiliary barrier problem formulation:

$$\min_{x \in \mathbb{R}^n} \varphi_\mu(x) := f(x) - \mu \sum_{i=1}^n \ln(x_i) \quad (\text{B.4})$$

$$s.t. \quad c(x) = 0 \quad (\text{B.5})$$

where the bound constraints (B.3) are replaced by a logarithmic barrier term which is added to the objective function. The optimal solution of new configuration problem (B.4)-(B.5) will be in the interior feasible space defined by (B.3) . Outside this region ($x_i < 0$) the term $\ln(x_i)$ is undefined.

The optimal solutions of (B.4)-(B.5) problem converge to an optimal solution of the original problem (5.5)-(5.7) when $\mu \rightarrow 0$. Moreover for a given value of the barrier parameter $\mu > 0$ the barrier objective function $\varphi_\mu(x)$ goes to infinity if any of the variables x_i approach their bound zero.

These considerations can be appreciated with the solutions of the two examples plotted in the below *Figure B.1* and *Figure B.2*. The example in *Figure B.1* is related to the barrier objective function $\varphi_\mu(x) := (x - 3)^2 - \mu \ln(x)$ instead the example in *Figure B.2* to the following $\varphi_\mu(x) := (x + 1)^2 - \mu \ln(x)$.

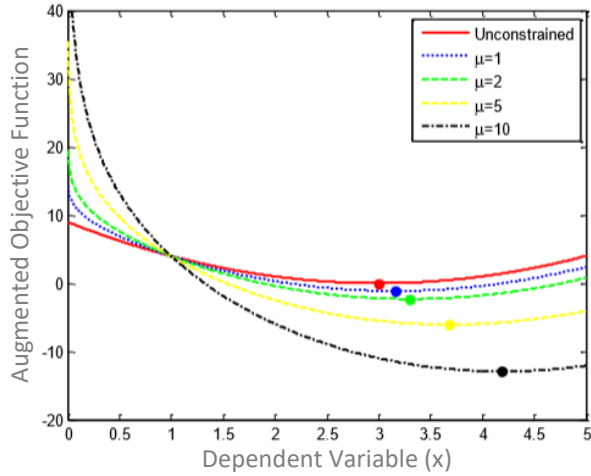


Figure B. 1 - Example A Barrier function

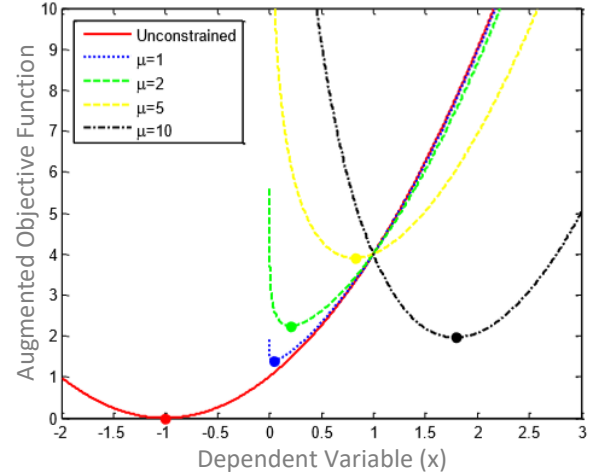


Figure B. 2 - Example B Barrier function

In both if $x_i \rightarrow 0$ the $\varphi_\mu(x) \rightarrow \infty$. The difference between the two examples is that in the second one the unconstrained solution is outside the feasible space ($x > 0$) and so the solutions converge near their bound zero instead the in the first example the optimal solution is internal to the feasible space.

Therefore, the overall solution strategy to solve the (B.4)-(B.5) problem is to do a sequence of barrier problems reducing each time the value of parameter μ . Starting with a moderate value of μ and a user-supplied starting point, the corresponding barrier problem (B.4)-(B.5) is solved to a relaxed accuracy; then μ is decreased and the next problem is solved with an tighter accuracy, using the previous approximate solution as a starting point. This is repeated until a solution for (B.1)-(B.3), or at least a point satisfying the first-order optimality conditions up to user tolerances, has been found.

Equivalently, this can be interpreted as applying a homotopy method to the primal-dual equations:

$$\nabla f(x) + \nabla c(x)\lambda - z = 0 \quad (\text{B.6})$$

$$c(x) = 0 \quad (\text{B.7})$$

$$XZe - \mu e = 0 \quad (\text{B.8})$$

with the homotopy parameter μ , which is driven to zero. Here, $\lambda \in \mathbb{R}^m$ and $z \in \mathbb{R}^n$ correspond to the Lagrangian multipliers respectively the first for the equality constraints (B.2) and the second for the bound constraints (B.3). Furthermore, the notation $X = \text{Diag}(x)$, $Z = \text{Diag}(z)$ and $e = (1, \dots, 1)^T$.

The equations (B.4)-(B.5) for $\mu = 0$ together with “ $x, z \geq 0$ ” are the Karush-Kuhn-Tucker (KKT) conditions for the original problem (B.1)-(B.3). Those are the first order optimality conditions for (B.1)-(B.3) if constraint qualifications are satisfied .

In order to solve the barrier problem (B.4)- (B.5) for a given fixed value of the barrier parameter μ_j , a *damped Newton's method* is applied to the primal-dual equations (B.6)- (B.8). Given an iterate (x_k, λ_k, z_k) , where k to denote the iteration counter for the “inner loop”, with $x_k, z_k > 0$, search directions $(d_k^x, d_k^\lambda, d_k^z)$ are obtained from the linearization of (B.6)-(B.8) at (x_k, λ_k, z_k) , namely

$$\begin{bmatrix} W_k & \nabla c(x_k) & -I \\ \nabla c(x_k)^T & 0 & 0 \\ Z_k & 0 & X_k \end{bmatrix} \begin{pmatrix} d_k^x \\ d_k^\lambda \\ d_k^z \end{pmatrix} = - \begin{pmatrix} \nabla f(x_k) + \nabla c(x_k)\lambda_k - z_k \\ c(x_k) \\ X_k Z_k e - \mu_j e \end{pmatrix} \quad (\text{B.9})$$

where W_k is the Hessian of the Lagrangian function for the original problem (B.1)-(B.3), i.e

$$W_k = \nabla_{xx}^2 L(x_k, \lambda_k, z_k) = \nabla_{xx}^2 (f(x_k) + c(x_k)^T \lambda_k - z_k)$$

and

$$Z_k = \begin{bmatrix} z_1 & 0 & 0 \\ 0 & \dots & 0 \\ 0 & 0 & z_n \end{bmatrix}; X_k = \begin{bmatrix} x_1 & 0 & 0 \\ 0 & \dots & 0 \\ 0 & 0 & x_n \end{bmatrix}$$

The (9) linear system is nonsymmetric so it is rearranged into a symmetric linear one:

$$\begin{bmatrix} W_k + \Sigma_x & \nabla c(x_k) \\ \nabla c(x_k)^T & 0 \end{bmatrix} \begin{pmatrix} d_k^x \\ d_k^\lambda \end{pmatrix} = - \begin{pmatrix} \nabla f(x_k) + \nabla c(x_k)\lambda_k \\ c(x_k) \end{pmatrix}$$

whit $\Sigma_k = X_k^{-1} Z_k$, derived from (9) by eliminating the last block row. The vector d_k^z is obtained after the linear solution to d_k^x and d_k^λ with explicit solution:

$$d_k^z = \mu_k X_k^{-1} e - Z_k - \Sigma_k d_k^x$$

After the Newton step has been computed, the algorithm first computes maximum step sizes as the largest $\alpha_k^{x,max}, \alpha_k^{z,max} \in (0,1]$ satisfying:

$$x_k + \alpha_k^{x,max} d_k^x \geq (1 - \tau)x_k ; \quad z_k + \alpha_k^{z,max} d_k^z \geq (1 - \tau)z_k$$

with $\tau = \min\{0.99, \mu\}$; this *fraction-to-the-boundary* rule ensures that the new iterate will again strictly satisfy $x, z \geq 0$. Then a line search with trial step sizes $\alpha_{k,l} = 2^{-l} \alpha_k^{max}$ (with $l = 0, 1, 2, \dots$) is performed. The determination of this trial step sizes α can be done by decrease in Merit Function or with Filter Methods.

Finally, the new iterate is obtained by setting

$$x_{k+1} = x_k + \alpha_k d_k^x$$

$$\lambda_{k+1} = \lambda_k + \alpha_k d_k^\lambda$$

$$z_{k+1} = z_k + \alpha_k d_k^z$$

and the next iteration is started.

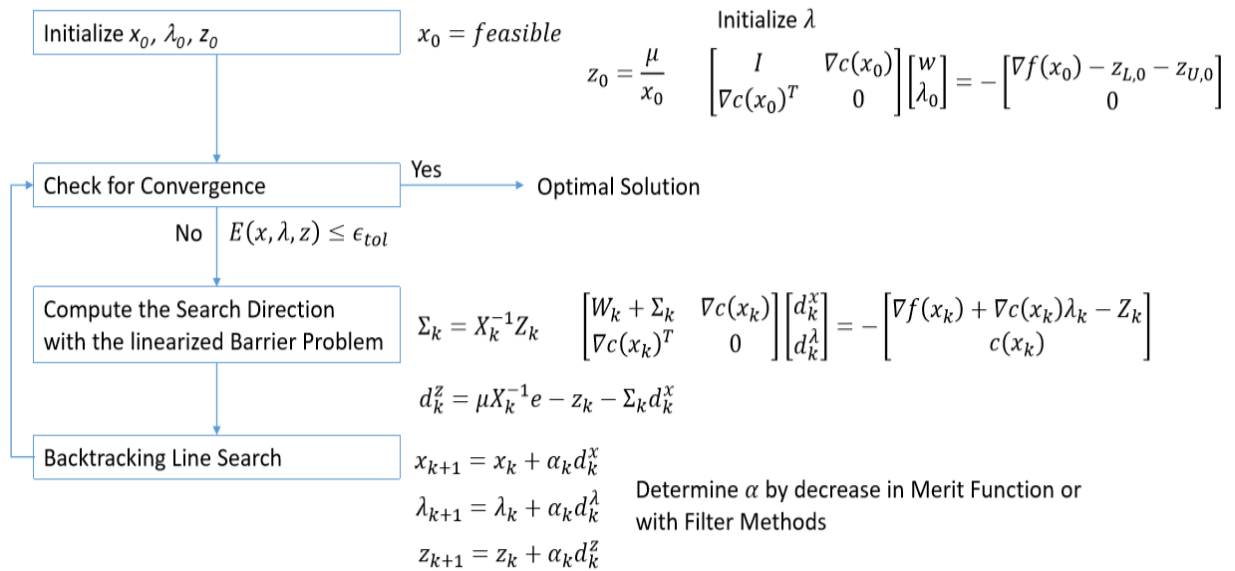
The convergence there is when KKT conditions are satisfied with a tolerance that for the constraint violation may be more restrictive.

$$\max |\nabla f(x) + \nabla c(x)\lambda - z| \leq \varepsilon_{tol}$$

$$\max |c(x)| \leq \varepsilon_{tol}$$

$$\max |XZe - \mu e| \leq \varepsilon_{tol}$$

The algorithm can be schematized with the following flow chart:



APPENDIX C: FSAE suspension rules

The FSAE event requires each team to design and built the formula small racing car according to the rules of the event. During the technical inspection if some request on the regulation is not respected the vehicle cannot access to the dynamic tests.

If the violation of the regulation is resolvable the vehicle can be inspected again by the judges before accessing to the dynamic tests.

The Formula SAE 2018 rules related to the suspensions with their reference chapter in the official text can be summarized in the following points:

T GENERAL TECHINCAL REQUIREMENTS

T 1 GENERAL DESIGN REQUIREMENTS

T 1.1 Vehicle Configuration

T 1.1.2 The vehicle must be open-wheeled, single seat and open cockpit (a formula style body) with four wheels that are not in a straight line.

T 1.1.3 Open wheel vehicles must satisfy (see also Figure 1):

- The wheels/tires must be unobstructed when viewed from the side.
- No part of the vehicle may enter a keep-out-zone defined by two lines extending vertically from positions 75mm in front of and 75mm behind the outer diameter of the front and rear tires in the side view of the vehicle, with tires steered straight ahead. This keep-out zone extends laterally from the outside plane of the wheel/tire to the inboard plane of the wheel/tire.

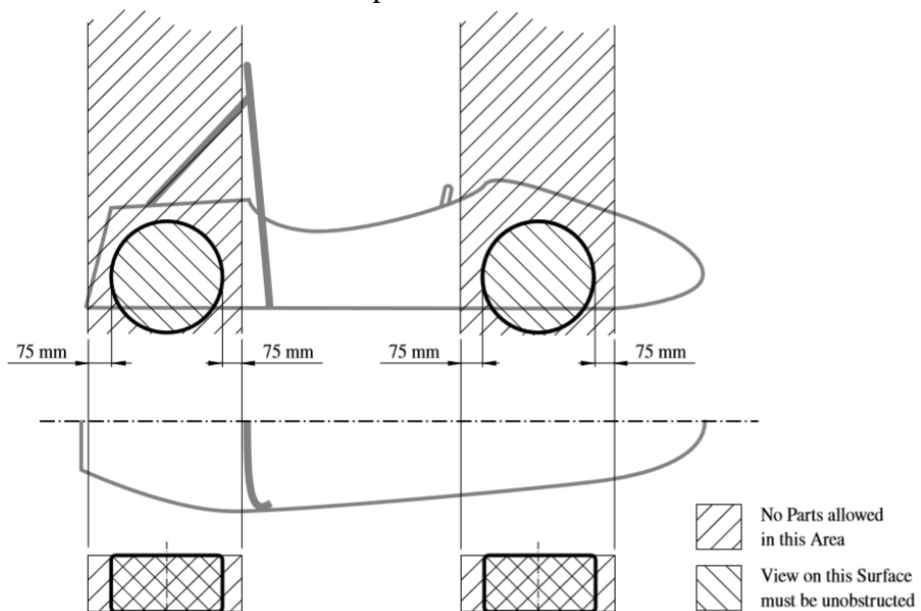


Figure C. 1 - Keep-out-zones for the definition of an open-wheeled vehicle
taken from: Formula Student Rules 2018

T 1.2 Bodywork

T 1.2.1 There must be no openings through the bodywork into the driver compartment other than that required for the cockpit opening. Minimal openings around the front suspension and steering system components are allowed.

T 1.3 Suspension

T 1.3.1 The vehicle must be equipped with fully operational front and rear suspension systems including shock absorbers and a usable wheel travel of at least 50 mm with driver seated (25 mm jounce and 25 mm rebound).

T 1.3.2 The minimum static ground clearance of any portion of the vehicle, other than the tires, including a driver, must be a minimum of 30 mm.

T 1.3.3 All suspension mounting points must be visible at technical inspection, either by direct view or by removing any covers.

T 1.6 Steering

T 1.6.2 The steering wheel must be mechanically connected to the front wheels.

T 1.6.3 The steering system must have positive steering stops that prevent the steering linkages from locking up. The stops must be placed on the rack and must prevent the tires and rims from contacting any other parts.

T 1.7 Wheelbase

T 1.7.1 The vehicle must have a wheelbase of at least 1525 mm.

T 1.8 Track and Rollover Stability

T 1.8.1 The smaller track of the vehicle (front or rear) must be no less than 75 % of the larger track.

T 1.8.2 The track and center of gravity of the vehicle must combine to provide adequate rollover stability

T 4 DRIVER RESTRAINT SYSTEM

T 4.9 Driver's Leg Protection

T 4.9.1 All moving suspension and steering components and other sharp edges inside the cockpit between the front hoop and a vertical plane 100 mm rearward of the pedals, must be shielded with solid material.

T 4.9.2 Covers over suspension and steering components must be removable to allow inspection of the mounting points.

T 9 FASTENERS

T 9.1 Critical Fasteners

- T 9.1.1 Critical fasteners are defined as bolts, nuts, and other fasteners utilized in the primary structure, the steering, braking, driver's harness, suspension systems and those specifically designated as critical fasteners in the respective rule.
- T 9.1.2 All threaded critical fasteners must meet or exceed metric grade 8.8 or equivalent.
- T 9.1.3 All threaded critical fasteners must be of the type hexagon bolts (DIN 933, DIN 931) or socket head cap screws (DIN 912, DIN 7984) including their fine-pitch thread versions.
- T 9.1.4 Bolts may be shortened in length as long as T 9.2.3 is fulfilled.
- T 9.1.5 Any bolted joint in the primary structure using either tabs or brackets, must have an edge distance ratio “e/D” of 1.5 or greater. “D” equals the hole diameter and “e” equals the distance from the hole centerline to the nearest free edge of the tab or bracket. Any tabs attaching suspension members to the primary structure are not required to meet this rule.

T 9.2 Securing Fasteners

- T 9.2.1 All critical fasteners must be secured from unintentional loosening by the use of positive locking mechanisms.
- T 9.2.2 The following methods are accepted as positive locking mechanisms:
- Correctly installed safety wiring.
 - Cotter pins.
 - Nylon lock nuts (DIN 982, DIN 9626 or equivalent) for low temperature locations (80 °C or less).
 - Prevailing torque lock nuts (DIN 980, DIN 6925, ISO 7042 or equivalent, and jet nuts or K-nuts).
 - Locking plates.
 - Tab washers.

Any locking mechanism based on pre-tensioning or an adhesive is not considered a positive locking mechanism.

- T 9.2.3 A minimum of two full threads must project from any lock nut.
- T 9.2.4 All spherical rod ends and spherical bearings on the steering or suspension must be in double shear or captured by having a screw/bolt head or washer with an outer diameter that is larger than the spherical bearing housing inner diameter.
- T 9.2.5 Adjustable tie-rod ends must be constrained with a jam nut to prevent loosening.

IN TECHNICAL INSPECTIONS

IN 1 GENERAL

IN 1.6 Modifications and Repairs

IN1.6.1 After technical inspection, the only modifications permitted to the vehicle are:

- Adjustment of the suspension where no part substitution, other than springs, sway bars and shims, is required.
-

Among the rules there is also a part related to describe the dynamic events:

D DYNAMIC EVENT REGULATIONS

D 4 SKIDPAD EVENT

D 4.1 Skidpad Track Layout

D 4.1.1 The skidpad course consists of two pairs of concentric circles in a figure of eight pattern.

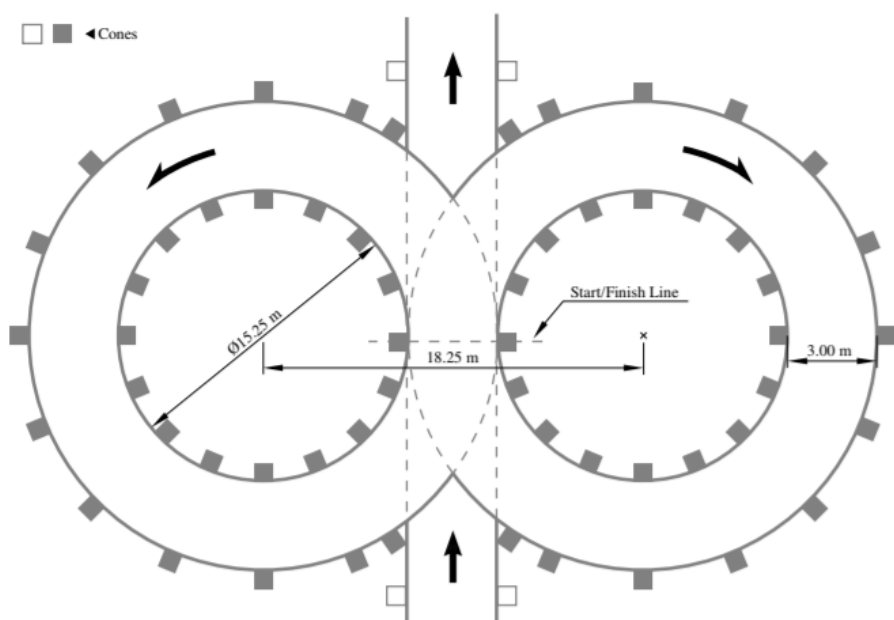


Figure C. 2 - Skidpad Track Layout
taken from: Formula Student Rules 2018

D 4.2 Skidpad Procedure

D 4.2.5 The vehicle will enter perpendicular to the figure of eight and will take one full lap on the right circle to establish the turn. The next lap will be on the right circle and will be timed. Immediately following the second lap, the vehicle will enter the left circle for the third lap. The fourth lap will be on the left circle and will be timed. Immediately upon finishing the fourth lap, the vehicle will exit the track perpendicular to the figure of eight and moving in the same direction as entered.

D 5 ACCELERATION EVENT

D 5.1 Acceleration Track Layout

D 5.1.1 The acceleration course is a straight line with a length of 75 m from starting line to finish line. The course is at least 5 m wide. Cones are placed along the course at intervals of about 5 m. Cone locations are not marked on the pavement.

D 6 AUTOCROSS EVENT

D 6.1 Autocross Track Layout

D 6.1.1 The autocross track layout is a handling course built to the following guidelines:

- Straights: No longer than 80 m
- Constant Turns: up to 50 m diameter
- Hairpin Turns: Minimum of 9 m outside diameter (of the turn)
- Slaloms: Cones in a straight line with 7.5 m to 12 m spacing
- Miscellaneous: Chicanes, multiple turns, decreasing radius turns, etc. The minimum track width is 3 m.

D 6.1.2 The length of the autocross track is less than 1.5 km.

D 7 ENDURANCE AND EFFICIENCY EVENT

D 7.1 Endurance Track Layout

D 7.1.1 The endurance track layout is a closed lap circuit built to the following guidelines:

- Straights: No longer than 80 m
- Constant Turns: up to 50 m diameter
- Hairpin Turns: Minimum of 9 m outside diameter (of the turn)
- Slaloms: Cones in a straight line with 9 m to 15 m spacing
- Miscellaneous: Chicanes, multiple turns, decreasing radius turns, etc.
- The minimum track width is 3 m.

D 7.1.2 The length of one lap of the endurance track is approximately 1 km.

D 7.1.3 The length of the complete endurance is approximately 22 km.

*This thesis work is dedicated to all the people who have always believed in
me during my academic career.*

*I would like to express my gratitude to my supervisor Prof. Francesco Biral
for his kind availability shown to me and for his useful advices.*

*I would also like to thank all the E-Agle Trento racing team where I found
excellent work colleagues and most importantly new friends.*

Finally, my gratitude goes to my family for their constant support.

Alessandro Luchetti